SELF-ASSEMBLING HUMAN PLURIPOTENT STEM CELL-DERIVED HEART ORGANOIDS FOR THE STUDY OF HEART DEVELOPMENT AND CONGENITAL HEART DISEASE

Ву

Yonatan Raz Lewis Israeli

A DISSERTATION

Submitted to
Michigan State University
in partial fulfillment of the requirements
for the degree of

Biomedical Engineering—Doctor of Philosophy

2023

ABSTRACT

Congenital heart defects (CHD) constitute the most common birth defect in humans, affecting approximately 1% of all live births. Our ability to understand how these disorders originate is hindered by our limited ability to model the complexity of the human heart in vitro. There is a pressing need to develop more representative organ-like platforms recapitulating complex in vivo phenotypes to study human development and disease in vitro. This dissertation outlines a novel method to generate physiologically relevant human heart organoids by self-assembly using pluripotent stem cells. This method is fully defined, highly efficient, scalable, exhibits high reproducibility, and is compatible with screening and highcontent approaches. Human heart organoids (hHOs) are generated through a three-step Wnt signaling modulation strategy using a combination of chemical inhibitors and growth factors in completely defined culture conditions. hHOs recapitulate aspects of human cardiac development and are comparable to agematched fetal cardiac tissues at the transcriptomic, structural, and cellular levels. hHOs develop sophisticated internal chambers with well-organized multi-lineage cell type regional identities reminiscent of the heart fields and the atrial and ventricular chambers, as well as the epicardium, endocardium, and vasculature, and exhibit robust functional activity. Finally, hHOs can recreate complex metabolic disorders associated with CHD by establishing the first in vitro human heart organoid model of pregestational diabetes (PGD) to study embryonic CHD. Our heart organoid model constitutes a powerful novel tool for translational studies in human cardiac development and disease.

This thesis is dedica	ited to my parents for help who I was, and to my pa	oing me become who I ar rtner for showing me who	m, to my brothers for o I want to be.	reminding me

ACKNOWLEDGEMENTS

I wish to thank Dr. Aitor Aguirre for his guidance and mentorship throughout my time at MSU, members of my committee: Dr. Assaf Gilad, Dr. Christina Chan, and Dr. Dana Spence, and all members of the Aguirre lab, present and past, who helped make my time in graduate school a pleasant journey.

A special thanks to Aguirre lab members including Aaron Wasserman, who helped greatly in the writing process of the Nature Communication and Biomolecules publications as well as with cell and organoid culture and immunofluorescence imaging; Brett Volmert, who created the FlipGFP cell line and help with live calcium imaging; Mitchell Gabalski, who dedicated hours of volunteer undergraduate work to this project by helping with cell culture, organoid culture and differentiation, immunostaining, and molecular biology; Amanda Huang, who helped with organoid culture and qPCR analyses; and Kristen Ball, who helped with cell and organoid culture. A special thanks to Dr. Mishref Abdelhamid for his help with designing and executing the experiments on modeling pregestational diabetes in human heart organoids. This work wouldn't have been possible without the generous contributions of members of the Zhou lab including Dr. Chao Zhou, Yixuan Ming, Jinyun Zou, and Guangming Ni, who performed all OPT imaging and help with the analysis; The tremendous help of members of the Li lab including Dr. Wen Li and Weiyang Yang, who constructed the microelectrode array and helped with the electrophysiology recordings of the organoids; And the incredible support of members of the Chatzistavrou lab including Dr. Xanthippi Chatzistavrou and Natalia Pajares, who helped in the preparation and conducted the imaging of the organoid samples using the TEM.

Many thanks to the MSU Genomics Core for their sequencing services, the Mass Spectrometry Core who performed the LC-MS on the organoids, and to the Advanced Microscopy Core and Dr. William Jackson at the MSU Department of Pharmacology and Toxicology for access to confocal microscopes.

Lastly, work in the Aguirre lab was supported by the National Heart, Lung, and Blood Institute of the National Institutes of Health under award numbers K01HL135464, R01HL151505, by the American Heart Association under award number 19IPLOI34660342, and by the Spectrum-MSU Foundation. Work in Dr. Zhou's laboratory was supported by grants from the National Institutes of Health under award number R01EB025209. Work in Dr. Li's laboratory was supported in part by the National Science Foundation under award number ECCS-2024270 and Michigan State University Graduate Excellence Fellowship.

TABLE OF CONTENTS

LIST	OF ABBREVIATIONS	. vi
1.	CHAPTER 1: INTRODUCTION	1
2.	CHAPTER 2: METHODS	20
	CHAPTER 3: AIM 1: ESTABLISHING A SELF-ASSEMBLING HUMAN HEART ORGANOID WIT	
	CHAPTER 4: AIM 2: MOLECULAR AND FUNCTIONAL CHARACTERIZATION OF ADVANCED RT STRUCTURES IN HUMAN HEART ORGANOIDS	
5. PRE	CHAPTER 5: AIM 3: CHARACTERIZING THE MOLECULAR PATHOLOGY OF GESTATIONAL DIABETES IN THE HUMAN HEART	84
6.	CHAPTER 6: CONCLUSION AND FUTURE DIRECTIONS1	80
REF	ERENCES1	11
APP	PENDIX1	25

LIST OF ABBREVIATIONS

ActA Activin A

BETi Bromodomain Extra Terminal inhibitors

bHLH basic Helix-Loop-Helix

BMP4 Bone Morphogenic Protein 4

BRD4 Bromodomain-Containing Protein 4

BSA Bovine Serum Albumin

CHD Congenital Heart Defects/Disease

CM Cardiomyocyte

CPC Cardiac Progenitor Cell

CVD Cardiovascular Disease

DOX Doxorubicin

EB Embryoid Body

ECAR Extracellular Acidification Rate

ECM Extracellular Matrix

EHT Engineered Heart Tissue

EMT Epithelial-Mesenchymal Transition

ER Endoplasmic Reticulum

ESC Embryonic Stem Cells

FHF First Heart Field

GFP Green Fluorescent Protein

Gj Gap junction

Gy Glycogen Granules

hChaMPs human Chambered cardiac Pumps/human Chambered Muscle Pumps

HCM Hypertrophic Cardiomyopathy

hCO human Cardiac Organoid

hESC human Embryonic Stem Cells

hHO human Heart Organoid

hiPSC human induced Pluripotent Stem Cell

hPSC human Pluripotent Stem Cell

HUVEC Human Umbilical Vein Endothelial Cells

hvCOC human ventricular-like Cardiac Organoid Chambers

Hz Hertz

iPSC induced Pluripotent Stem Cell

KO Knockout

Ld Lipid droplet

MEA Microelectrode Array

mESC mouse Embryonic Stem Cell

Mi Mitochondria

MI Myocardial Infarction

MSC Mesenchymal Stem Cell

N Nucleus

NHO Normoglycemic Heart Organoid

OCT Optical Coherence Tomography

OCR Oxygen Consumption Rate

Org Organoid

PC Principal Component

PC (OCT) Personal Computer

PDMS Polydimethylsiloxane

PEO Proepicardial Organ

PFA Paraformaldehyde

PGD Pregestational Diabetes

PGDHO Pregestational Diabetes Heart Organoid

PSC Pluripotent Stem Cell

RFP Red Fluorescent Protein

RNA-Seq RNA Sequencing

ROS Reactive Oxygen Species

S Sarcomeres

SD-OCT Spectral Domain Optical Coherence Tomography

SD Standard Deviation

SEM Standard Error of Mean

SHF Second Heart Field

SLD Superluminescent Diode

T1D/T2D Type 1/Type 2 Diabetes

TEM Transmission Electron Microscopy/Microscope

TUNEL Terminal deoxynucleotidyl transferase dUTP nick end labeling

VSDI Voltage-Sensitive Dye Imaging

WGA Wheat Germ Agglutinin

1. CHAPTER 1: INTRODUCTION

1.1. CARDIOVASCULAR DISEASE AND CONGENITAL HEART DEFECTS

Cardiovascular-related disorders are a significant worldwide health problem. Cardiovascular disease (CVD) is the leading cause of death in developed countries, making up a third of the mortality rate in the US¹. Congenital heart defects (CHD) affect ~1% of all live births², making it the most common birth defect in humans, and the leading cause of death in the first year of infant life^{3,4}. There has been an increase in the prevalence of CHDs⁵, with millions of people around the world living with congenital heart malformations³. Although the CDC reports that ~97% of newborn children survive non-critical CHD and ~75% survive critical CHD⁶, it is commonly associated with significant morbidity and medical interventions in later years, burdening the lives of patients and the healthcare system^{7–9}. While the number of studies relating to the etiology and underlying mechanisms associated with CHD has been increasing in recent years, less than 20% of cases have an identifiable cause¹⁰. Access to early human tissues for the study of the early stages and etiology of CHD is very limited, if at all possible, due to unavoidable ethical limitations¹¹. The multifaceted etiology of CHD has remained largely elusive to research and medical professionals and can be broadly categorized as genetic in origin or environmentally induced, though often both must be taken into consideration.

1.2. IN VITRO MODELS OF THE HEART

1.2.1.Stem cell-derived cardiomyocytes

Human Pluripotent Stem cells (hPSCs) — including human embryonic stem cells (hESCs) and induced pluripotent stem cells (hiPSCs) — enable us to recapitulate important developmental steps *in vitro* to produce specific cardiac cell types with relative ease, high purity, and in large amounts^{12–14}. However, current cell models are still far away from the structural and cellular complexity of the tissues and organs they intend to represent (e.g., lack of 3-dimentional (3D) matrix, disorganized cells, and absence of multicell-type interactions). These models frequently study isolated cell types and minimize or ignore other heart cells (e.g., epicardial cells, endocardial cells) or the contribution of cell-cell communication to a disease phenotype. There is a strong demand to bridge this technological and knowledge gap, as producing

more faithful *in vitro* models of the human heart will allow us to better model healthy and diseased states for research and translational applications.

The *in vitro* generation of complex 3D cardiac tissues ("miniature hearts") that faithfully recapitulate human cardiac cell type composition, structure, and function will be paramount in advancing basic research studies as well as pre-clinical CVD research.

1.2.2. Engineered 3D tissue, spheroids, and organoids

Organoids are 3D *in vitro* cell constructs that recapitulate organ properties and structure to a significant extent. They constitute particularly useful models to study unapproachable states in humans, such as embryonic and fetal development, or early disease progression in adults.

In recent years, human pluripotent stem cells (hPSCs) and primary cells have been successfully used to create organ-like (organoid) models of the brain¹⁵⁻¹⁸, lung ¹⁹⁻²¹, liver²²⁻²⁴, pancreas²⁵⁻²⁷, intestine²⁸⁻³⁰, colon³¹⁻³³, and kidney³⁴⁻³⁶. However, there has been less progress on human heart organoids, likely due to its significant structural complexity and challenges associated with its biomechanics and vascularization. The potential applications of human heart organoids are wide-ranging. Because they recapitulate the structural complexity of the heart and follow developmental tissue maturation steps, they can be used to study human cardiac development in a dish and model congenital heart diseases. More mature cardiac organoids can be used to study heart disease in adults and the pathophysiology of myocardial infarction and cardiac injury. In preclinical studies, heart organoids might prove to be a valuable screening tool for determining the therapeutic or cardiotoxic effects of drugs. Patient-specific hPSCs can be used to generate organoids that can greatly advance the field of personalized medicine³⁷. In the long term, heart organoids might become viable sources of transplant tissue. For all these applications, however, creating more sophisticated and reproducible human heart organoids is a key necessary preliminary step that still presents

1.3. HEART ORGANOIDS FABRICATION AND DIFFERENTIATION APPROACHES

significant challenges.

Over the last few decades, a multitude of studies explored the concept of 3D engineered heart tissues, or heart organoids to a certain extent. While these studies significantly advanced the field of *in vitro* heart modeling, the sophistication of self-assembling heart organoids still lag behind that of other organ models. There are two different general schemes for producing heart organoids, directed assembly and self-

organization/self-assembly (**Figure 1**). It is worth noting that throughout this section, the term "organoids" will be used to refer to directly assembled and self-organizing tissues indistinctly in the most general sense of the term, albeit some authors may prefer the specific distinction of engineered heart tissues (EHT) vs. organoids proper. The rationale for this choice is the fact that both methods attempt to recreate constructs with tissue-like structure and functionality. In addition, even though the 3D tissues generated in some of the studies may classify more as EHTs than organoids, the nomenclature used by the original authors will be employed out of respect to their work.

In directed assembly, stem cell-derived differentiated cardiac cells or primary cardiac cells are co-cultured and seeded onto a scaffold or bioengineered device that allows them to develop their 3D structure. In some cases, this structure is obtained by simply growing the cells on an extracellular matrix (ECM) hydrogel or in microwell molds, but it can also be done through more complex means, such as using a biocompatible elastic pillar or a custom-designed bioreactor^{38,39}. The earliest reports attempting to create in vitro organlike heart tissues (sometimes referred to throughout the literature as engineered heart tissues or EHTs) employed cells obtained from primary sources, such as rat and mouse tissues, and aggregated them into a spherical structure, producing what is commonly known as cardiac spheroids^{40–43}. Originally made from only one or two relevant cardiac cell types in co-culture, the cells in these constructs would stick together via cell-cell adhesions and organize into a loosely spherical mass⁴⁴⁻⁵². Other early studies utilized micropatterning of cardiac cells to form non-spherical structures that were more elongated and linear in shape^{53,54}. While the above pioneering constructs were utilized for disease modeling and engraftment with a certain degree of success, they did not develop noteworthy morphological or anatomical complexity and lacked many of the cell types found in the human heart. More recently, however, EHTs have experienced significant innovations raising their complexity and modeling capabilities^{55–59}, as discussed in more detail below.

In recent years, self-organization, a technique that is based on our growing understanding of heart embryonic development and advances in stem cell culture, has gained increased popularity. In this approach, stem or progenitor cells form the 3D structure autonomously, with minimal exogenous intervention, due to the presence of morphogens and growth factors in the media and ECM⁶⁰. Driving developmental cues are provided in the medium in a carefully time-controlled stepwise fashion to induce

differentiation into heart lineages. The established cardiac stem cell lineages produced release their own local morphogens and trigger higher levels of complexity and organization quickly. Organoids generated via this method can develop very high levels of complexity, with most or all of the cell types found in the heart, and spontaneously acquire relevant rudimentary anatomical morphology, such as chamber organization and atrioventricular specification^{61–64}. The cost of this approach is lower control over the final result in comparison to organoids fabricated via direct assembly.

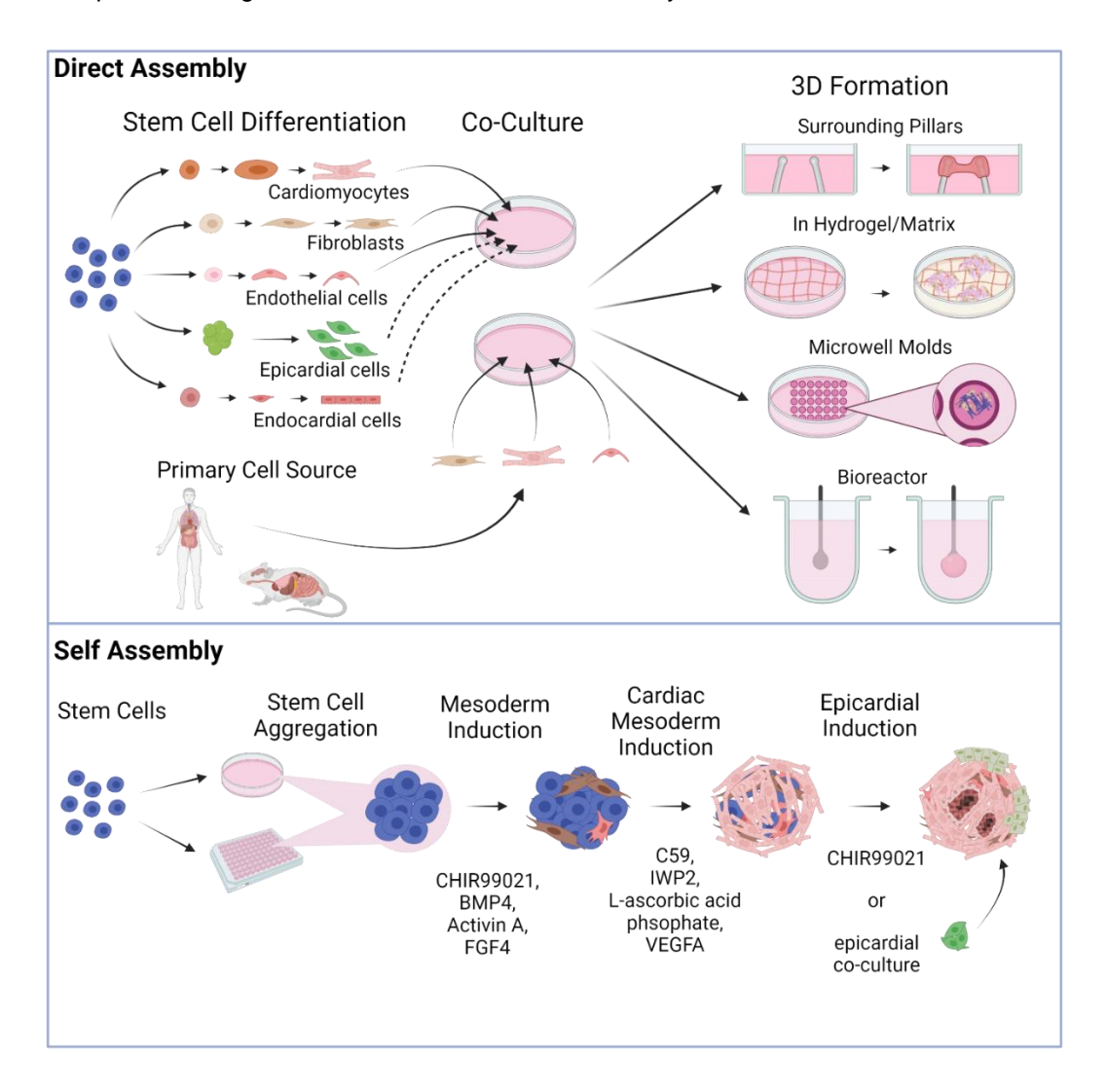


Figure 1. Fabrication approaches for cardiac organoid generation in a dish. Direct assembly approaches (**top**) are organoid techniques where specific cell types are co-cultured and structurally maneuvered to give rise to 3D tissue. Self-assembly approaches (**bottom**) rely on the aggregation of stem cells (often pluripotent) and the induction of differentiation protocols to guide these aggregates towards a cardiac lineage, aiming to mimic physiological development, and allowing the stem cells to self-organize without external structural constraints.

1.3.1. Engineered heart tissue by direct assembly

Several studies have been published demonstrating the directed assembly of 3D heart organoids *in vitro*. These methods differ widely in terms of differentiation protocols, cardiac cell type compositions, and potential applications. However, they all utilize some type of scaffold, biomaterial, or ECM component to drive the formation of 3D cell aggregates from dissociated cell suspensions. One example of a directed organoid differentiation protocol that has been studied extensively in recent years is the heart dynamometer (Heart-Dyno) microtissue platform⁵⁷. At its core, this method involves taking pre-differentiated cardiac cells and allowing them to condense around two elastic scaffolds, forming a circular structure. The Heart-Dyno is a 96-well plate with a custom-designed culture insert inside each well containing two polydimethylsiloxane (PDMS) elastomeric posts spaced 1.0 mm apart. In the first study utilizing this system, Mills et al. took hiPSC-derived cardiomyocytes and stromal cells at a ~70:30 ratio, mixed them with collagen I and Matrigel (synthetic ECM), and added this mixture to the culture insert⁵⁷. They then allowed the cells to gel for ~30–45 min at 37 °C before immersing them in culture media, which led to them condensing around the two elastic poles within two days, forming human cardiac organoids (hCOs). The presence of the posts stabilizes hCO contraction and allows contraction force to be measured in response to specific inotropic agents⁵⁷.

The applications of the Heart-Dyno platform are numerous, as it provides a 96-well device for functional screening of agents that promote organoid growth, maturation, and function. Mills et al.⁵⁷ first set out to study cardiac maturation by supplementing the hCOs with palmitate, causing them to switch their metabolism from glycolysis to fatty acid oxidation. They found that fatty acids induced the organoids to display more mature contractile, electrophysiological, and transcriptional properties. In addition, the maturation medium caused cardiomyocytes (CMs) to proliferate less and activate the DNA damage response, which drives terminal CM differentiation ⁵⁷. In another study, the Heart-Dyno system was utilized to screen 105 small molecules for their pro-regenerative capacity in immature and mature hCOs⁶⁵. The authors identified two compounds that not only increased CM proliferation but also had no detrimental effects on hCO contractile function. Transcriptomic analysis revealed that these hit molecules activated the cell cycle network and the mevalonate pathway, which synthesizes the precursors for cholesterol and steroid hormones⁶⁶, thereby suggesting a mechanism for inducing pro-regenerative effects in human

hearts⁶⁵. One final application of the Heart-Dyno is in the study of cardiac damage that occurs as a result of COVID-19 infection. In this recent study⁶⁷, the effects of candidate pro-inflammatory cytokines on hCO function were investigated, leading to the identification of a cocktail of compounds that induced diastolic dysfunction. They found that bromodomain-containing protein 4 (BRD4) is activated in response to this "cytokine storm" and that bromodomain extra terminal inhibitors (BETi) improved hCO function. Importantly, one specific BETi (INCB054329) also prevented SARS-CoV-2 infection of cardiac cells, a finding that can have important public health implications in the near future⁶⁷.

A very similar hCO platform (with CMs differentiated from hESCs instead of hiPSCs) was also recently used to develop an *in vitro* cardiac injury model⁶⁸. In this study, the authors induced cryoinjury in cardiac organoids by applying a dry ice probe directly to its surface, leading to localized cell death and reduced contractile function. Remarkably, the injured hCOs displayed high levels of CM proliferation and full functional recovery after two weeks, further suggesting that they can be used to study heart regeneration in a dish⁶⁸.

Recently, one burning issue that directly-assembled organoids have been used to model is cardiac tissue maturation. In a landmark study, Ronaldson-Bouchard et al.³⁸ made 3D human cardiac tissues by growing cell populations of 75% hiPSC-derived CMs and 25% human dermal fibroblasts and encapsulating them in a fibrin ECM. They then dispensed these mixtures into a polycarbonate-based tissue bioreactor platform consisting of 12 tissue culture wells with flexible elastomeric pillars in each well. After the cardiac tissues formed around these pillars (approximately one week of culture), the authors subjected them to gradually increasing electrical stimulation, with the goal of forming structures that were as mature as possible. Indeed, after three weeks of intensity training, the human cardiac tissues displayed enhanced cardiac ultrastructure, oxidative metabolism, T-tubule formation, and calcium handling dynamics, thereby demonstrating the potential of this system for modeling adult cardiac disease³⁸. Another platform that utilized electrical stimulation to mature three-dimensional heart tissues is the Biowire system^{69,70}. Here, hESC-CMs and supporting cells were seeded into template PDMS channels containing a sterile surgical suture and embedded in type I collagen gel. Over the course of seven days, the cardiac cells remodeled around the suture, forming 3D rectangular tissues with aligned CMs (biowires). Throughout this time, the biowires were matured via gradually increasing electrical stimulation at low frequency (1 Hz to 3 Hz) or high frequency (1

Hz to 6 Hz). After stimulation, the biowires showed increased CM myofibril organization, elevated action potential conduction velocity, and improved calcium handling dynamics compared to control constructs^{69,70}. In recent years, the Biowire system has been further expanded to generate chamber-specific cardiac tissues⁵⁸. It should be noted that not all cardiac maturation studies utilize electrical stimulation, as mechanical force can also be employed to mature 3D heart tissue. Indeed, several recent papers have reported the generation of EHTs between two posts, one rigid, and one flexible, and subjected them to successively increasing stretch in one direction at the flexible end. In general, mechanical stimulation improved the efficiency of excitation-contraction coupling, calcium handling, myofibril alignment, and expression of cardiac maturation markers. However, applying too much stretch led to signs of pathological hypertrophy and fibrosis accumulation^{71,72}. Overall, the above studies demonstrate the utility of organoid direct assembly approaches for testing different methods of cardiac maturation. Once matured, these tissues can be used to model adult cardiac pathologies, such as hypertrophic cardiomyopathy (HCM) and heart failure^{38,56}.

Other groups have generated their own custom platforms to engineer human heart tissue *in vitro*. In a recent study, Keung et al.³⁹ generated human ventricular-like cardiac organoid chambers (hvCOCs) to study their responses to various inotropic drugs. First, they grew hESC-CMs as embryoid bodies, resuspended them with human dermal fibroblasts and ECM components, and fabricated them into a custom bioreactor designed to construct hvCOCs resembling a heart pump. In short, the authors took a silicon balloon Foley catheter and filled it with water, then immersed it in an agarose mold. They added the cell-ECM tissue mixture directly to the mold and changed the agarose to culture media after two hours, allowing the hvCOC to spontaneously form around the balloon over the course of 10 days (protocol first developed in⁷³). They then exposed these tissues to 25 cardioactive compounds and found that they faithfully recapitulated the expected response to positive inotropic agents, such as isoproterenol (a beta-adrenergic receptor agonist) and levosimendan (a calcium sensitizer)³⁹. Finally, one unique study utilized undifferentiated cells to generate human chambered cardiac muscle pumps (hChaMPs) *in vitro*. In this paper, Kupfer et al.⁵⁹. took hiPSCs and combined them with an optimized ECM-based bioink that they used to 3D print a structure with two chambers and two flow outlets in two weeks. The presence of the ECM proteins allowed the stem cells to proliferate over 14 days to fill the empty spaces in the construct, after which time, they were differentiated

to CMs *in situ*. Remarkably, the 3D structure contained discrete vessels that allowed for perfusion and a continuous muscular wall that formed an enclosed chamber. Longer-term culture allowed the hChaMPs to mature, resulting in functional CMs, calcium transients, action potentials, and beating activity. The authors suggest that these bioengineered heart pumps may be useful for medical device testing and regenerative medicine, demonstrating yet another example of the benefits of using scaffolds to generate 3D human heart tissues⁵⁹.

Not all protocols involving directed assembly of organoids use scaffolds to embed their cells of interest. Instead, some utilize hydrogel molds and culture cardiac cells on top, allowing them to form spheres. Varzideh et al. 74 grew organoids from three different cardiac cell types: hESC-derived cardiac progenitor cells (hESC-CPCs), hESC-derived mesenchymal stem cells (hESC-MSCs), and HUVECs, cultured at a 10:5:5 ratio. They first coated 24-well plates with Matrigel and allowed it to solidify for 20 minutes, resulting in a Matrigel bed (first described in⁷⁵). They then suspended the three cardiac cell types in media and cultured them directly on the hydrogels. Exposure to the ECM components present in the Matrigel allowed the suspensions to acquire a 3D rounded shape within three days, with maximum beating observed after seven days. Once the hCOs reached this point, the authors encapsulated them in collagen type I, transferred them into a bio-compatible 3D-printed basket (made of polylactic acid), and sutured the baskets directly into the peritoneal cavity of nude mice. One month after transplantation, the CMs were more mature at the transcriptional and ultrastructural level and the organoids also developed primitive vasculature 74. In another study utilizing hydrogel molds to direct assembly of 3D structures, Richards et al. 76 made organoids from a 50:50 ratio of CMs to non-CMs (primary human fibroblasts, endothelial cells, and adipose-derived stem cells). Cell suspensions were added to non-adhesive agarose hydrogel molds with 35 microwells each (800 µm diameter) and allowed to settle to the bottom of the mold (protocol first developed in 77). Microtissue formation and beating were observed within four days, at which point the authors subjected them to an oxygen diffusion gradient by placing them in a hypoxia chamber (10% O₂). They then added norepinephrine to the media to trigger adrenergic stimulation, thereby developing an organoid model of myocardial infarction (MI). The infarcted organoids displayed increased cell death and fibrosis accumulation, abnormal calcium handling, and pathological shifts in their metabolism. Importantly, these hCOs were also used to model chemotherapy-induced cardiotoxicity, potentially providing a platform to recapitulate cardiac responses to various drugs at the tissue level⁷⁶.

The studies described above provide ample evidence that directed assembly of human cardiac organoids presents exciting opportunities for disease modeling, drug discovery, and advances relevant to public health. These protocols may even allow us to generate tissues from different germ layers in the same construct, allowing for the study of paracrine interactions between nearby organs. Indeed, a recent study utilized rotary orbital suspension culture of mesendoderm progenitor cells to produce multi-lineage organoids containing cells from the mesoderm (heart) and endoderm (gut) lineages⁷⁸. While directed assembly protocols do have clear applications, it should be noted that many of these studies do not explore the presence of cardiac cell types other than cardiomyocytes and present an oversimplified view of the heart. The human heart is composed primarily of cardiomyocytes (~60%), with the remaining 40% being composed mostly of endothelial cells and cardiac fibroblasts, followed by smaller amounts of smooth muscle cells, epicardial cells, conductance cells, and immune cells⁷⁹. Directed assembly protocols often present few cell types, and cell type ratios that are not close to those observed physiologically. In addition, they all rely on physical structures for proper organization, and despite the fact that some of these materials may recapitulate structural features of the heart, naturally, they are not involved in heart development *in vivo*. A summary of the recent organoid protocols that rely on directed assembly is presented in **Table 1**.

Table 1. Cardiac organoids by direct assembly: techniques, characteristics, and applications

Reference	Cell Source	Aggregation Technique	Functional Assessment	Translational Applications
Mills et al., 2017	hiPSC-CMs, stromal cells	Heart-Dyno: grow hCOs around two elastomeric posts	Force/contractile analysis, electrophysiology, calcium imaging, metabolic profiling	Cardiac maturation studies
Mills et al., 2019	hiPSC-CMs, stromal cells	Heart-Dyno: grow hCOs around two elastomeric posts	Force/contractile analysis	Drug screening: regenerative responses
Mills et al., 2021	hiPSC-CMs, stromal cells	Heart-Dyno: grow hCOs around two elastomeric posts	Force/contractile analysis	Modeling cardiac effects of COVID-19
Voges et al., 2017	hESC-CMs, stromal cells	Grow hCOs around two elastic exercise poles	Force/contractile analysis	Cardiac regeneration studies
Ronaldson-Bouchard et al., 2018	hiPSC-CMs, human DFs	Grow human cardiac tissues around flexible elastomeric pillars	Force/contractile analysis, electrophysiology, calcium imaging, metabolic profiling	Cardiac maturation/adult disease modeling
Keung et al., 2019	hESC-CMs, human DFs	Grow hvCOC around silicon balloon Foley catheter (custom bioreactor)	Force/contractile analysis	Drug screening: inotropic responses
Kupfer et al., 2020	hiPSCs-CMs	3D print hChaMP, culture hiPSCs on construct, differentiate in situ	Force/contractile analysis, pressure/volume analysis, calcium imaging, optical mapping	Medical device testing/tissue grafting
Varzideh et al., 2019	hESC-CPCs, hESC-MSCs, HUVECs	Culture on Matrigel-coated hydrogel	Electrophysiology, voltage- sensitive dye imaging (VSDI)	Transplantation into mice
Richards et al., 2020	human CFs, HUVECs, hADSCs	Culture in microwells containing agarose hydrogels	Calcium imaging, metabolic profiling, mechanical testing	Myocardial infarction modeling
Devarasetty et al., 2017	hiPSC-CMs, human CFs	Culture in round-bottom well plates, immobilize in hydrogel	Force/contractile analysis	Drug screening: chronotropic responses
Buono et al., 2020	hiPSC-CMs, HCMECs, human CFs	Invert cell suspension, gravity- enforced aggregation ("Hanging Drop")	Calcium imaging	Modeling hypertrophic cardiomyopathy
Silva et al., 2020	hiPSC-mesendoderm progenitor cells	Rotary orbital suspension culture	Electrophysiology, calcium imaging	Modeling multi-tissue interactions

1.3.2. Heart organoids by self-assembly

Recently, and throughout the development of this dissertation project, self-assembling organoid technologies have become available for several tissues. These approaches explore the differentiation of PSC aggregates in an attempt to recapitulate early cardiogenesis *in vitro*. Mouse ESCs have been used to generate precardiac organoids showing distinct heart field specifications⁸⁰, cardiac crescent-like structures juxtaposed with primitive gut tube⁸¹, and atrial and ventricular cardiomyocyte lineages⁸². These studies provide us with a great deal of understanding of early heart development but are faced with the traditional limitations associated with mouse models. Cardiac organoids from human PSCs have also seen great advancements, with heart-forming organoids with an internal endodermal core⁸³. These, however, present limitations as a model of the heart associated with their cells of non-cardiac origin, lack of minor cardiac cell lineages, and non-physiological organization. Most recently, cardioids have been reported with a large internal chamber, relevant cardiac cell lineages and impressive transcriptomic analysis⁸⁴. While demonstrating a large leap in self-assembling capabilities, these cardioids still rely on co-culture approaches to include epicardial clusters and rely on multiple differentiation protocols to achieve this model of the developing human heart.

Formation of PSC aggregates can be performed by either high-density cell seeding, allowing 3D aggregates to form and transferring them to ultra-low-attachment wells⁸⁰, or by seeding the cells into round bottom ultra-low-attachment plates to allow 3D aggregate formation by undisturbed incubation^{61,85} or centrifugation of the plate^{62–64}. For aggregates prepared in 96-well plates, the number of seeded cells ranges from as little as 300–700 cells per well⁸⁵ up to 10,000 cells per well (as described in this dissertation and corresponding publication)⁶³. Most protocols initiate differentiation of the PSC aggregates 2 days after seeding^{81,83,86,87}, with the exception of Hofbauer et al., which starts 1 day after⁶⁴, and Lee et al., which starts 4 days after⁶¹. These protocols yield a range of cardiac organoids mimicking various aspects of cardiogenesis. While these organoids demonstrate some overlap in the resulting features, there are key differences between them when it comes to cell lineages, morphological structure, functional capabilities, and demonstration of translational applicability. Several of the reported protocols used mouse ESCs (mESCs)^{80,81,88}, while the most recent ones used human iPSCs or ESCs^{62–64}, with the added benefit of pre-clinical and translational applicability to humans.

Andersen et al.89 generated precardiac organoids to model the formation of the first and second heart field using transgenic mouse ESC lines. They tested the effects of various concentrations of the growth factors bone morphogenic protein 4 (BMP4) and Activin A (ActA) on cardiogenesis and found that variations in BMP4 concentration significantly affected organoid formation, while the effect of ActA variation was only moderate. This finding illustrates the importance of such a platform to facilitate the study of morphogens in cardiac development. Using their transgenic line containing an Hcn4/GFP reporter for the first heart field (FHF) and a Tbx1/RFP reporter for the second heart field (SHF), they were able to demonstrate that FHF progenitors are more likely to give rise to cardiomyocytes (~89%) compared with SHF progenitor cells (~50%). They concluded that the SHF progenitor cells are more likely to give rise to non-myocyte cardiac lineages, which may include cardiac fibroblasts and endothelial cells. They also found that cardiomyocytes arising from the SHF progenitor cells had a delay in differentiation and experienced CM specification up to 2 days after those derived from FHF progenitors, a phenomenon that is also observed in vivo⁹⁰. Lastly, they used their organoids to show that the chemokine receptor CXCR4 can be used to identify SHF progenitors in both mice and humans using an hiPSC cell line. Taking mouse ESC-derived cardiac organoids one step further, Lee et al.⁶¹ cultivated heart organoids with cardiomyocytes, endothelial cells, and smooth muscle cells, with both atrial and ventricular regions. Like Andersen et al., they found that their organoids contain FHF and SHF markers and observe cardiac crescent-like structures in heart development. These organoids, however, develop further than the heart field stage. The authors observed the presence of the atrial-specific cardiomyocyte marker MLC2a and the ventricular-specific marker MLC2v, with a clear spatial separation between them, suggesting atrioventricular specification. Electron microscopy revealed that the ultrastructure was specific to atrial (atria-specific granules, secretory vesicles, and high density of mitochondria), or to ventricular (well-structured sarcomeres, myofibrils containing glycogens) cardiomyocytes, features they also observed in E11.5 mouse heart tissue. Lastly, they analyzed the functional capability of their heart organoids using calcium transient analysis and evaluated electrophysiological parameters using isoproterenol treatment. These studies support the ability of heart organoids to model mouse cardiac development and illustrate their value in understanding novel aspects of morphogen signaling, heart field formation, and atrioventricular specification.

The recent study by Drakhlis et al.⁹¹ used human ESCs to differentiate 3D aggregates embedded in a drop of Matrigel to provide matrix support. They found that their organoids form three distinct layers containing lineages beyond those found in the heart. The inner core had endodermal features and was encircled by endocardial-like cells and a dense myocardial layer. The outer layer had endodermal regions and clustered positive for the liver anlagen marker HNF4a. While not exclusively cardiac in nature, these organoids allow the modeling of early heart and foregut development. Aside from cardiomyocyte and endocardial cell markers, they also observed vessel-like endothelial cells, mostly in the inner core. By generating an NKX2.5 knockout (KO) line, they were able to demonstrate that these organoids recapitulate phenotypes of NKX2.5 knockout mice. NKX2.5 is a crucial transcription factor in cardiac development, and its absence is lethal to mouse embryos⁹². Notably, KO organoids appeared less compact, with disorganized sarcomeres and increased cardiomyocyte size. Similar to the organoids produced by Drakhlis et al., the mouse gastruloids produced by Rossi et al.85 comprise more than just cardiogenic lineages. These gastruloids form a cardiac crescent-like structure adjacent to a primitive gut-like tube. Unlike aggregate generation methods employed by other groups, Rossi et al. seeded under 1000 cells per well in a small volume of media (40 µL) and did not centrifuge the plate, allowing the aggregates to form over 48 h undisturbed, a method reminiscent of an older protocol93. Gastruloids display high levels of self-organization and allow for the study of early germ layer interactions. Further development of these gastruloids past the cardiac crescent stage could significantly increase the applicability of this system to study diseases affecting cardiac and foregut development in vitro.

Recently, a study that was published alongside the published work corresponding to this dissertation, reported heart organoids with more complex morphological features than those described above, including chamber formation and self-vascularization^{63,64}. Hofbauer et al.⁶⁴ created self-organizing cardioids by seeding 2500–7500 cells in 96-well plates. The method involved a two-step WNT pathway activation/inhibition followed by co-culture of the organoids with epicardial aggregates (differentiated via a separate protocol) to simulate the formation of the proepicardial organ. These organoids generated clear chamber-like structures larger in size than those described here, with chamber formation beginning right after mesoderm induction and smaller chambers forming after 2–3 days of differentiation. The authors showed that cardioids can be used as a platform for the study of fetal heart injury by performing cryoinjury

and documenting necrosis (using TUNEL staining) and evaluating the contribution of fetal cardiac fibroblasts to the injury.

The recent advancements in self-assembling cardiac organoid technology in the past five years greatly increase our capabilities of studying heart development and disease *in vitro*. These platforms allow stem cell aggregates to differentiate without physical constraints or supporting forces and organize into morphological structures in suspension directed only by the inherent forces of the 3D cellular environment, better resembling *in vivo* development. By guiding the stem cells onto a mesoderm/cardiac mesoderm path, these organoids give rise to a more diverse population of cells than co-culture protocols allow and facilitate more physiologically relevant cellular interactions. While self-assembling organoids do show a great deal of promise in modeling heart development and disease, they are not without their limitations. The self-assembling nature of the methods to create these organoids allows researchers to guide cell type specifications but does not allow for precise control over the cell-to-cell ratios, the overall composition, or the resulting structural organization. Furthermore, the lack of supporting material results in 3D constructs that are more delicate in nature compared to many of their directly assembled counterparts. A summary of the recent organoid protocols that rely on self-assembly is presented in **Table 2**.

Table 2. Cardiac organoids by self-assembly: techniques, characteristics, and applications

Reference	Cell Source	Aggregation Technique	Differentiation Protocol	Cell Types Observed	Stage of Development	Translational Applications
Andersen et al., 2018	mESCs, hiPSCs	high-density cell seeding	D0: BMP4/ActA (40 h)	Cardiac progenitor cells, FHF cells, SHF cells, cardiomyocytes, endothelial cells, smooth muscle cells, fibroblasts	Precardiac heart field specification. No beating reported.	Discovery of CXCR4 as SHF progenitor marker in human organoids
Lee et al., 2020	mESCs	round-bottom, low-attachment well plate	D0–D9: FGF4 D9–D15: FGF4, BMP4, BIO, LIF	Cardiac progenitor cells, FHF cells, SHF cells, cardiomyocytes (atrial), cardiomyocytes (ventricular), smooth muscle cells, endothelial cells	Atrioventricular chamber specification. Representing embryonic day E7.5–E9.5. Beating after 10 days.	
Drakhlis et al., 2021	hESCs	round-bottom, low-attachment well plate with centrifugation, embedded in Matrigel	D0: CHIR99021 (24 h) D3: IWP2 (48 h)	Cardiac progenitor cells, cardiomyocytes, mesenchymal cells, endothelial cells, endocardial cells, liver anlagen	Cardiac mesoderm and foregut endoderm specification. Beating after 7–10 days.	NKX2.5 knockout recapitulates <i>in vivo</i> congenital heart defects
Rossi et al., 2021	mESCs	round-bottom, low-attachment well plate	D0: CHIR99021 (72 h) D4: bFGF, VEGF165, L- ascorbic acid phosphate (48 h)	Cardiac progenitor cells, FHF cells, SHF cells, cardiomyocytes, endothelial cells, endodermal cells	Cardiac crescent and gut- like tube. Beating after 6 days.	
Hofbauer et al., 2021	hiPSCs, hESCs	round-bottom, low-attachment well plate with centrifugation	D0: CHIR99021, ROCKi (36–40 h) D2: VEGF-A (96 h, with medium change every 48 h) D8.5: co-culture with epicardial aggregates	Cardiac progenitor cells, FHF cells, cardiomyocytes (atrial), cardiomyocytes (ventricular), endothelial cells, epicardial cells, endocardial cells, fibroblasts	First heart field specification and chamber formation. Beating after 7 days.	Cardiac injury model

1.4. PREGESTATIONAL DIABETES AND CONGENITAL HEART DEFECTS

1.4.1. Risk of congenital heart defects

CHD constitutes the most common type of congenital defect in humans⁹⁴. Pregestational diabetes (PGD), defined in this case as diabetes of the mother before and during the first trimester of pregnancy (regardless of whether it is type 1 diabetes (T1D) or type 3 diabetes (T2D)) is one of the most prominent non-genetic factors contributing to CHD⁹⁵ and is present in a significant, growing population of diabetic female patients of reproductive age^{96,97}. Newborns from mothers with PGD have an increased risk of CHD (PGD-CHD, 4–12% depending on the sources), versus ~1% in the normal population (up to a 12-fold increase)^{95,98–100}. PGD is challenging to manage clinically due to the extreme sensitivity of the developing embryo to glucose oscillations and constitutes a critical health problem for the mother and the fetus. The prevalence of PGD-CHD is increasing significantly due to the ongoing diabetes epidemic, and although preventative and therapeutic interventions are critically needed, no significant advances have occurred to treat this condition yet.

1.4.2. PGD Case studies

A clear association between PGD and CHD in the newborn has been shown in the literature both in clinical studies^{9,101–103}. The prevalence of CHDs has been rapidly increasing, ⁵ and it is estimated that ~2.4 million Americans, including 1 million children, are living with a congenital malformation of the heart ³ Diabetes mellitus (DM) complicates 1–2% of all pregnancies. It carries a high prenatal disease and mortality risk despite this relatively low prevalence. Numerous retrospective case studies reported a clear correlation between maternal DM during pregnancy and an increase in the risk of CHDs^{9,101–103}. A national study from Denmark investigated the prevalence of CHD and its association with PGD, looking at over 2 million births in a period of about 13 years¹⁰¹. The prevalence of CHD in offspring of mothers with PGD was 318 per 10,000 live births compared to 80 per 10,000 in the baseline group, establishing an adjusted relative risk of 4.00 for CHD¹⁰¹. Interestingly, they found that factors such as year of birth, maternal age at the onset of diabetes, the duration of the diabetes, or whether it was type 1 or type 2, did not significantly affect the relative risk¹⁰¹. Correspondingly, the Pediatric Cardiac Genomics Consortium identified maternal PGD as a one of the few listed non-genetic risk factors of CHD, among others such as obesity and smoking¹⁰². The association between PGD and CHD is evident yet understanding the mechanism and causes of this

association cannot be done in a clinical setting. As such, research scientists diverted their attention to animal models to investigate the underlying etiology of PGD-CHD.

Clinical practice largely precludes studies of PGD-CHD in humans, or severely limits them, thus direct studies of human embryos are not viable. This is understandable given the care that pregnant mothers need, particularly if they suffer from potential increased risk to their fetus. However, the result is significantly limited access to human tissues for research of early-stage disease and mechanisms of PGD-CHD, forcing an overreliance on animal models and stalling progress.

1.4.3. In vivo research of PGD

Significant efforts have been devoted to understanding the molecular pathology of PGD-CHD using animal models^{9,104}, leading to the identification of increased reactive oxygen species (ROS) production, abnormal lipid metabolism, and mitochondrial stress among other contributing factors^{99,105–107}. However, the molecular links and the overall contribution of these abnormalities to the different phenotypes observed in PGD-CHD remain elusive. It also remains unclear to what extent rodent models recapitulate abnormalities present in human PGD-CHD, particularly given critical species differences in heart size and cardiac physiology, and bioenergetics^{108–110}. For example, there are major species differences between mice and humans in how the heart utilizes glucose, lactate, ketone bodies, and fatty acids. *In vivo* studies in mice investigated the symptoms and potential mechanisms in which pregestational diabetes affects fetal development. Many studies demonstrate that maternal diabetes alters the expression of some genes that are involved in the development of the heart, leading to congenital heart defects, including developmental morphogens and transcription factors, such as Bmp4, Msx1, Pax3¹¹¹, Gata4, Tbx5, Nkx2.5, Gata5, Bmp10, and Notch1¹⁰⁵. These studies also alluded to the involvement of increased oxidative stress during development^{105,111–113}.

1.4.4. In vitro research

In vitro studies using 2D monolayers of cardiomyocytes derived from hiPSCs have been used to investigate the effects of diabetic conditions in human cells^{114–116}. To create the diabetogenic environment, hiPSC-derived cardiomyocytes were exposed to a high glucose (HG) environment. HG-treated cardiomyocytes were 5-fold larger than normal glucose-treated cardiomyocytes. In line with the observed hypertrophic

changes, high glucose treatment significantly increased the expression of the cardiac hypertrophy markers ACTA1, FHL, and MLC2A¹¹⁶.

In recent years, novel stem cell-based technologies have enabled the creation of engineered, highly complex, human organ-like 3D tissues *in vitro*, with properties that recapitulate the physiological setting to a significant extent^{117–121}. These organoids are particularly useful for studying unapproachable disease states in humans (e.g., early disease progression when symptoms are not still present), or states for which animal models are not well-suited^{11,122,123}. Organoids can also be powerful tools to verify in human models what we have learned in animal studies, complementing them. While organoids have been used to model a wide range of human tissues and conditions, their use in cardiovascular research has been lagging until very recently^{83,86,122,124,125}. Human heart organoids are an ideal platform to study the etiology of PGD-CHD and investigate the underlying mechanisms.

1.5. SIGNIFICANCE

1.5.1. Improvement on current models

While traditional animal models, such as mice and rats, have proven useful for studying CVD etiology and pathogenesis, there is a critical need for human-derived models to be able to fully translate these findings to the clinic. The project described here shows a crucial technical step forward by engineering one of the first synthetic development models of human heart development⁸⁶. These heart organoids recapitulate critical steps of cardiac development in humans, while containing high complexity in cardiac cell types and structural organization. They simultaneously exhibit high reproducibility and are amenable to screening approaches^{86,122}.

1.5.2. Sophistication and novelty of the model

This dissertation reports a novel small molecule-based methodology to create highly complex and physiologically relevant human heart organoids (hHOs) using hPSCs by manipulating cardiac developmental programs. This protocol relies mainly on three sequential Wnt modulation steps (activation/inhibition/activation) at specific time points on suspension embryoid bodies (EBs) and produces significant heart-like structures in terms of structure, organization, functionality, cardiac cell type complexity, ECM composition, and vascularization. Additionally, this method is inexpensive compared to growth factor-based approaches and relatively simple in terms of procedure.

1.5.3. In vitro applications and translational relevance

The organoid platform described here is automatable, scalable, and amenable to high-content/high-throughput pharmacological screenings. It can be used to both study human heart development and investigate the onset of human heart diseases from a mechanistic and a pharmacological approach. At the time of writing, published works using this organoid platform have been used to model human fetal heart development⁸⁶, the onset of PGD-CHD⁸⁶, and the effect of COVID-19 on the human heart¹²⁶.

1.5.4. Novelty of pregestational diabetes model

This organoid system is utilized here to model the effects of PGD — clinically defined as diabetes before pregnancy and affecting the first trimester embryo — on the developing embryonic heart and explore its potential to identify therapeutic targets. To date, research on the effects of PGD on the developing human heart and its association with CHD are limited to retrospective case/cohort studies, animal models, and overly simple 2D cardiomyocyte *in vitro* models, as described in sections 1.4.21.4.4, respectively. This dissertation and its corresponding publications^{86,122}, are the first to describe the onset effects of human fetal-like heart tissue in organoid form in response to diabetic (hyperglycemic and hyperinsulinemic) conditions, paving the way to mechanistic understanding and therapeutic discovery.

1.6. AIMS

Aim 1: Establishing a self-assembling human heart organoid with myocardial and epicardial tissue

Aim 2: Molecular and functional characterization of advanced heart structures in human heart

organoids

Aim 3: Characterizing the molecular pathology of pregestational diabetes in the human heart

2. CHAPTER 2: METHODS

2.1. CELL AND TISSUE CULTURE

2.1.1. Stem cell culture

The following human iPSC lines were used in this study: iPSC-L1, AICS-0037-172 (Coriell Institute for Medical Research, alias AICS), iPSCORE_16_3 (WiCell, alias iPSC-16; UCSD013i-16-3), iPSC GCaMP6f^{127,128}, and human ESC line H9 (WiCell, WA09). All PSC lines were validated for pluripotency and genomic stability. hPSCs were cultured in Essential 8 Flex medium containing 1% penicillin/streptomycin (Gibco) on 6-well plates coated with growth factor-reduced Matrigel (Corning) in an incubator at 37°C, 5% CO₂ until 60–80% confluency was reached, at which point cells were split into new wells using ReLeSR passaging reagent (Stem Cell Technologies). The sources for the cell lines used in this dissertation can be found in the appendix (**Table 5**)

2.1.2. Monolayer differentiation

Differentiation was performed using the small molecule Wnt modulation strategy adapted from a previous protocol 129 , (referred to as monolayer 1 in the text), with small modifications. Briefly, differentiating cells were maintained in RPMI with B27 minus insulin from day 0–7 of differentiation and RPMI with B27 supplement (Thermo) from day 7–15 of differentiation. Cells were treated with 10 μ M CHIR99021 (Selleck) for 24 hours on day 0 of differentiation and with 2 μ M Wnt-C59 (Selleck) for 48 hours from day 3–5 of differentiation.

2.1.3. Embryoid body formation

Accutase (Innovative Cell Technologies) was used to dissociate PSCs for spheroid formation. After dissociation, cells were centrifuged at 300 g for 5 minutes and resuspended in Essential 8 Flex medium containing 2 μM ROCK inhibitor Thiazovivin (Millipore Sigma). hPSCs were then counted using a Moxi Cell Counter (Orflo Technologies) and seeded at 10,000 cells/well in round bottom ultra-low attachment 96-well plates (Costar) on day -2 at a volume of 100 μl per well. The plate was then centrifuged at 100 g for 3 minutes and placed in an incubator at 37°C, 5% CO₂. After 24 hours (day -1), 50 μl of media was carefully removed from each well, and 200 μl of fresh Essential 8 Flex medium was added for a final volume of 250 μl/well. The plate was returned to the incubator for an additional 24 hours.

2.1.4. Inducing cardiac mesoderm in organoids

On day 0, 166 µl (~2/3 of total well volume) of media was removed from each well and 166 µl of RPMI 1640/B-27, minus insulin (Gibco) containing CHIR99021 (Selleck) was added at a final concentration of 4 µM/well a for 24 hours. On day 1, 166 µl of media was removed and replaced with fresh RPMI1640/B-27, minus insulin. On day 2, RPMI/B-27, minus insulin, containing Wnt-C59 (Selleck) was added for a final concentration of 2 µM Wnt-C59 and the samples were incubated for 48 hours. The media was changed again on day 4 and day 6, but insulin was not added to the RPMI1640/B-27 (Gibco) mixture until day 6, as it has been shown to decrease cardiomyocyte yield before this time point²¹. Subsequently, media was changed every 48 hours until organoids were ready for analysis.

2.1.5. Inducing proepicardial formation in organoids

The differentiation process is identical to the procedure in section 2.1.4 up until day 6. On day 7, a second 2 µM CHIR99021 exposure was conducted for 1 hour in RPMI1640/B-27. Subsequently, media was changed every 48 hours until organoids were ready for analysis.

2.1.6. Organoid differentiation with added growth factors

The organoid differentiation process as described in section 2.1.42.1.5 were modified with the following modification to day 0: on day 0, 166 μ l (~2/3 of total well volume) of media was removed from each well and 166 μ l of RPMI 1640/B-27, minus insulin (Gibco) containing CHIR99021 (Selleck) was added at a final concentration of 4 μ M/well along with BMP4 at 0.36 pM (1.25ng/ml) and Activin A at 0.08 pM (1ng/ml) for 24 hours.

2.1.7. Media changes

A partial media change (referring to the steps described in sections 2.1.4 & 2.1.5) was conducted on the organoids by removing 166 μ l, or 2/3 of the total media in each of the 96 wells. This technique allows the organoids to remain in 84 μ l of media and results in the changing of media with minimal disturbance to the organoids at the bottom of the well. As the plates used are ultra-low attachment, the organoids are cultured in suspension, and settle at the bottom of each well. For this reason, media changes must be performed with care to avoid the accidental pipetting of the organoids and minimize any organoid movements that may result from the removal or addition of media to the well. Furthermore, this partial media change allows gradient exposure to differentiation inhibitors and growth factors, as some remain in the media after media

changes. This allows the effects of the inhibitors and growth factors to gradually fade instead of an abrupt removal of the differentiation agents, suggesting a more physiological exposure to external stimuli.

2.1.8. Lentiviral transduction

Lentiviral transduction was conducted by Brett Volmert from the Aguirre Lab. iPSC-L1s were tagged with GFP to be present when the active form of caspase-3 is present in the cell, occurring during the apoptosis cascade. Lentiviruses, which are a type of retroviruses such as HIV, can permanently integrate into the genome of a host mammalian cell. Through reverse transcription, the lentivirus RNA becomes double-stranded DNA and lentiviral enzymes (integrase) allow the integration of this DNA into the genome of the host cell. Recombinant lentiviral constructs can be used to insert or remove target genes from the genome of cells and include antibody resistance to help select successfully transfected cells (**Figure 2**). For lentiviral production HEK293T (ATCC) cells were transfected with the Flip-GFP plasmid (VectorBuilder) and the packaging plasmids (pMD2; psPAX2) using lipofectamine with Plus reagent (Thermo Fisher). Lentivirus was added to iPSC-L1 cells with 8 µg/ml polybrene (Fisher Scientific) and incubated overnight. Puromycin selection was carried out for ~3–5 days. Surviving clones were collected, replated, and expanded to give rise to the FlipGFP line.

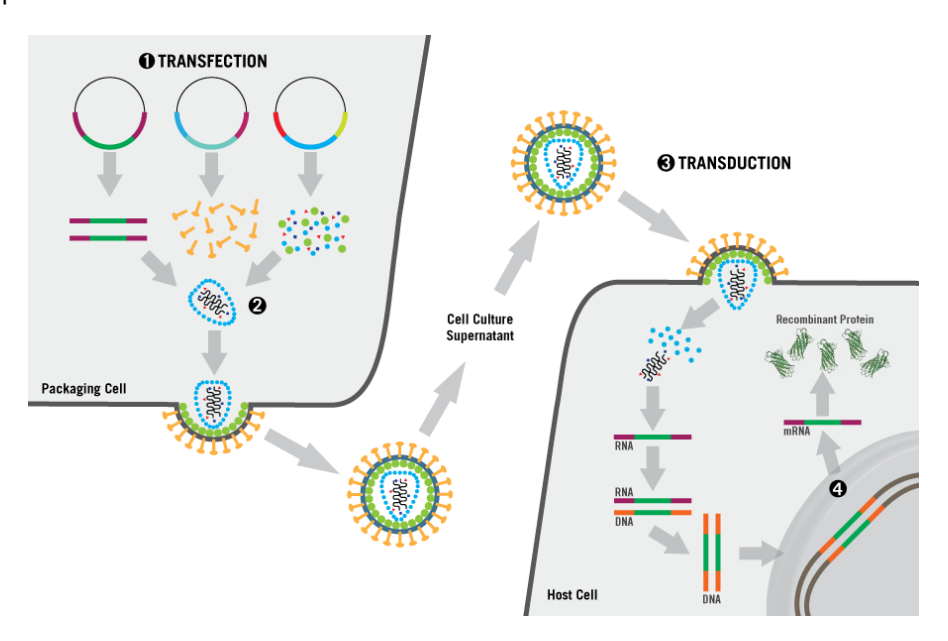


Figure 2. Overview of lentiviral transfection and transduction. (1) Packaging cells, such as HEK293t, are transfected with lentiviral vectors containing target gene and antibody resistance (e.g., puromycin). (2) The virus is assembled and secreted into the media. (3) Target cells (e.g., iPSC-L1) are transduced with recombinant lentivirus particles in the presence of polybrene to increase the uptake. The viral RNA is transcribed and integrated into the host genome. Figure taken from: https://www.mirusbio.com/applications/high-titer-virus-production/lentivirus-production.

2.1.9. Organoid culture and differentiation modeling pregestational diabetes

Diabetic conditions were simulated by using basal RPMI media with 11.1 mM glucose and 1.14 nM insulin and compared with control media containing 3.5 mM glucose and 170 pM insulin. 40.5 uM Oleate-BSA (Sigma), 22.5 uM Linoleate-BSA(Sigma), and 120 uM L-Carnitine (Sigma) were added at day 7 to increase fatty acid metabolism, concentrations previously described 130. The differentiation of the healthy or diabetic organoids was conducted in the same manner discussed in 2.1.42.1.7, and are summarized in **Figure 3**.

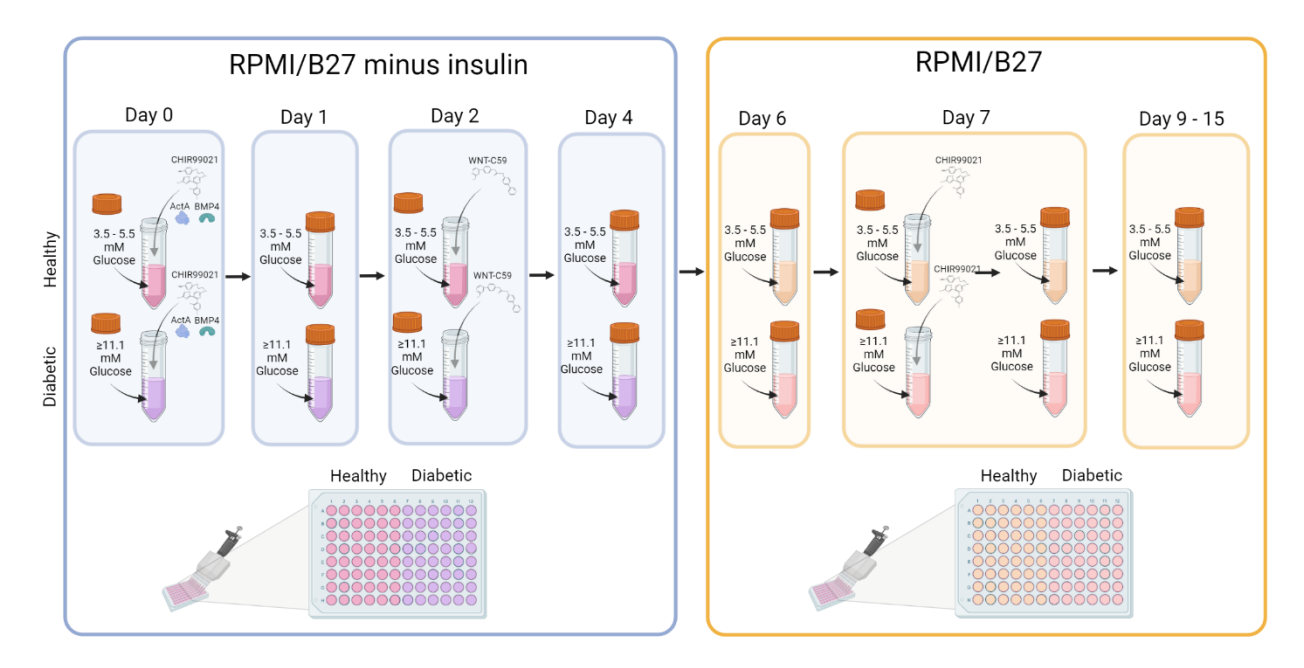


Figure 3. A schematic diagram depicting the differentiation protocols of hHOs under healthy and diabetic conditions. The cardiac organoid differentiation protocol described in this thesis has been modified to allow for the modeling of human heart development under diabetic conditions. The protocol is made up of 2 phases, the first includes a mesoderm and cardiac mesoderm induction under insulin-free conditions (days 0-5), and the second phase that includes epicardial induction and organoid maintenance in the presence of insulin. The diabetic developmental condition (bottom) relay on the elevation of the glucose concentration throughout the protocol and the elevation of insulin in the second phase of the protocol, compared to healthy conditions (top). Organoids are cultured on the same 96-well plate (half healthy and half diabetic) to minimize unintended differences between the conditions.

2.2. IMMUNOFLUORESCENCE AND IMAGING

2.2.1.Immunofluorescence staining

Immunofluorescence is a method where antibodies conjugated with fluorescent dyes are used to visualize the presence of target proteins under a fluorescence microscope. In this method, cells or tissue (such as organoids) are fixed using a fixation agent such as PFA, in order to preserve the tissue in a "life-like" state, and subsequently exposed to specific antibodies. A primary antibody that is specific for a target protein (e.g., cardiac troponin T, aka cTnT) that was produced in a host species (e.g., mouse) is placed in solution

with the organoid, and is then washed away. A secondary antibody that has a conjugated fluorescent dye and is specific to the host animal in which the primary antibody was produced, is then placed in solution with the organoid, allowing it to attach to the attached primary antibodies (**Figure 4**). Fluorescent microscopy, such as confocal microscopy, can be used to image the stained organoids and visualize the structure and location of the target proteins within the organoid. A step-by-step protocol of the immunostaining process is described here:

hHOs were transferred to microcentrifuge tubes (Eppendorf) using a cut 1000 µL pipette tip to avoid disruption to the organoids and fixed in 4% paraformaldehyde solution. Fixation was followed by washes in phosphate-buffered saline (PBS)-Glycine (20 mM) and incubation in blocking/permeabilization solution containing 10% Donkey Normal Serum, 0.5% Triton X-100, 0.5% bovine serum albumin (BSA) in PBS on a thermal mixer (Thermo Scientific) at minimum speed at 4°C overnight. hHOs were then washed 3 times in PBS and incubated with primary antibodies (**Table 4** in Appendix) in Antibody Solution (1% Donkey Normal Serum, 0.5% Triton X-100, 0.5% BSA in PBS) on a thermal mixer at minimum speed at 4°C for 24 hours. Primary antibody exposure was followed by 3 washes in PBS and incubation with secondary antibodies (**Table 4** in Appendix) in Antibody Solution on a thermal mixer at minimum speed at 4°C for 24 hours in the dark. Stained hHOs were washed 3 times in PBS before being mounted on glass microscope slides (Fisher Scientific) using Vectashield Vibrance Antifade Mounting Medium (Vector Laboratories). 90 µm Polybead Microspheres (Polyscience, Inc.) were placed between the slide and the coverslip (No. 1.5) to preserve the 3D structure of the organoids. T-tubules staining was conducted using Wheat Germ Agglutinin (WGA) lectins conjugated with FITC (Millipore Sigma).

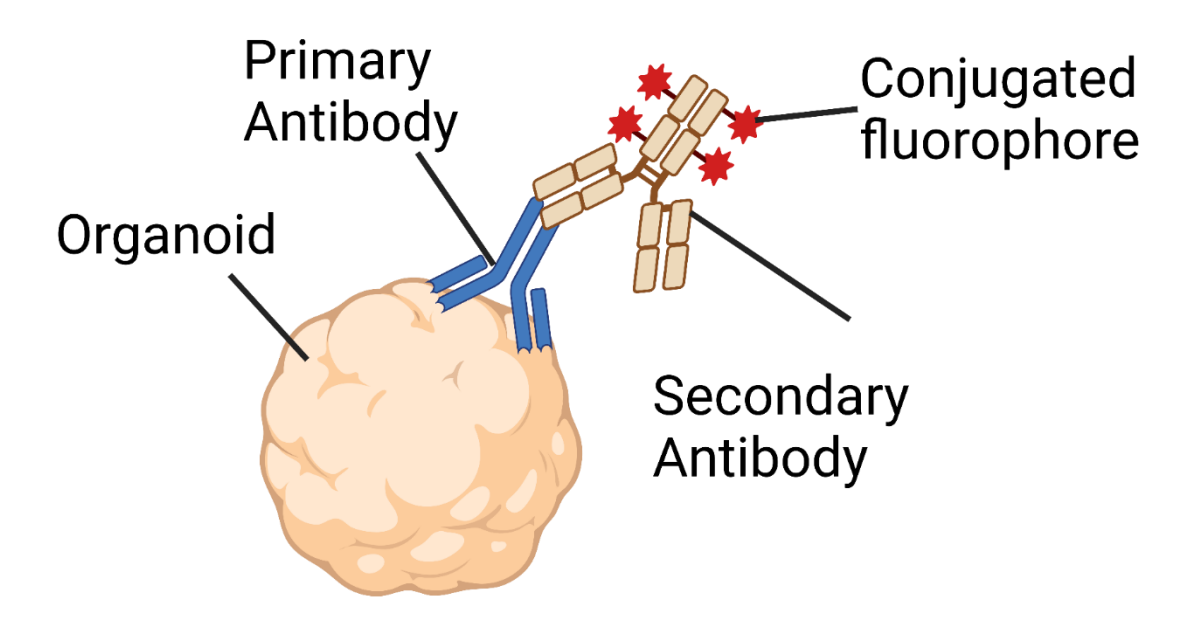


Figure 4. Immunostaining of heart organoid. Primary antibodies are specific to a target protein, and secondary antibodies, which are conjugated with a fluorophore, are specific to a host animal where the primary antibodies were produced (e.g., mouse, rabbit), thus allowing visualization of proteins and structural organization using fluoresce microscopy.

2.2.2. Immunofluorescence imaging and analysis

Samples were imaged using confocal laser scanning microscopy (Nikon Instruments A1 Confocal Laser Microscope; Zeiss LSM 880 NLO Confocal Microscope System). Images were analyzed using Fiji (https://imagej.net/Fiji). For cell quantification in the organoids, DAPI positive cells were counted and used for normalization against the target cell marker of interest across at least three z-planes throughout each organoid for each target cell marker.

2.2.3. Optical coherence tomography

Optical Coherence tomography (OCT) was conducted in collaboration with the Zhou lab at Washington University in St. Louis (WUSTL). All imaging and processing were conducted on site at WUSTL by the Zhou lab, with collaboration on image analysis. OCT uses near infrared light waves and reconstructs a tissue depth profile using the scattered light reflected by the tissue sample, as the light beam scans across the organoid. The scanned planes can then be reconstructed to form a 3D structure. A customized spectral-domain optical coherence tomography (SD-OCT) system was developed by the Zhou lab to acquire 3D images of the cardiac organoids. As shown in **Figure 5**, a superluminescent diode (SLD 1325, Thorlabs) was used as the light source to provide broadband illumination with a central wavelength of 1320 nm and

a spectral range of 110 nm. The output of the SLD was split 50/50 with a fiber coupler and transmitted to the sample and reference arms, respectively. A galvanometer (GVSM002-EC/M, Thorlabs) was used to scan the optical beam in transverse directions on the sample. The SD-OCT setup used a custom-designed spectrometer consisting of a 1024-pixel line scan camera (SU1024-LDH2, Sensors Unlimited), an 1145-line pairs per mm diffraction grating (HD 1145-line pairs per mm at 1310 nm, Wasatch Photonics), and an f = 100 mm F-theta lens (FTH100-1064, Thorlabs). The sensitivity of the OCT system was measured as ~104 dB when operating at 20 kHz A-scan rate. The axial resolution of the SD-OCT system was measured to be ~7 mm in tissue. A 5X objective lens (5X Plan Apo NIR, Mitutoyo) was used to achieve a transverse image resolution of ~7 mm, and the scanning range used for the cardiac organoids imaging was ~2 mm X 2 mm. Fixed hHOs were placed into a 96-well plate with PBS and imaged at a 20-kHz A-scan rate. Obtained OCT datasets of the cardiac organoids were first processed to generate OCT images with corrected scales. Then OCT images were further de-noised using a speckle-modulation generative adversarial network¹³¹ to reduce the speckle noise. 3D renderings of OCT images were performed using Amira software (Thermo Fisher Scientific).

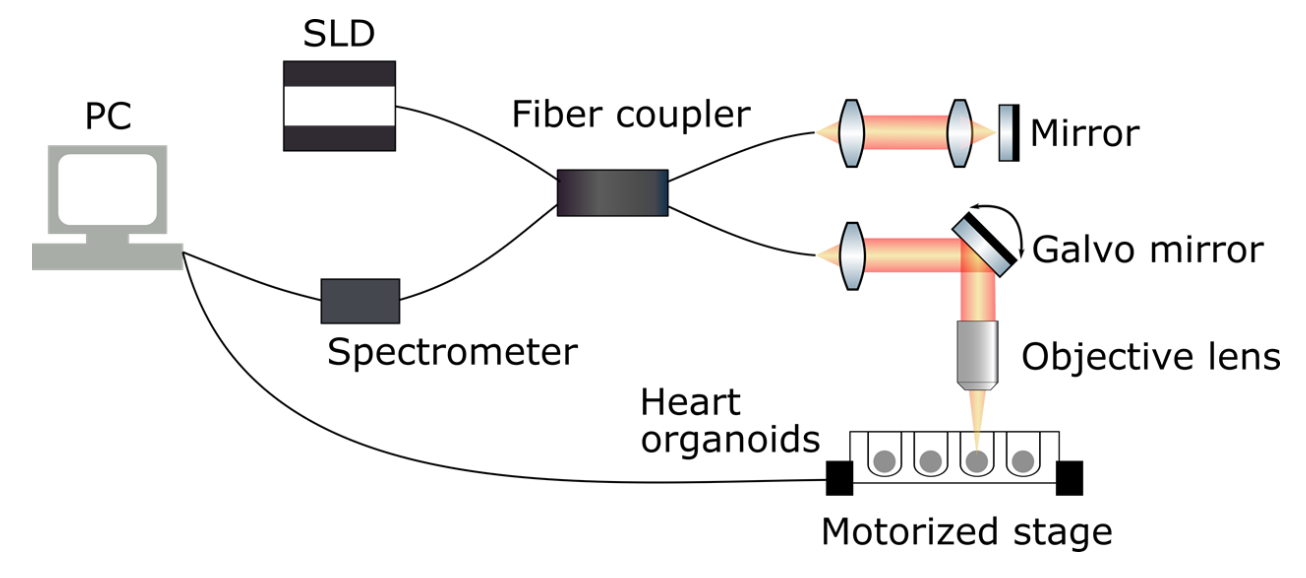


Figure 5. OCT imaging system. Illustration of a custom spectral-domain Optical Coherence Tomography imaging system, PC: personal computer, SLD: superluminescent diode. Figure prepared by the Zhou lab: Dr. Chao Zhou, Dr. Yixuan Ming, Jinyun Zou, Guangming Ni.

2.2.4. Transmission electron microscopy

Transmission electron microscopy (TEM) is an imaging technique that uses electrons instead of light, to achieve very high-resolution images. A beam of electrons is directed at a thin sample slice and passes

through it and onto a detector. This detects ultrastructure boundaries in the thin sample slice, such as sarcomeres and gap junctions in cardiomyocytes. TEM sample preparation and imaging was conducted in collaboration with the Chatzistavrou Lab. Organoids were fixed in 4% PFA for 30 minutes followed by 3 washes in water, 10 minutes each. Post fixation sample preparation and subsequent imaging was conducted by Natalia Pajares from the Chatzistavrou Lab. Post fixation was performed in 1% osmium tetroxide in cacodylate buffer (pH 7.3) for 60 minutes at room temperature. Organoids were embedded in 2% agarose in water, solidified using ice, for manipulation. Then, a serial dilution of acetone was used for dehydration (25%, 50%, 75%, 90%, and 3 times in 100%) for 10 minutes each. Organoids were infiltrated with Spurr resin (Electron Microscopy Sciences) by immersion in 1:3, 2:2, and 3:1 solutions of resin in acetone, 3 hours each under agitation, following embedding in 100% resin for 24 hours, and polymerization at 60°C overnight. Ultra-thin sections (50–70 nm) were cut using RMC PTXL Leica Ultramicrotome and collected in carbon-coated copper grids 200 mesh. Before observation, all samples were positively stained in 2% uranyl acetate and 1% lead citrate for 6 and 3 minutes, respectively. The grids were examined at 100 keV using a JEOL 1400 Flash transmission electron microscope.

2.3. TRANSCRIPTOMICS

2.3.1. Bulk RNA-Sequencing

In order to track the developmental stages of the hHOs, RNA-Sequencing (RNA-Seq) was employed. This technique allows the analysis of the transcriptome of a given sample using next-generation sequencing, exploring which genes are being upregulated or downregulate and to what extent. By comparing different time points throughout the hHO protocol to day 0 embryoid body (pluripotent) controls, we can track developmental stages of the organoids through transcriptomic expression. RNA-Seq works by first extracting the RNA from a sample, conducting some quality control to ensure purity and quality RNA, followed by a reverse transcription into cDNA, known as a cDNA library, which is then fragmented. The next step, called adapter ligation, in which oligonucleotides with known sequences are added to each side of the cDNA fragment. These are then amplified, subsequently sequenced and aligned to a reference genome (Figure 6). The data can then be analyzed with a variety of bioinformatic tools, as described below. Often, clustering of genes is accomplished by k-means cluster analysis, in which a number of clusters is given (e.g., 15 clusters), and genes are sorted into the clusters based on how close they are to the mean

of the cluster. This results in groups of genes that are expressed similarly being assigned to the same cluster and reveals information about the transcriptomic activity of the sample. These clusters can be run through gene ontology tools to reveal the information about the cluster's molecular function, biological processes, associated diseases and more.

RNA was extracted at 11 different time points throughout the hHO fabrication and differentiation protocol. The time points are as follows: days 0, 1, 3, 5, 7, 9, 11, 13, 15, 17, and 19. At each time point, eight organoids were removed and stored in RNAlater (Qiagen) at -20°C until all samples were collected. RNA was extracted using the Qiagen RNEasy Mini Kit according to manufacturer instructions (Qiagen), and the amount of RNA was measured using a Qubit Fluorometer (Thermo). RNA samples were sent to the MSU Genomics Core, where the quality of the samples was tested using an Agilent 2100 Bioanalyzer followed by RNA sequencing using an Illumina HiSeq 4000 system. For RNA-Seq sample processing, a pipeline was created in Galaxy. Briefly, sample run quality was assessed with FASTQC, and alignment to hg38 was carried out using HISAT2. Counts were obtained using featureCounts and differential expression analysis was performed with EdgeR. Further downstream bioinformatic analysis was performed in Phantasus 1.11.0 (artyomovlab.wustl.edu/phantasus) and ToppGene Suite (http://toppgene.cchmc.org).

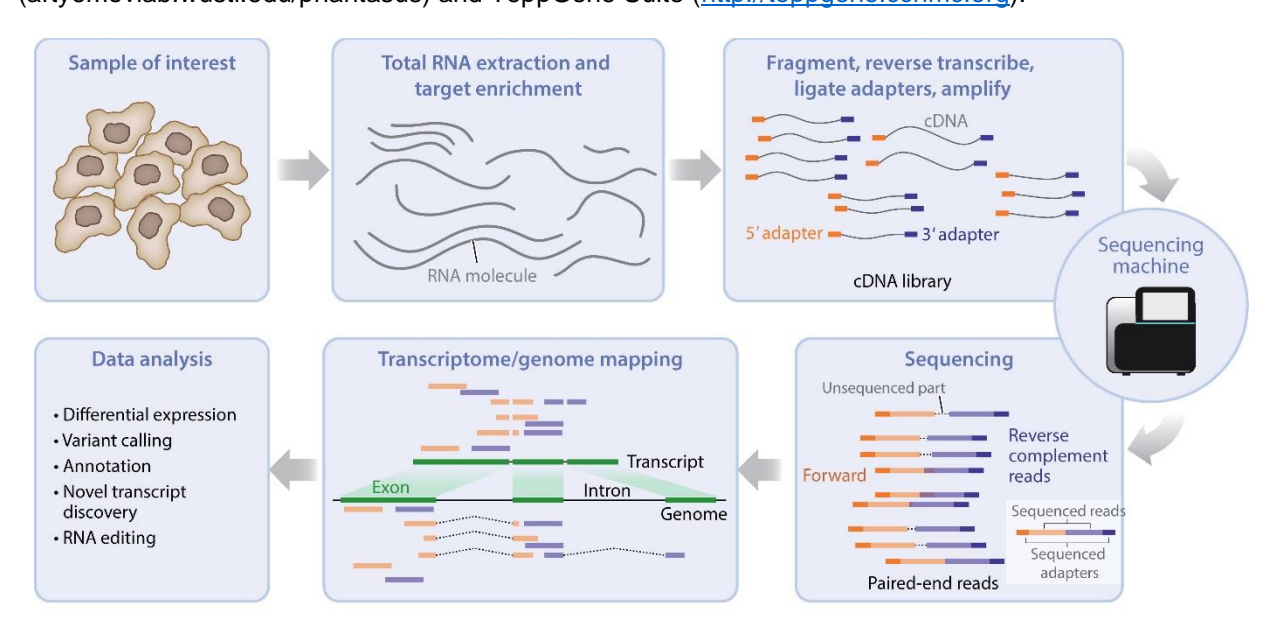


Figure 6. RNA-Seq workflow. The steps required to perform RNA-Seq, from RNA extraction, to reverse transcription, adapter ligation, amplification, sequencing, genome mapping and downstream analysis. Figure retrieved from Van de Berge et al., 2019¹³².

2.3.2. Gene expression analysis

Total RNA was extracted from 4 pooled organoids in at least 3 replicates for each condition/time point using the RNeasy Mini Kit (Qiagen). Organoids were lysed Eppendorf tubes. Once extracted, RNA was quantified using a NanoDrop (Mettler Toledo), with a concentration of at least 20 ng/μL being required to proceed with reverse transcription. cDNA was synthesized using the Quantitect Reverse Transcription Kit (Qiagen) and stored at -20°C for further use. Primers for qRT-PCR were designed using the Primer Quest tool (Integrated DNA Technologies) and SYBR Green (Qiagen) was used as the DNA intercalating dye. qRT-PCR plates were run using the QuantStudio 5 Real-Time PCR system (Applied Biosystems) with a total reaction volume of 20 μL. Expression levels of genes of interest were normalized to HPRT1 levels and fold change values were obtained using the 2-ΔΔCT method. At least three independent samples were run for each gene expression assay.

2.3.3. Organoid dissociation to single cell suspension

Organoids were dissociated at day 15 into single cell suspension using a modified protocol of the STEMdiff Cardiomyocyte Dissociation Kit (STEMCELL Technologies). 4 organoids from each condition were dissociated and pooled into the same tube to reach the desired cell concentration. Individual organoids were placed in separate Eppendorf tubes and washed once with PBS. The PBS was then removed, and the organoid is submerged in pre-warmed (37°C) dissociation media and placed on a thermoshaker at 37°C set to 300 RPM for 10 minutes. The supernatant was then collected and pipetted into a falcon tube containing RPMI+B27 with 1% BSA with the respective concentrations of glucose and insulin (see section 2.1.9). The organoid was then submerged in fresh pre-warmed (37°C) dissociation media, and placed on a thermoshaker at 37°C set to 300 RPM for 5 minutes. The supernatant was collected and pipetted to the same tube containing the RPMI+B27 with 1% BSA. The organoid was then resuspended in fresh, prewarmed dissociation media and pipetted up and down gently 3-4 times to induce further dissociation and placed on a thermoshaker at 37°C set to 300 RPM for 5 minutes. If the organoid is still visible, the process is repeated for 5 more minutes. If the organoid is no longer visible, it is pipetted up and down gently 3-4 times and the entire media is transferred to the tube containing the RPMI+B27 with 1% BSA. The dissociated organoids were then centrifuged for 5 minutes at 300 x g. The supernatant was aspirated, and the pellet is resuspended in 1 ml of RPMI+B27 with 1% BSA with the respective concentrations of glucose and insulin. The cells are run through a 40 µm cell strainer to remove remaining aggregates. Cell count, viability and percentage aggregates were retrieved using a hemocytometer.

2.3.4. Single cell RNA-Sequencing

Single cell RNA-sequencing (scRNA-Seq) allows the sequencing of individual cells within the organoid separately, thus producing data of specific cell types. This high-throughput transcriptional profiling allows us to identify cell population clusters within the organoid and compare target genes or group of genes on the single cell basis. In this process, the organoids are first dissociated into a single cell suspension and analyzed for viability and aggregation. The cells are then processed using a microfluidics and barcoded with gel beads before being lysed. The beads capture the mRNA molecules and through reverse transcription, cDNA libraries are created. The cDNA from each cell contains a unique molecular identifier (UMI) which have been tagged with a unique barcode. The cDNA is pooled, amplified and adapters are added as in RNA-Seq (see 2.3.1), to create the final library (**Figure 7**). The library is then sequenced and the data analyzed as described below.

Sequencing of the 10x Genomics Single Cell 3' Gene Expression library was prepared from the cells dissociated from four pooled organoids per condition. The libraries were prepared using the 10x Chromium Next GEM Single Cell 3' Kit, v3.1 and associated components. Quality control was performed on completed libraries and quantified using a combination of Qubit dsDNA HS, Agilent 4200 TapeStation HS DNA1000 and Invitrogen Collibri Library Quantification qPCR assays. The library was loaded onto an Illumina NextSeq 500 v1.5 Mid Output flow cell. Sequencing was performed in a custom paired end format: 28 bases for read 1 which captures the 10x cell barcode and Unique Molecular Identifier (UMI), and 90 bases for read 2 which is the RNA portion of the library fragment. Base calling was done by Illumina Real Time Analysis (RTA) v2.4.11 and output of RTA was demultiplexed and converted to FastQ format with Illumina Bcl2fastq v2.20.0. After demultiplexing and FastQ conversion, secondary analysis was performed using cellranger count (v6.0.0). Analysis was executed using 10X Loupe Browser 6 for k-means clustering and t-SNE visualization, Enrichr (https://maayanlab.cloud/Enrichr/) for gene ontologies and DiVenn 2.0 (https://divenn.tch.harvard.edu/) for differentially expressed genes analysis.

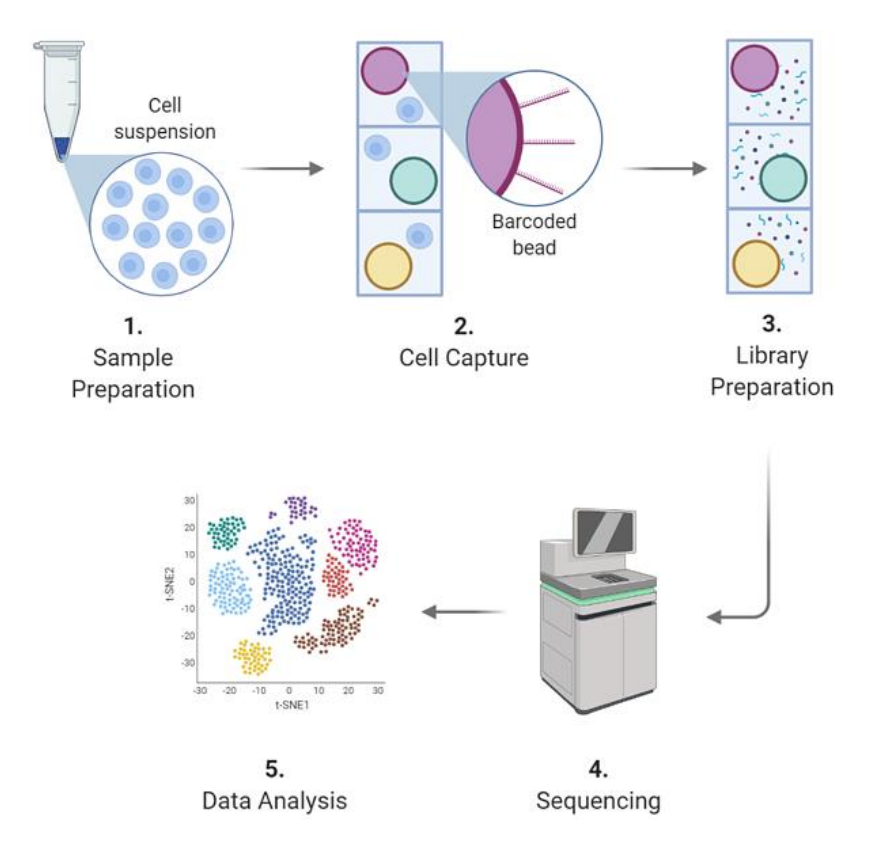


Figure 7. Single cell RNA-Seq workflow. scRNA-Seq includes a sample preparation step (1) in which cells are dissociated into a single cell suspension. The cells are then tagged with unique barcodes (2) before being lysed and used to generate a cDNA library (3). The libraries from all cells are pooled the sequenced (4). The data is then analyzed (5), where the transcriptomic data more each cell can be identified due to the barcode tag. Figure retrieved from https://web.azenta.com/how-single-cell-sequencing-works.

2.4. FUNCTIONAL ANALYSES

2.4.1. Measuring beating metrics

Organoids were video recorded under a light microscope (Olympus CKX53) at room temperature, within 10 minutes of removal from incubator at 37°C, 5% CO₂. Beating frequency was measured by counting the number of beats per minute observed for each organoid. Organoid plate was returned to the incubator for at least an hour between recording sessions to allow organoids to return to physiological conditions.

2.4.2. Electrophysiology

Electrophysiology recordings were conducted in collaboration with the Li Lab. Organoids electrophysiology recordings were measured in collaboration with Weiyang Yang (Li Lab) and data processing was conducted by Weiyang Yang. An in-house microelectrode array (MEA) system described previously¹³³ was used to record the electrical activity of individual organoids (**Figure 8**). The MEA was fabricated with the following

cleanroom procedures. First, 10 µm Parylene C was deposited on a cleaned 3-inch silicon wafer (PDS 2010, Specialty Coating System, Inc). Then, 500 nm Au was evaporated on the substrate. Next, a photoresist layer was spun on Au and photolithographically patterned the areas of 32-channel microelectrodes, interconnection wires, and contact pads. Finally, 2 µm Parylene C was deposited on the substrate as an insulating layer, and then Parylene C on the contact pads and microelectrodes were removed completely using oxygen plasma dry etching (RIE-1701 plasma system, Nordson March, Inc). Live organoids were placed on the MEA inside a PDMS well in culture media supplemented with 15 mM HEPES. The MEA was placed within a Faraday cage inside an incubator at 37°C at low humidity to avoid damage to the MEA system. Each organoid was recorded for a period of 30 minutes, and the PDMS well was washed with PBS between organoids. The recorded signals were amplified and digitalized using a commercial Intan RHD2132 system (Intan Technologies) and then recorded with Intan RHD2000 interface and analyzed using the Matlab Chronux toolbox to extract the electrocardiogram from the recordings.

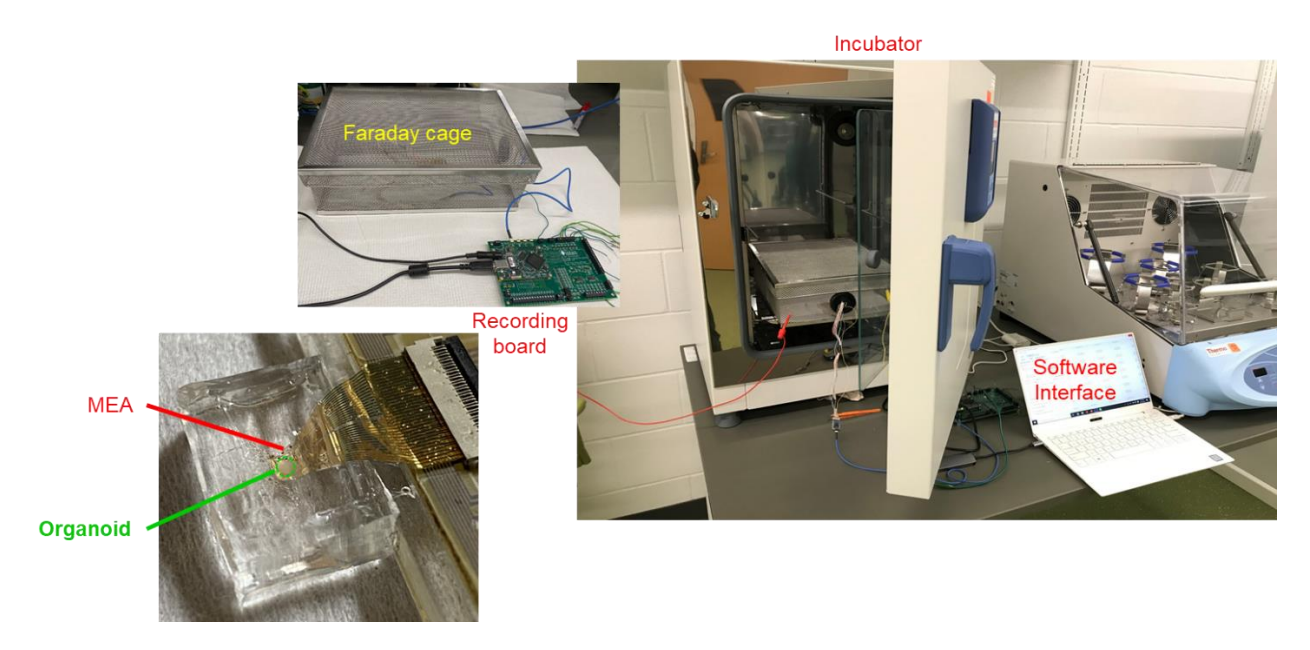


Figure 8. MEA recording system showing the gold electrode array in a PDMS chamber where the organoid is placed within a Faraday cage inside an incubator. This system facilitates the live recording of electrophysiological measurements of individual organoids at physiological temperature. MEA contraption was designed and built by the Li lab: Dr. Wen Li and Weiyang Yang.

2.4.3. Calcium imaging

Calcium transients were observed in heart organoids developed from iPSCs expressing the fast calcium indicator GCaMP6f^{127,128}. Dynamic fluorescence changes in the heart organoid were recorded at 10 frames

per second on an inverted fluorescence microscope (IX71, Olympus). Data analysis of fluorescence recordings was performed in MATLAB. 10 by 10 pixel binning was applied to the fluorescence recordings to minimize impact of contraction of heart organoids. Baseline F_0 of the fluorescence intensities F was calculated using asymmetric least squares smoothing¹³⁴. Fluorescence change $\Delta F/F_0$ was calculated by:

$$\frac{\Delta F}{F_0} = (F - F_0) / F_0 \tag{1}$$

2.5. METABOLIC ANALYSES

2.5.1. Seahorse metabolic analysis

A Seahorse analyzer (Agilent) was used to conduct glycolysis rate assay as per manufacturer instructions. The glycolytic rate was detected by measuring the basal extracellular acidification rate (ECAR) and then sequentially introducing rotenone/antimycin A (Rot/AA), which is an inhibitor of the mitochondrial electron transport chain, and then 2-deoxy-D-glucose (2-DG), which is a glucose analog. The Rot/AA inhibits the oxygen consumption rate in the mitochondria, and the 2-DG inhibits glycolysis by competing for glucose binding. This results in a decrease in proton efflux rate that confirms basal levels of glycolysis before the introduction of Rot/AA and 2-DG (**Figure 9**).

Organoids were carefully dissociated using STEMDiff cardiomyocyte dissociation kit and checked for viability using a hemocytometer before analysis. Only samples with over 90% viability were used in the assay. Identical numbers of cells were plated for the assay. Measurements were performed immediately after dissociation.

Seahorse XF Glycolytic Rate Assay Profile

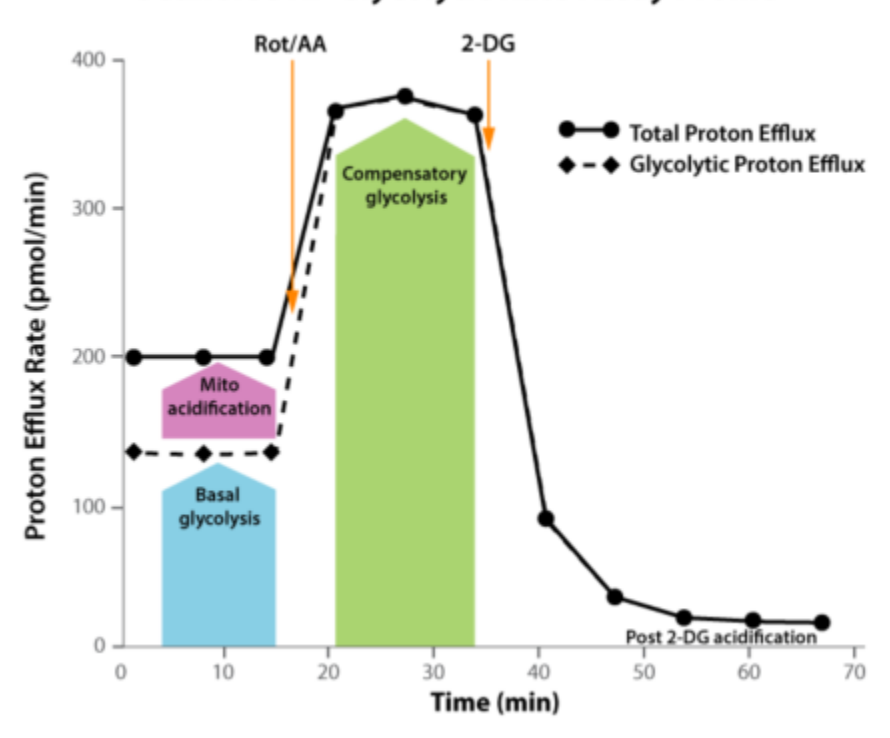


Figure 9. Seahorse glycolytic rate assay. The basal proton efflux rate is measured from live cells. Rot/AA is then introduced to inhibit mitochondrial oxygen consumption. 2-DG is followed to inhibit glycolysis, resulting in a decrease in the proton efflux rate. Figure retrieved from the Agilent Seahorse XF Glycolytic Rate Assay Kit User Guide.

2.5.2. Liquid chromatography–mass spectrometry

Liquid chromatography—mass spectrometry (LC-MS) was conducted in collaboration with the MSU Mass Spectrometer Core who performed sample extraction, LC gradient, mass spectrometry and data analysis. This two-part analytical technique combines the compound separation capability of LC with the mass analysis capability of MS. Samples were extracted (described below) and the sample solution was injected through a flowing stream (called the mobile phase) in a column filled with coated particles (usually silica) which are known as the stationary phase. The components of the sample interact with different coated particles depending on their chemical and physical properties, resulting in their separation as a result of strength of affinity to the column as the mobile phase passes through. The column eluent (the out-flow of the mobile phase) was then evaporated by heat and was vaporized and ionized so it can be detected by the mass spectrometer (MS). Using electric and magnetic fields, the MS detects mass-to-charge values for the different components of the sample.

Sample preparation: At day 15, 10 organoids per condition were placed in individual tubes without any media, and flash frozen in a -80°C freezer. The media from each organoid was centrifuged and the supernatants were placed in individual Eppendorf tubes and flash frozen in a -80°C freezer.

Sample extraction: Sample metabolite extraction and solid phase extraction (SPE) sample cleanup followed the methods outlined previously¹³⁵. 100 µL of media (thawed on ice) or individual organoid samples (on dry ice) were spiked with 5 ng of d8-arachidonic acid. To each organoid sample, 250 µL of -20°C chilled 75% ethanol was added, and samples were homogenized in a ThermoFisher bead mill for 2 minutes. Homogenates were transferred to 2.0 mL centrifuge tubes, and an additional 750 µL of -20°C chilled 75% ethanol was added. Samples were vortexed for 30 minutes, then incubated at -20°C for one hour to precipitate proteins. Samples were then centrifuged at 15,000 x g for 20 minutes. The supernatants were transferred to new 2.0 mL centrifuge tubes, and the remaining protein pellets were re-extracted and the supernatants pooled with those from the first extraction. Media samples were processed similarly using a 3:1 ratio of ethanol:media, with omission of the homogenization step. The pooled supernatants were diluted with 1.0 mL of HPLC water, and applied to preconditioned SPE columns (Phenomenex Strata-X polymeric reverse phase, 10 mg/1 mL, 33 µm) using vacuum assisted pull-through. The flow-through was discarded, and the SPE columns were washed with 900 µL of 10% methanol, then eluted with 400 µL of 100% ethanol. Samples were dried under vacuum in a speedvac centrifuge, reconstituted in 50 µL of acetonitrile by vortexing for 15 minutes, then transferred to LC-MS vials containing small volume inserts. Samples were stored at -80°C until analysis.

LC gradient: The LC-MS platform consisted of a Shimadzu Prominence HPLC coupled to a Thermo LTQ-Orbitrap Velos mass spectrometer. The LC system included two LC20AD pumps, a vacuum degassing system, autosampler, and column oven. The HPLC column was a Phenomenex 2.0 mmx150 mm Synergi HydroRP-C18 (4 μm, 80 Angstrom pore size) equipped with a guard cartridge of the same column chemistry. The LC gradient was adapted from previous work¹³⁵. Solvent A was 70:30 water:acetonitrile (v:v) containing 0.1% acetic acid. Solvent B was 50:50 isopropanol:acetonitrile containing 0.02% acetic acid. The flow rate was 200 μL per minute and the column oven was held at 45 degrees C. The autosampler was held at 4°C. 10 μL of each sample was injected. The gradient conditions used were:

Time 0–2 minutes, 1% solvent B. Column eluant was diverted to waste using a 2-position 6 port valve. At time=2 minutes, Solvent B was increased to 50%, and a linear gradient from 50% to 65% B was run between 2 and 10 minutes. Solvent B then increased linearly to 99% B between 10 and 16 minutes, and solvent B was held constant at 99% until 24 minutes. Solvent B was then returned to 1 to re-equilibrate the column for 5 minutes.

Mass spectrometry: Column eluent was introduced to a Thermo LTQ-Orbitrap Velos mass spectrometer via a heated electrospray ionization source. The mass spectrometer was operated in negative ion mode at 30,000 resolution with full scan MS data collected from 200–700 m/z. Data-dependent product ion spectra were collected on the four most abundant ions at 7,500 resolution using the FT analyzer. The electrospray ionization source was maintained at a spray voltage of 4.5 kV with sheath gas at 30 (arbitrary units), auxiliary gas at 10 (arbitrary units) and sweep gas at 2.0 (arbitrary units). The inlet of the mass spectrometer was held at 350°C, and the S-lens was set to 35%. The heated ESI source was maintained at 350°C.

Data analysis: Chromatographic alignment, isotope correction, peak identification and peak area calculations were performed using MAVEN software. Concentrations of each analyte were determined against the peak area of the internal standard (D8-arachidonic acid). Confirmed analytes were identified by comparison against authentic reference standards. Additional fatty acids (C24–C28) were identified by comparison against natural products as no reference standards are commercially available.

2.6. STATISTICS AND DATA AVAILABILITY

2.6.1. Statistics and reproducibility

All analyses were performed using GraphPad software and all raw data was collected in Microsoft Excel. All data presented a normal distribution. Statistical significance was evaluated with a standard unpaired Student t-test (2-tailed; P<0.05) when appropriate. For multiple-comparison analysis, 1-way ANOVA with the Tukey's or Dunnett's post-test correction was applied when appropriate (P<0.05). All data are presented as mean ± SD and represent a minimum of three independent experiments with at least three technical replicates unless otherwise stated. All micrograph images are representative of at least six independent experiments per condition/marker and calcium transient graphs are representative of six independent experiments. Critical parameters relating to the protocol as well as troubleshooting suggestions can be found in the appendix (**Table 6Table 8**).

2.6.2. Data availability

The organoid RNA-Sequencing data sets have been deposited in the National Center for Biotechnology Information Gene Expression Omnibus repository under accession code "GSE153185" ([https://www.ncbi.nlm.nih.gov/geo/query/acc.cgi?acc=GSE153185]. The RNA-Seq from monolayer differentiation method 2 and fetal heart data were obtained from the National Center for Biotechnology Information Gene Expression Omnibus repository under accession code "GSE1066901".

3. CHAPTER 3: AIM 1: ESTABLISHING A SELF-ASSEMBLING HUMAN HEART ORGANOID WITH MYOCARDIAL AND EPICARDIAL TISSUE

3.1. INTRODUCTION

3.1.1. 2D in vitro models

In recent years, hPSC-derived cardiomyocytes (CMs) have become critically useful tools to model aspects of heart development¹³⁷⁻¹³⁹, human genetic cardiac disease¹⁴⁰⁻¹⁴³, therapeutic screening^{144,145}, and cardiotoxicity testing^{146–149}. Several of these studies go further to fabricate heart muscle tissue in vitro to show cardiac maturation, 150,151 potential regeneration, 152,153 and modeling of cardiac muscle disorders^{150,151,154} such as hypertrophic cardiomyopathy. Although protocols for CM differentiation in different studies are not identical, several aspects seem to play an important role in the differentiation process. These include either the temporal inhibition of two key pathways of heart development, GSK3 and WNT pathways, or the manipulation of members of the transforming growth factor-β (TFG-β) family. While CMs make up a large portion of heart cell composition, they are far from the only cell type present and alone cannot accurately depict the heart. Other cells present in the heart have previously been differentiated from iPSCs, including fibroblasts, 155 endothelial cells, 156 smooth muscle cells, 157 and more recently, epicardial cells. 158 While CMs make up a significant portion of the human heart, in vitro studies using CMs alone cannot accurately depict its complexity¹⁵⁹. Furthermore, the use of 2D monolayer models come short of accurate representation of the intricate interactions of tissues in the physiological 3D environment¹⁶⁰. Reliable in vitro 3D human heart models are needed to mimic its development, function, structural organization, and the higher-order interactions between different heart tissues to study CHD etiology and progression.

3.1.2. Modeling the heart using organoid technology

Significant attempts have been made over the last decade to address the lack of relevant heart-on-a-chip or heart organoid models, particularly using tissue engineering techniques¹⁶¹. These approaches often rely on direct assembly of various heart cell types in a 3D construct by co-culture, cell layering, 3D bioprinting and the use of hydrogel molds which give the user high control over the structure of the end product. However, they frequently do not faithfully represent the original cell composition (e.g., use of dermal fibroblasts or HUVECs)^{161,162} and organization (e.g., cardiospheres¹⁶³) of the heart. These approaches yield

functional tissues but fall short in terms of physiological and structural relevance, as well as cell and ECM complexity. In more recent times, self-assembling organoid technologies have become available for the heart. These approaches are exploring the differentiation of PSC embryo-like aggregates in an attempt to recapitulate early cardiogenesis *in vitro*. Recently, mouse embryonic stem cells (mESCs) were used to create embryoid bodies that were differentiated into precardiac organoids with distinct heart field markers⁸⁰, cardiac crescent-like formation with foregut endoderm¹⁶⁴, and atrial and ventricular cardiomyocyte lineages¹⁶⁵. These studies provided us with a great deal of understanding and information of early heart development *in vitro* but are faced with limitations associated with mouse models. Hybrid cardiac-foregut organoids from human PSCs have also been reported very recently, with external heart layers and an internal endodermal core⁹¹, and cardioids (an alternative nomenclature for heart or cardiac organoids) with a large internal chamber and relevant cardiac cell lineages¹⁶⁶. Nevertheless, these studies rely on multiple protocols and co-culture techniques, and lack the formation of endothelial vasculature.

3.1.3. Advantages and limitations of current 3D heart models

The development of the heart is a complex process that utilizes the coordinated effort of a multitude of progenitor cells to give rise to a complex organ. Modeling such a process *in vitro* is a difficult feat, but in recent years, researchers have made significant advances on this front. Both direct and self-assembled cardiac organoids provide us with indispensable tools to study the process of human heart development and disease in extraordinary detail. Organoids created by direct assembly grant researchers extensive control over the composition and organization of the 3D tissue, allowing the exploration of specific functions and attributing the effects to their cells of interest. Studies using direct assembly have shown progress in cardiomyocyte tissue maturation strategies and have employed techniques such as mechanical and electrical stimulation. In contrast to direct assembly strategies, which have been around for well over a decade, the field of self-assembling cardiac organoids is still very much in its infancy but shows enormous promise. Much work remains to be performed, such as further refinement of developmental models and maturation of these organoids beyond the fetal stage to model adult conditions. Both approaches to creating heart organoids come with advantages and disadvantages (summarized in **Table 3**) and both are likely to remain the focus of future studies for some time. Organoids created by direct assembly are likely to lead the research in heart tissue constructs capable of withstanding high mechanical forces and have a head

start on targeting more adult heart tissues and are therefore more ideal for surgical intervention in the form of patches and replacement tissue. On the other hand, organoids created by self-assembly will likely take the lead in the study of developmental diseases and disorders and are more capable of physiologically representing the complexity of the human heart as a whole.

Overall, heart organoids open the window into a wide range of basic studies and translational applications. Organoids created by directly assembly have been used in functional screening, cryoinjury studies, response to COVID-19 infection, and modeling chemotherapy-induced cardiotoxicity and myocardial infarction. Organoids created by self-assembly have been used to investigate heart field progenitor cell markers, the effects of gene knockouts (e.g., *NKX2-5*), the response to isoproterenol compared to that observed *in vivo*, cryoinjury studies, and disease modeling (pregestational diabetes). Future steps will aim at improving developmental modeling by refining protocols and lengthening the viability of the organoids over time, as well as creating more mature heart organoids to closely resemble the adult heart, thus opening the field to a range of applications beyond fetal heart development and disease.

Table 3. Direct assembly vs. self-assembly: advantages and disadvantages

Direct Assembly		Self-Assembly	
Advantages	Disadvantages	Advantages	Disadvantages
 Precise control over cell composition Relative control over size and shape Can be comprise of more mature cells Pillars can be used for mechanical 	 Often only include cardiomyocytes or a small number of cell types Rely on physical structures for support Not as physiologically relevant to heart 	 Embryoid body differentiation more closely represents physiological heart development Multi-cellular composition High tissue complexity Can be used to model various stages of early heart 	Minimal control over cell type composition Minimal control over shape Comprised of immature (fetal-like) cells
stimulationScaffolding allows for stronger tissue construct	development and structureMiss out on early heart developmental stages	 development Self-organizing capabilities unhindered by physical restraints 	• Constructs are more feeble in nature

3.1.4. A self-assembling human heart organoid with myocardial and epicardial tissue

This chapter reports a methodology based on small molecules to manipulate the Wnt pathway and create complex self-assembling human heart organoids (hHOs) that closely resemble physiological development stages using hPSCs. Our protocol relies mainly on three sequential modulations of the Wnt pathway which include an activation followed by an inhibition and then a final activation step, at specific time points.

This protocol generates highly reproducible heart-like organoids resembling the structure and organization of the myocardium and epicardium in the developing human heart.

3.2. RESULTS

3.2.1. Myocardial differentiation optimization

Our method was designed to meet four initial milestones: 1) high organoid quality and reproducibility; 2) high-throughput/high-content format; 3) relative simplicity (no need for special equipment outside of traditional cell culture instrumentation); and 4) defined chemical conditions for maximum control and versatility for downstream applications. The first iteration of the protocol started by assembling hPSCs into EBs by centrifugation in ultra-low attachment 96-well plates followed by a 48-hour incubation at 37°C and 5% CO₂ prior to induction (Figure 10). This incubation allowed for spheroid stabilization and was important to increase efficiency, as other incubation times (12 hours, 24 hours) provided inferior results once differentiation started (data not shown). After induction, two-thirds of the spent medium was removed and replaced with fresh medium at each medium change, resulting in gradual transitions in exposure to the different signals employed and minimizing agitation of the organoids at the bottom of the well. Induction of mesoderm and cardiogenic mesoderm was achieved by sequential exposure to CHIR99021, a canonical Wnt pathway activator (via specific GSK3 inhibition), and Wnt-C59, a Wnt pathway inhibitor (via PORCN inhibition) (Figure 10), modifying previously described differentiation protocols 129,145,167. Brightfield and immunofluorescence imaging of hHOs showed a significant increase in size throughout the differentiation protocol (Figure 11). Confocal microscopy of hHOs stained with cardiomyocyte-specific TNNT2 antibody showed that organoids started to develop sarcomeres as early as day 7 (Figure 11), with clear sarcomere formation and fiber assembly readily apparent by Day 15 (Figure 12). Beating hHOs appeared as early as Day 6 of the differentiation protocol, with robust and regular beating appearing by Day 10 in all samples and lasting for at least 8 weeks in culture. Given the 3D nature of EBs and the increased tissue density compared to monolayers, determining the optimal conditions for initial Wnt activation, required exposing EBs to different concentrations of CHIR99021 (1 μM, 2 μM, 4 μM, 6.6 μM, and 8 μM) on Day 0 for 24 hours. On Day 15, hHOs were evaluated for cardiac lineage formation by confocal microscopy (Figure 13). Optimal cardiogenic mesoderm induction for all human embryonic stem cell (hESC) and induced pluripotent stem cell (hiPSC) lines tested occurred at lower CHIR99021 concentrations than previously reported for

optimal cardiomyocyte monolayer differentiation protocols, which typically range from 10 to 12 μ M CHIR99021^{129,137,145,167–171}. A 4 μ M CHIR99021 exposure resulted in the highest cardiomyocyte content with 64.9 \pm 5.3% TNNT2⁺ cells at Day 15 (**Figure 13Figure 14**). This difference is probably due to endogenous morphogen production and paracrine signaling within the developing hHOs, bestowed by the 3D environment and inherent self-assembling properties of the organoids^{172–176}. Moreover, the optimal CHIR99021 concentration compared with previous monolayer protocols are likely affected by the 3D nature and therefore higher tissue density of the hHOs. hHOs treated with 4 μ M CHIR99021 also displayed the best functional properties of the tested concentrations (**Figure 15**).

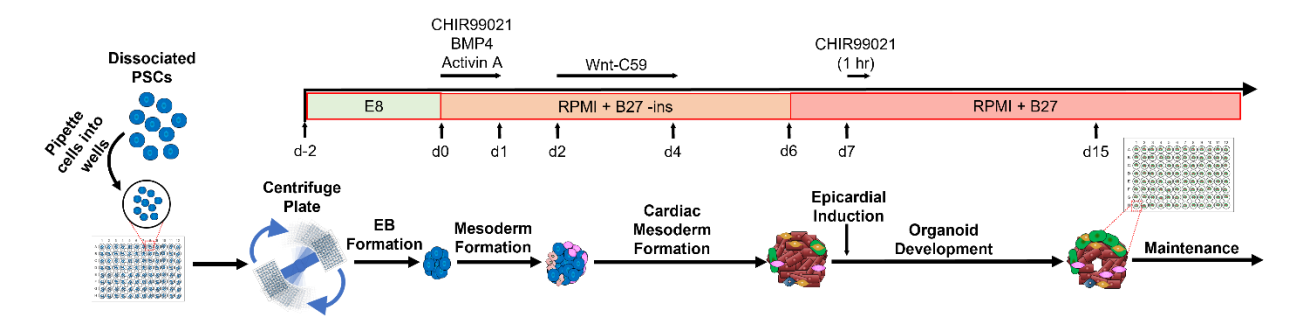


Figure 10. Organoid differentiation protocol. A schematic diagram depicting the protocol used to differentiate cardiac lineages in embryoid bodies. Various CHIR99021 concentration were tested at day 0 and day 7 in the optimization of this protocol. Organoids are cultured in round-bottom, ultra-low attachment 96 well plates, with a single organoid per well allowing for biological replicates. (Blue cells represent PSCs, red cells represent cardiomyocytes, all other colors represent non-myocyte cells).

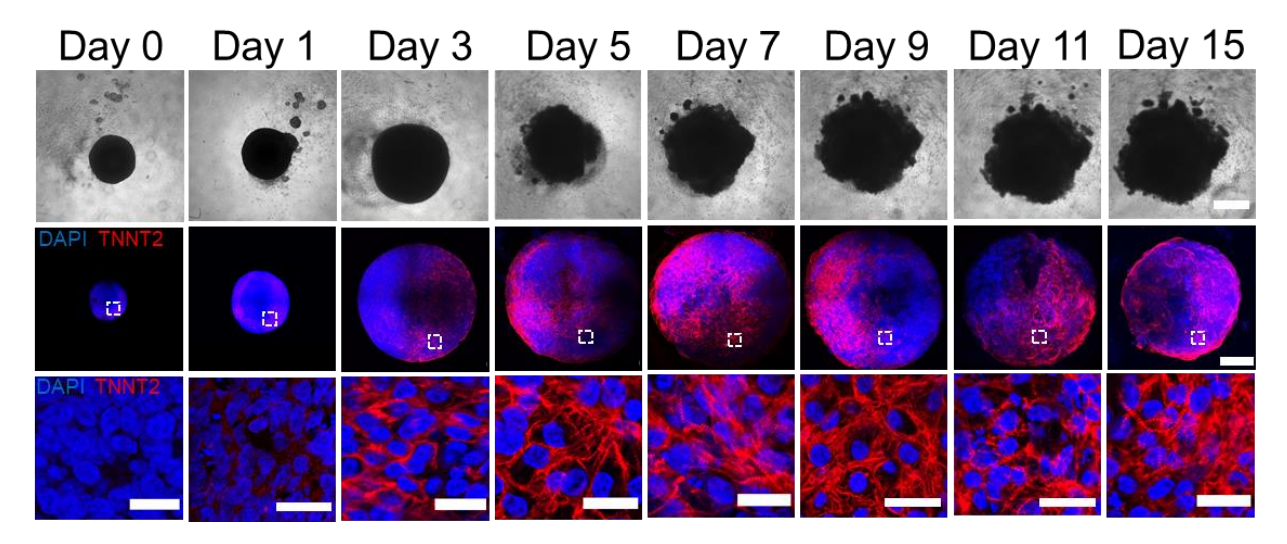


Figure 11. Microscopy images of developing organoids. **(Top)** brightfield images of developing organoid over 15 days of differentiation, **(center, bottom)** confocal immunofluorescence images for DAPI (blue), and TNNT2 (red), of representative organoids by day from day 0 to 15, showing the development of cardiomyocytes tissue; scale bar: 500µm, inset: 50µm (n=20).

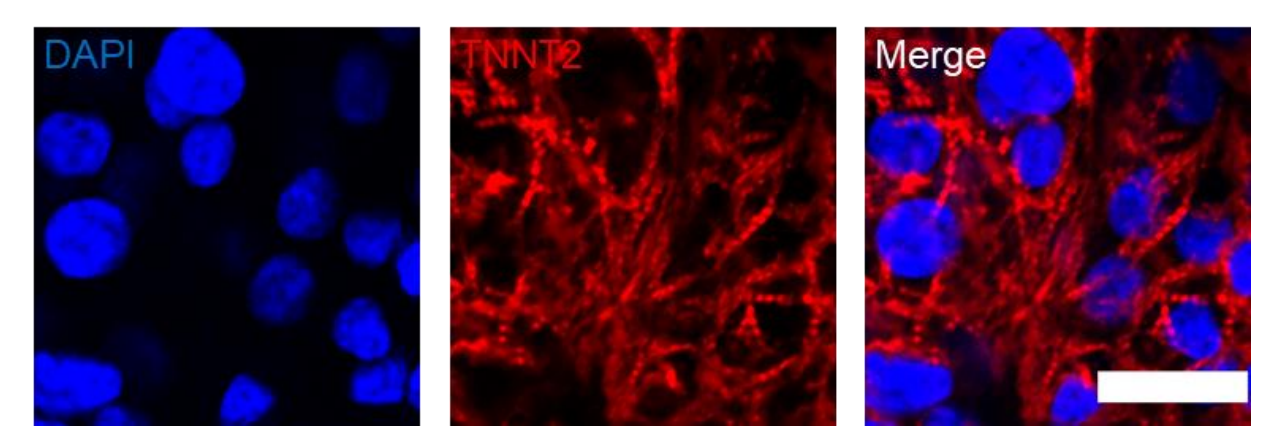


Figure 12. High magnification confocal immunofluorescence images for TNNT2 (red) and DAPI (blue), in day 15 organoids differentiated using 4 μ M CHIR99021 showing sarcomere bands in developed cardiomyocyte tissue; Scale bar: 25 μ m.

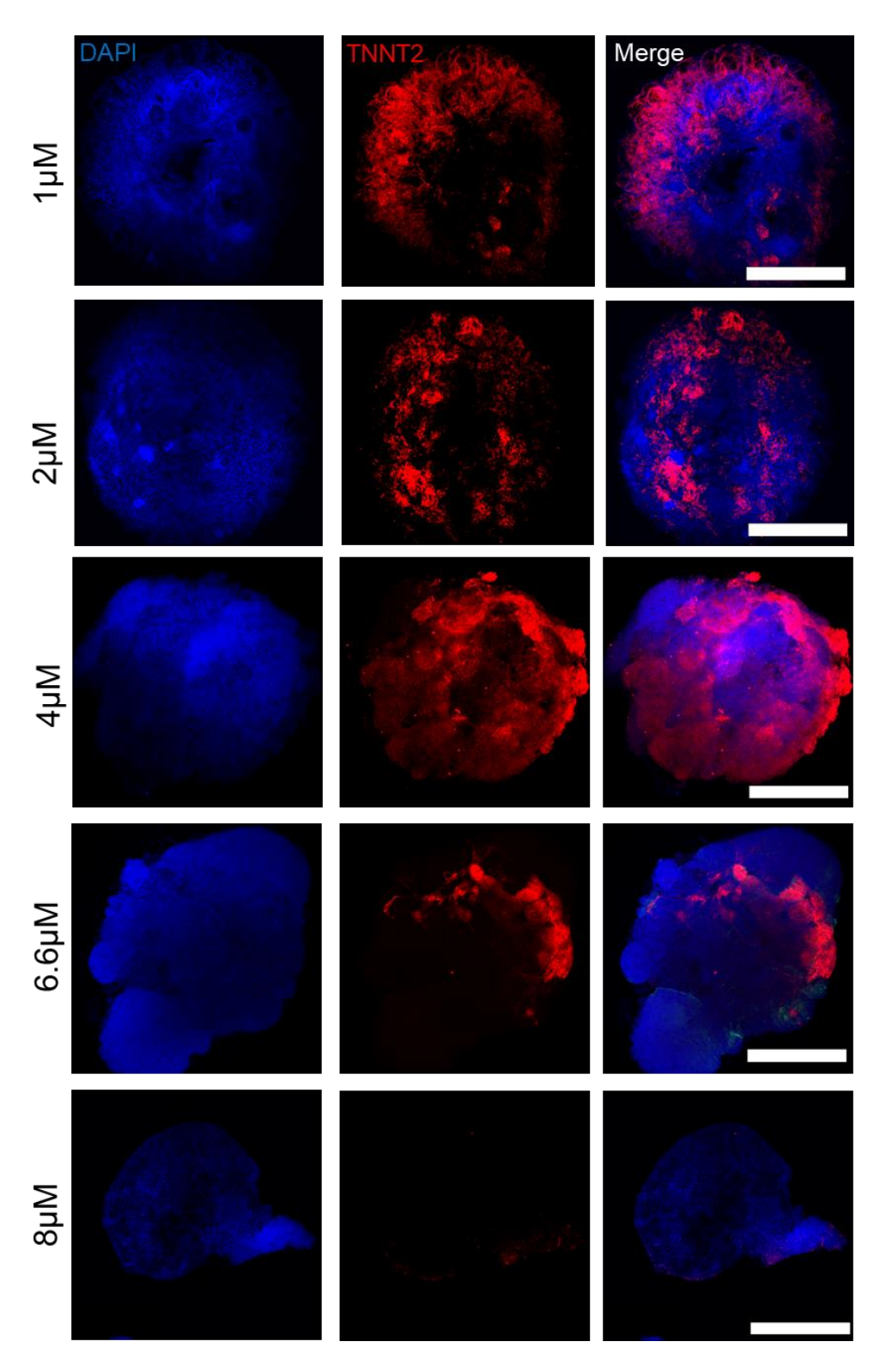


Figure 13. Confocal immunofluorescence images for TNNT2 (red) and DAPI (blue), in day 15 organoids with CHIR99021 exposure concentrations of 1, 2, 4, 6.6, and 8 μ M, at day 0, showing the effect of the small molecule at day 0 on the differentiation of cardiomyocytes in human stem cell derived heart organoids; scale bars, 500 μ m (n=12).

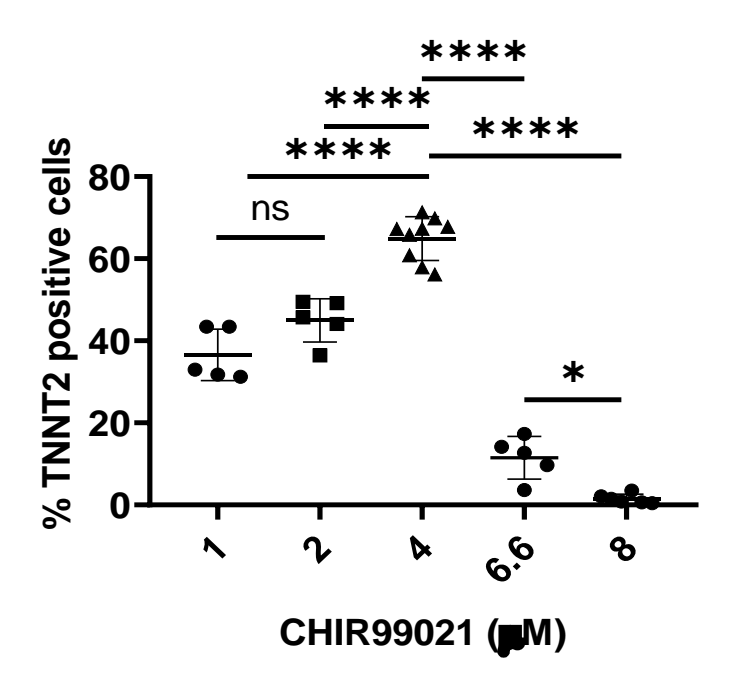


Figure 14. Cell quantification of cardiomyocytes within day 15 organoids taken at multiple z-planes as a percentage of TNNT2+ cells to total cells of each organoid for the five CHIR99021 concentrations at day 0 (n=5 organoids).

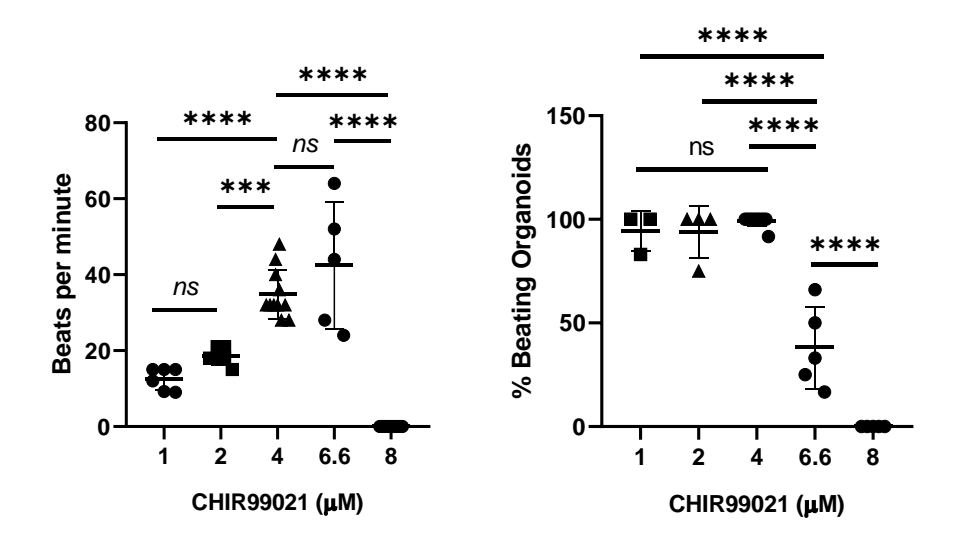


Figure 15. Beating frequency and reproducibility. (**left**) Quantification of beat frequency in hHOs (n=6) and (**right**) percentage of beating hHOs per treatment (1 μ M n=288 organoids, 2 μ M n=384 organoids, 4 μ M n=960, 6.6 and 8 μ M n=480 organoids). Value = mean \pm SD, 1-way ANOVA multiple comparison test; ***p=0.00.

3.2.2. Epicardial differentiation optimization

To increase organoid complexity and produce more developmentally relevant structures, a method to induce proepicardial organ specification was introduced into the protocol, based on a second Wnt activation step¹⁶⁷ on differentiation days 7–9. To determine if this second activation would prime our hHOs to increase complexity and better recapitulate heart development, the effects of a second CHIR99021 exposure on day 7 and continued culturing of the hHOs to day 15 for fixation and imaging (Figure 10), was explored. CHIR99021 was added to developing hHOs at varying concentrations (2, 4, 6, and 8 µM), and exposure duration (1, 2, 12, 24, and 48 hours). The efficiency of epicardial cell and cardiomyocyte formation was evaluated using confocal imaging and quantification for well-established epicardial (WT1, TJP1) and cardiomyocyte (TNNT2) markers at Day 15 (Figure 16Figure 20). It was found that the treatment robustly promoted the formation of proepicardium and epicardial cells (Figure 16Figure 18Figure 19), however, high concentrations or long exposure times inhibited the formation of cardiac cell types other than epicardial cells, particularly cardiomyocytes (Figure 17Figure 18Figure 20). It was further found that a single 2 µM CHIR99021 treatment for 1 hour on differentiation Day 7 produced the most physiologically relevant epicardial to myocardial ratio (60% cardiomyocytes, 10-20% epicardial cells) (Figure 16Figure 20). Structurally, a significant part of the epicardial tissue was found on external layers of the organoid and adjacent to well-defined myocardial tissue (TNNT2+) (Figure 16Figure 18Figure 19), thus recapitulating the structural organization found in the heart. The robust expression of TJP1 on epicardial cell membranes also confirmed the epithelial phenotype of these cells (Figure 19). Overall, the resulting hHO were mainly myocardial in origin, with epicardial clusters near the outer surface of the organoid (Figure 21).

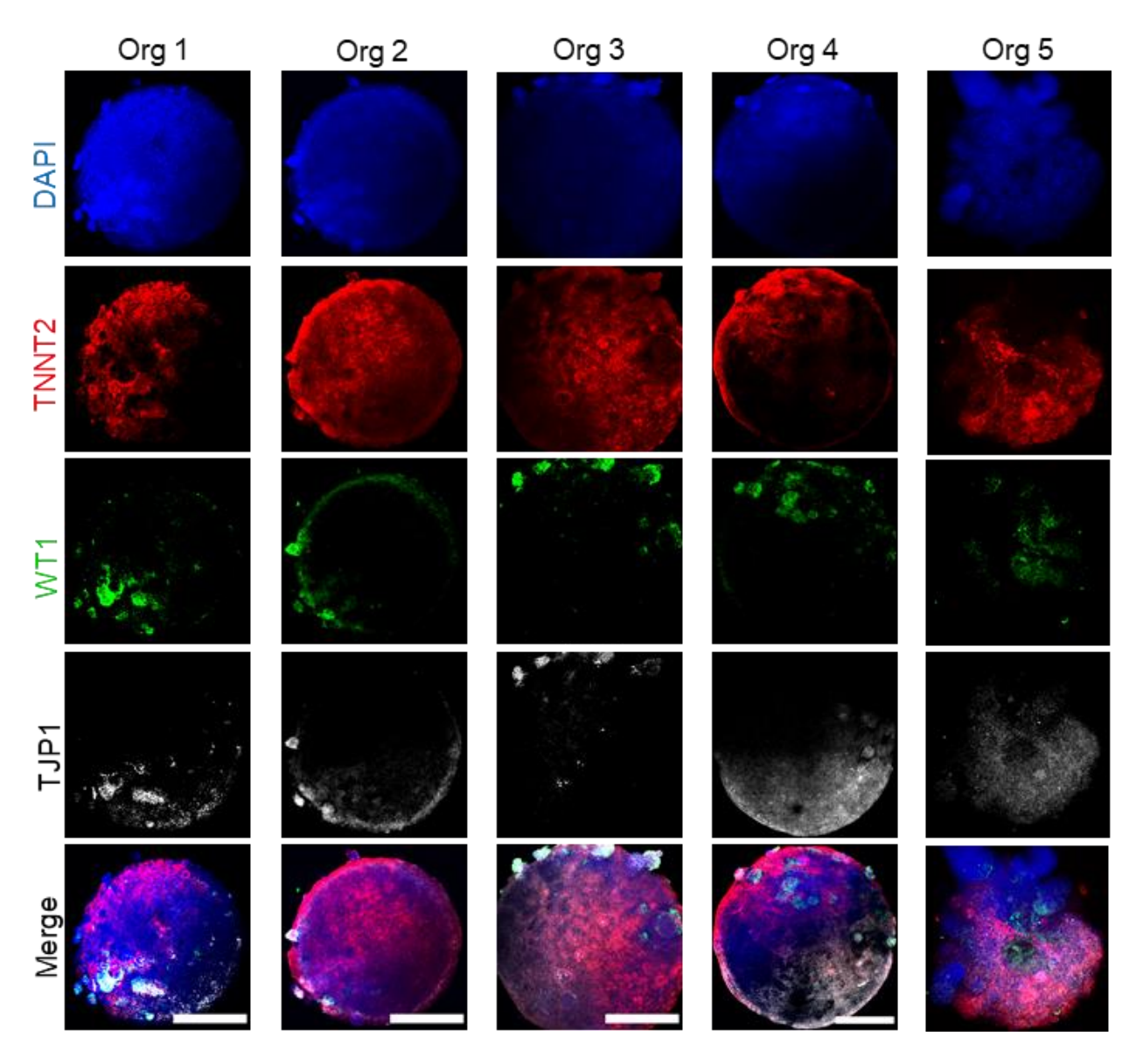


Figure 16. Confocal immunofluorescence images of hHOs at differentiation day 15 for DAPI (blue), epicardial marker WT1 (green), cardiomyocyte marker TNNT2 (red), and epithelial marker TJP1 (white) after day 7 epicardial induction with 2 μ M CHIR99021 (n=12 organoids), showing the formation of epithelial epicardial tissue in the organoids. Org = organoid.

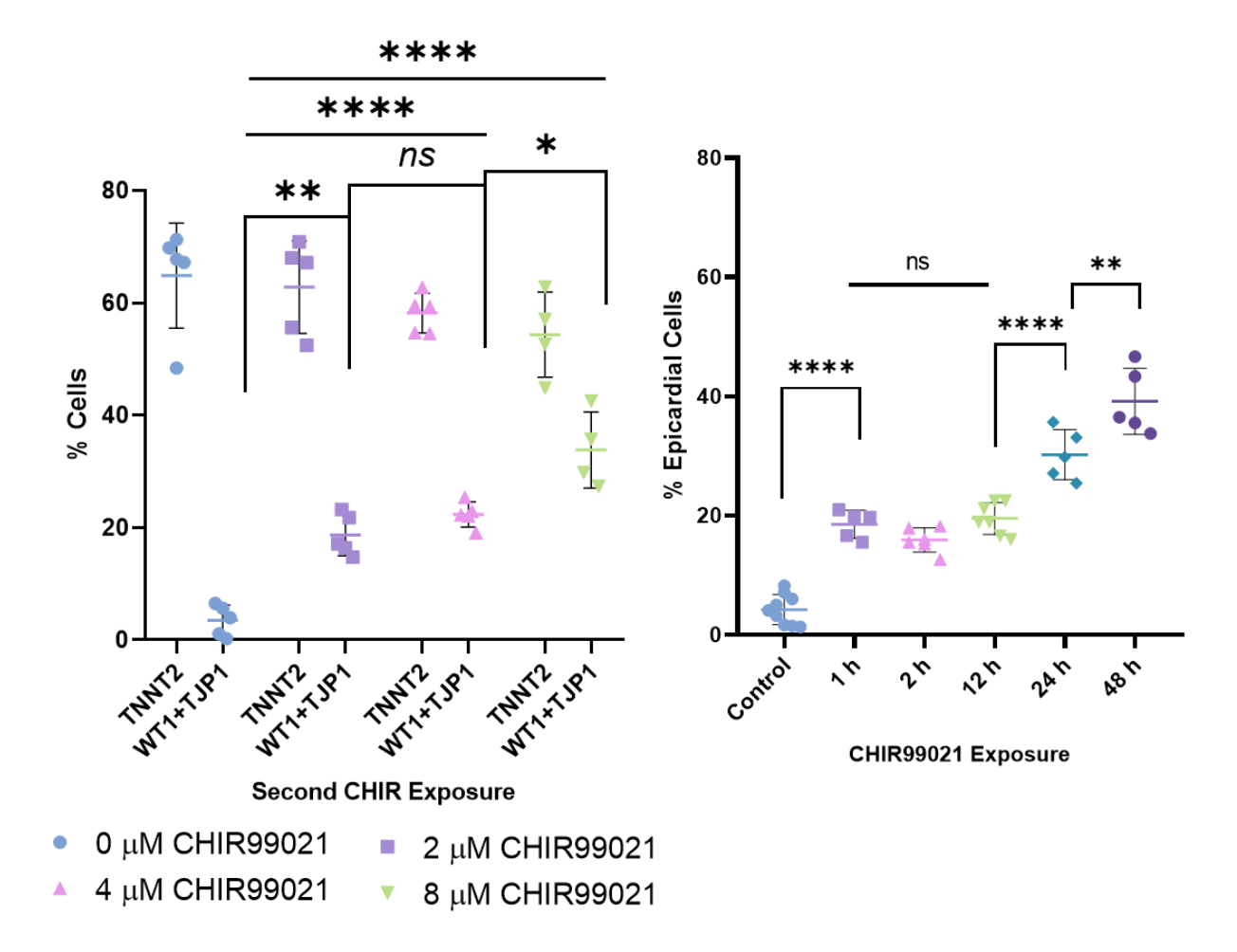


Figure 17. Epicardial differentiating optimization. (**left**) Cell quantification of cardiomyocyte (TNNT2+) and epicardial cells (WT1+ and TJP1+) within organoids taken at multiple z-planes as a percentage of total cells of each day 15 organoid (n=5 organoids). Value = mean \pm SD, 1 way ANOVA multiple comparison test; *p=0.04, **p=0.0023, ****p<0.0001, otherwise ns: no significance p=0.9. (**right**) Cell quantification analysis of epicardial cells (WT1+ and TJP1+) within organoids taken at multiple z-planes as a percentage of DAPI+ cells of each organoid treated with CHIR99021 at day 7 for different time durations (control n=9 organoids, 1, 24 and 48 hours n=5 organoids, 2 hours n=6 organoids, 12 hours n = 7 organoids); value = mean \pm SD, 1-way ANOVA multiple comparison test; **p=0.0018, ****p<0.0001, otherwise ns: no significance.

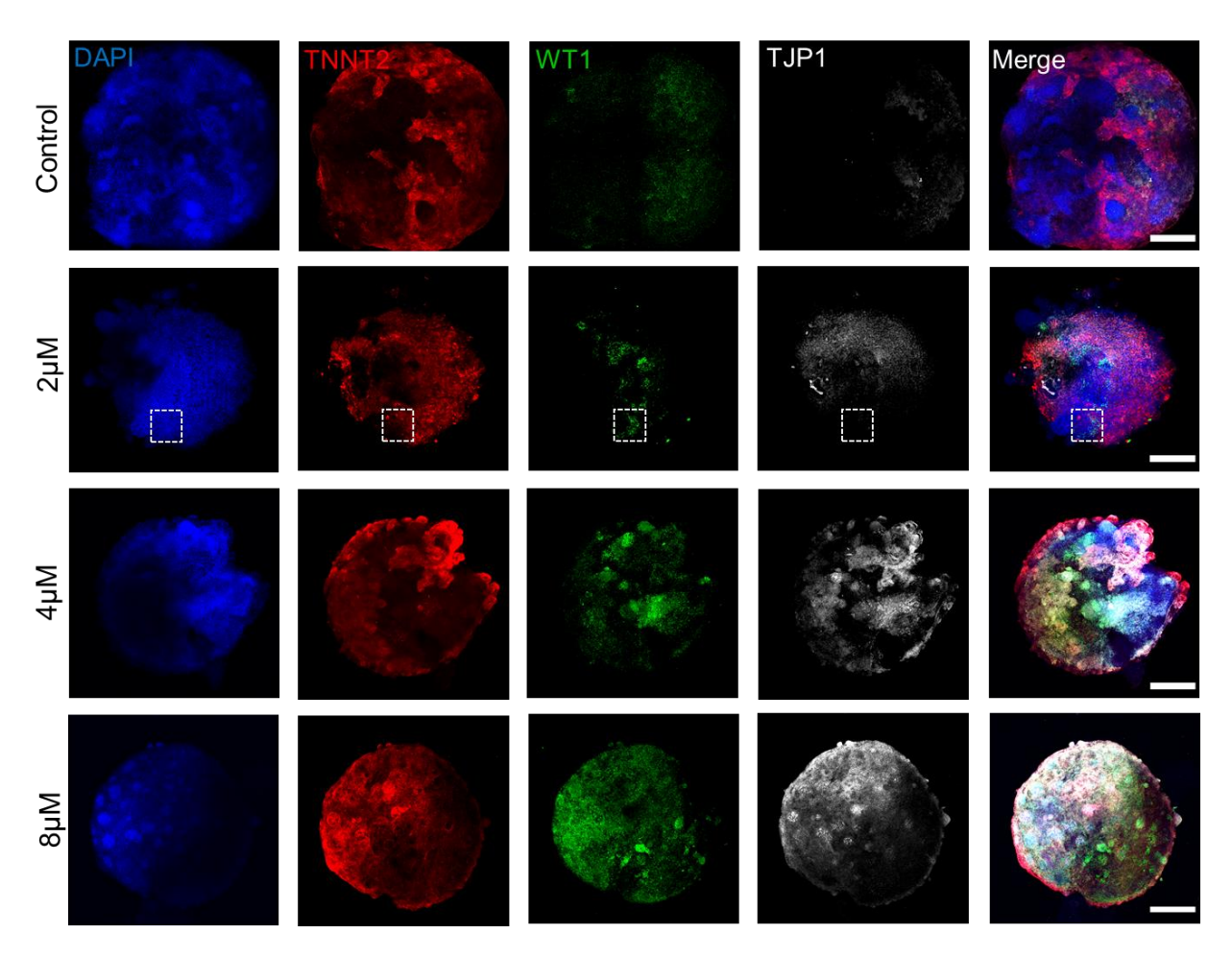


Figure 18. Epicardial optimization by CHIR99021 concentration. Confocal immunofluorescence images of hHOs at differentiation day 15 for DAPI (blue), WT1 (green), TNNT2 (red), and TJP1 (white), with variable concentrations of the second CHIR99021 exposure at day 7 vs. control with no second CHIR99021 exposure; scale bars: 500 μm. Dash-lined squares are shown in higher magnification in the following figure.

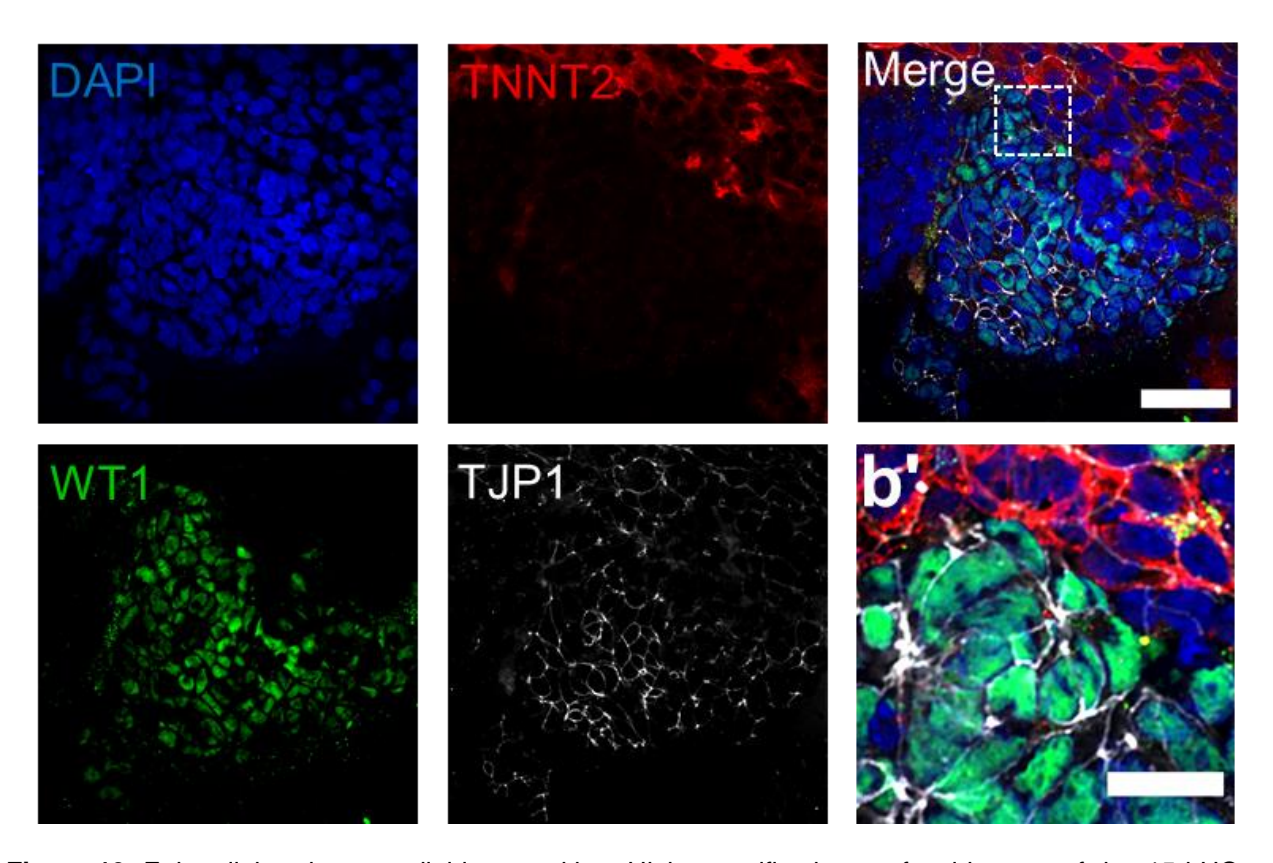


Figure 19. Epicardial and myocardial juxtaposition. High magnification confocal images of day 15 hHOs after 2 μ M second CHIR99021 exposure at day 7 showing, an adjacent region of TNNT2+ myocardial tissue and WT1+/TJP1+ epicardial tissue, showing the capacity of the organoids to facilitate the interaction between epicardial cells and cardiomyocytes; scale bar: 50 μ m.

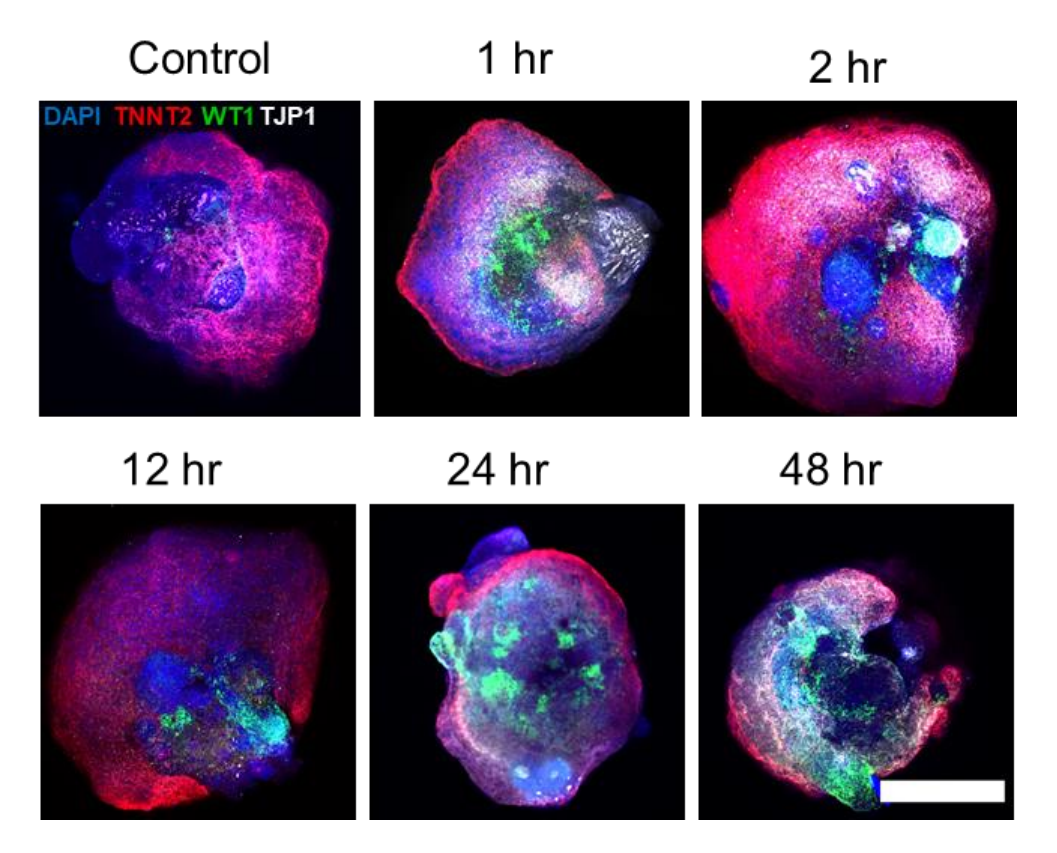


Figure 20. Epicardial optimization by CHIR99021 duration. Representative confocal immunofluorescence images of organoids from the time durations quantified in **Figure 17** (**right**); scale bar: 500 µm.

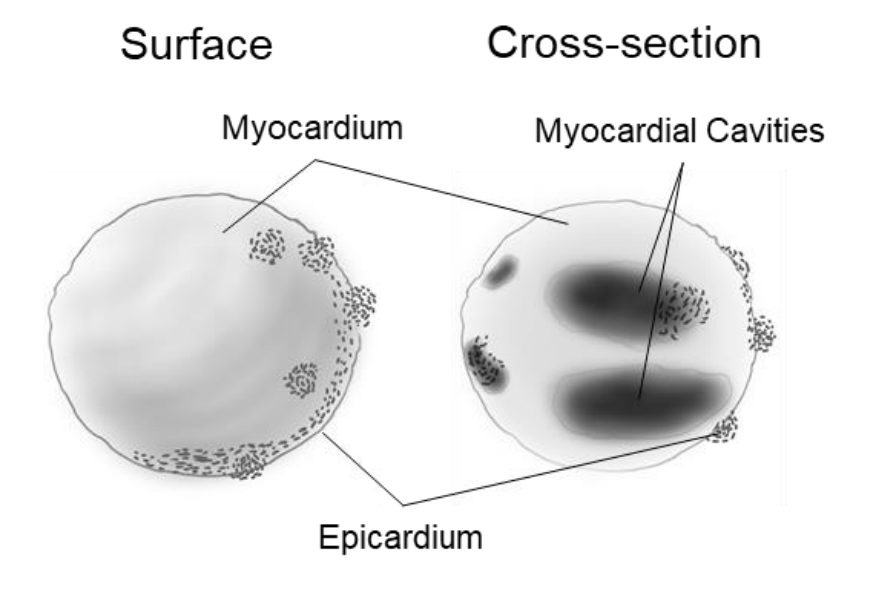


Figure 21. Sketch of hHO structure showing surface (**left**) and cross-section (**right**) features of the hHOs. Key features in the organoid noted at this stage were the myocardium body of the organoids, made up of cardiomyocytes, epicardial cluster formation near the outer surface of the organoids, and internal cavities that upon further investigation proved to have features of myocardial chambers (see Chapter 3).

3.2.3. Cell line reproducibility

Our initial hHO differentiation protocol was reproducible across multiple hPSC lines (iPSC-L1, AICS-37-TNNI1-mEGFP, iPSCORE_16_3, H9, iPSC GCaMP6f). hHOs derived from different hPSC lines exhibited similar differentiation efficiencies, beat metrics, growth rates, and sizes (Figure 22). iPSC line L1 was used for the majority of the experiments and is the line from which the organoids shown in previous figures are derived. The efficiency of this differentiation protocol was further verified using another hiPSC cell line (iPSC-AICS) as well as an iPSC line with a genetic mutation known to cause Danon Disease, a genetic disorder affecting the heart and the brain^{177,178}. Organoids were successfully generated from this diseased cell line (iPSCORE16), showing myocardial and epicardial markers (Figure 23). These organoids also appeared to develop morphological deformities compared to other cell lines, and may hint towards developmental disorders as a result of Danon Disease (Figure 23). Further studies into the use of these organoids to study Danon Disease and other genetic disorders may prove very valuable. Lastly, to confirm that the organoid derivation method works in embryonic stem cell (ESC) lines as well as iPSCs, the ubiquitous ESC line H9 was successfully used to generate healthy organoids with healthy beating frequency (Figure 22) similar to the iPSC lines discussed thus far. Organoids derived from iPSC line GCaMP6f are discussed in further detail in section 4.2.5.

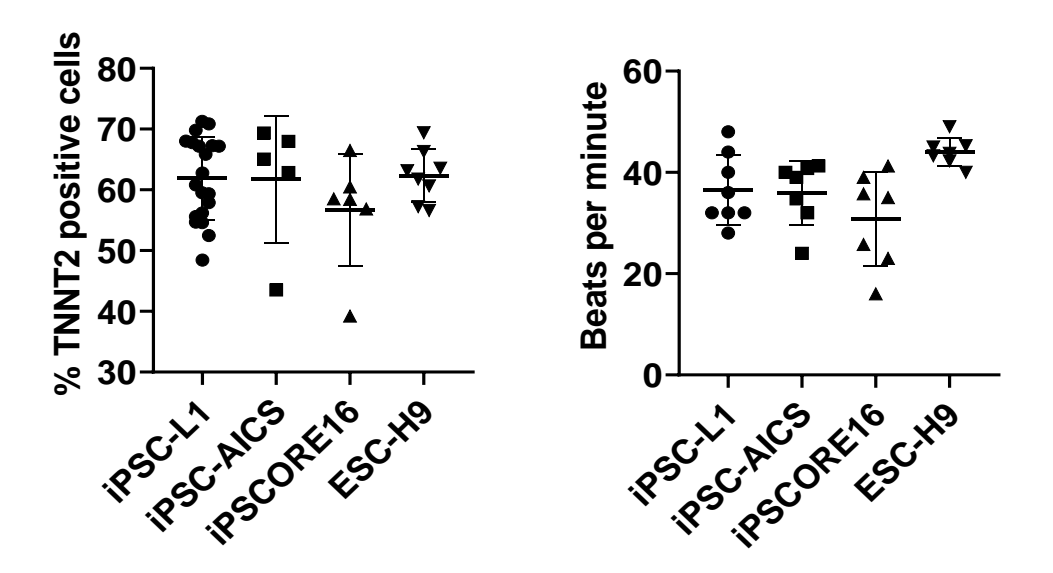


Figure 22. Protocol reproducibility across cell lines. (**left**) Percentage of TNNT2+ cells normalized to total cells in confocal images of hHOs (n=20 organoids), showing the reproducibility of cardiomyocyte formation and (**right**) beating frequency (n=7 organoids), in 3 iPSC lines and 1 ESC line. Value = mean ± SD.

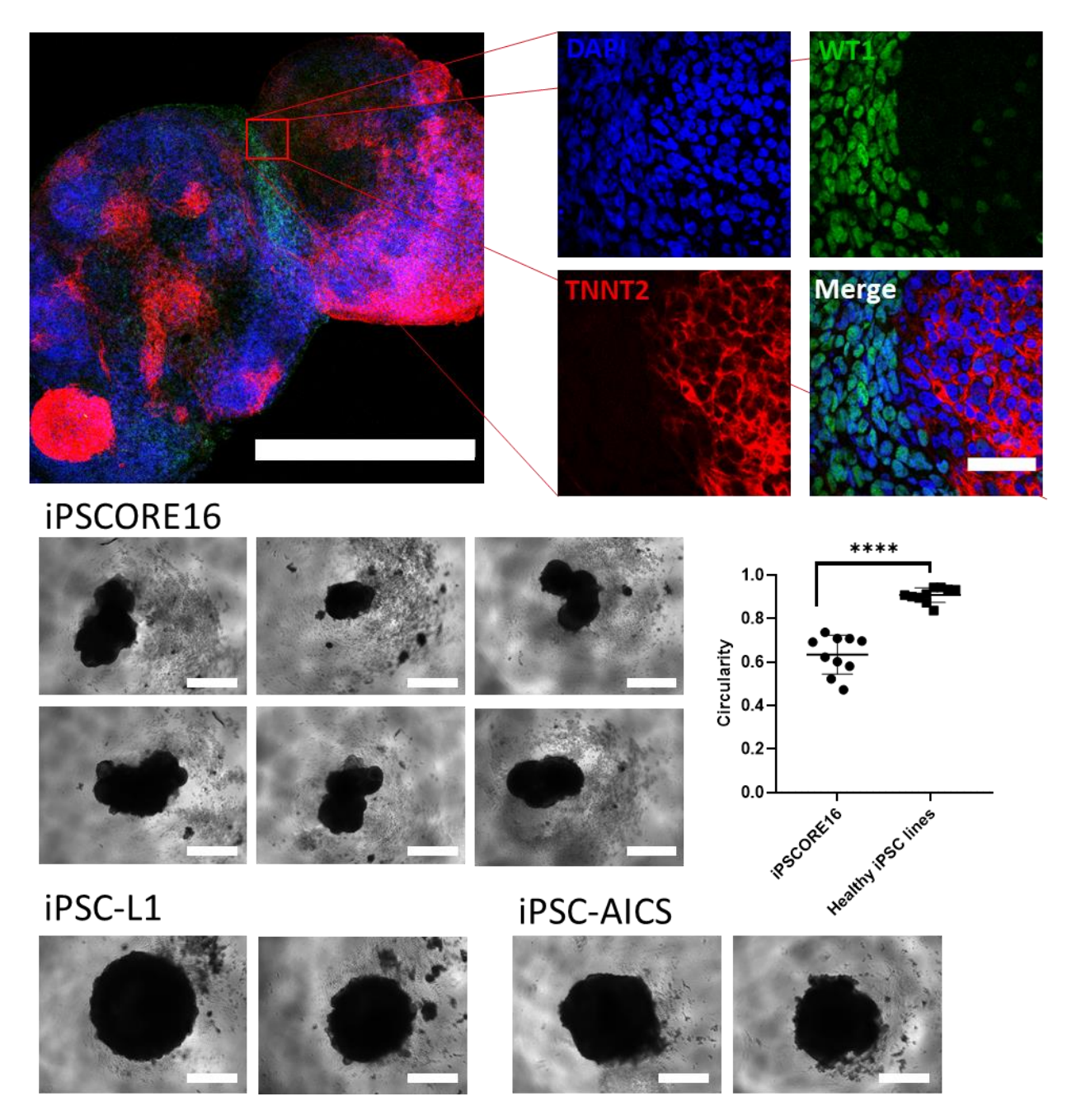


Figure 23. Organoids derived from iPSCORE16 with the genetic mutation for Danon Disease. **(top)** Immunofluorescence image of iPSCORE16-derived hHO showing CM and EC markers; DAPI (blue), WT1 (green), TNNT2 (red); scale bar: 500 μ m, inset: 50 μ m. **(bottom)** Deformed morphology of iPSCORE16 organoids shown by light microscopy and by measure of circularity compared with organoids derived from healthy iPSC cell lines. Value = mean \pm s.d, two-tailed, unpaired t-test, ****p<0.0001.

3.3. DISCUSSION

The study of human heart development is conducted using animal models and overly simplistic 2D cell models *in vitro* that are limited by cross-species differences and lack of physiological complexity, respectively. However, recent advances in stem cell bioengineering approaches have facilitated the

emergence of human stem cell-derived organoid model systems^{179–183}. Organoids are 3D tissue constructs that resemble the properties of an organ in structure or function¹⁸⁴. They are particularly useful in studying unapproachable disease states in humans, or for which animal models are not readily available^{185,186}. While organoids have been used to model a wide range of tissues (colon^{187–189}, pancreas^{121,180,190}, kidney^{42,182,191,192}) and conditions (cancer, host-microbe interactions)^{180,193}, their application to cardiovascular studies has been lacking.

There is an unmet need for human heart models to study disease development and provide a platform on which therapeutics can be tested and screened. Animal models do not meet the recapitulation capacity to mimic human-specific diseases and respond to human-specific drugs. Engineered heart tissue derived from human induced pluripotent stem cells (hiPSCs) provide a medium which human heart diseases can be modeled, studied, and treated. The differentiation of iPSCs to different cell types of the heart such as cardiomyocytes (CMs), cardiac fibroblasts, smooth muscle cells and epicardial cells, have been previously established 158,194,195. Furthermore, engineered heart tissue has been constructed from iPSCs to study various aspects of cardiac tissue including regeneration, developmental maturation, and disease modeling (see section 1.3.1). These models, however, need to be optimized to better match the properties and cell composition of the human heart during development

Previous attempts at generating 3D human cardiac tissues typically included cardiomyocytes and only one or two other cardiac cell lineages ^{196–198}. This aim sought to create a highly reproducible, scalable, and cost-effective differentiation protocol that yields physiologically relevant human heart organoids with high structural and multicell type complexity using hPSCs. The created and optimized protocol is comprised of multistep manipulation conditions for canonical WNT signaling using GSK3 and *PORCN* inhibitors in multiple PSC lines. These conditions lead to the formation of most cardiac tissue lineages in a self-assembling heart organoid with similar properties to the fetal heart. This method consistently yields cardiac organoids composed of approximately 60% cardiomyocytes and between 15-20% epicardial cells. Notably, hHOs were successfully derived from three independent iPSC lines and one ESC line, demonstrating reproducibility.

To increase the complexity of this system and inspired by a previous epicardial monolayer differentiation method¹⁶⁷, the protocol was modified and optimized for producing heart organoids with well-defined regions

of epicardial tissue adjacent to myocardial tissue. These epicardial-myocardial interactions are important in mammalian heart development and function, as epicardial cells increase cardiomyocyte growth in 3D engineered heart tissues, and co-transplantation of both cell types into rat hearts increases endothelial cell production¹⁹⁹. These organoids model human cardiac development to an unprecedented degree of detail, while also exhibiting high level of reproducibility as well as being amenable to high-throughput screening approaches. Our hHO protocol will facilitate the study and modeling of epicardial-myocardial interactions *in vitro*.

4. CHAPTER 4: AIM 2: MOLECULAR AND FUNCTIONAL CHARACTERIZATION OF ADVANCED HEART STRUCTURES IN HUMAN HEART ORGANOIDS

4.1. INTRODUCTION

4.1.1. Capturing complex heart features in vitro

Organoids have been implemented to model a wide range of different organs and disease conditions. However, the technology for their fabrication and application to cardiovascular studies has been lagging significantly when compared to other organoid types (e.g., brain, pancreas, kidney, intestine). This is a surprising fact since cardiovascular disease (CVD) and congenital heart disease (CHD) constitute the leading cause of mortality and morbidity in the developed world, and the most common birth defect in humans, respectively, and collectively constitute one of the largest unmet medical needs in the modern world. There is a critical need to establish *in vitro* models of the human heart that faithfully recapitulate its biology and function, thus enabling basic and translational studies to develop new therapeutics. Generating heart organoids that truly resemble the heart has proven difficult due to its complexity, but significant progress has been made recently to overcome this obstacle.

Significant attempts have been made over the last two decades to produce more complex, multicell-type 3D heart tissue *in vitro* using tissue engineering techniques. While these approaches allow for high control of the end construct, they tend to be expensive, work-intensive, and not readily scalable. Furthermore, they do not faithfully represent the original cell composition (e.g., use of dermal fibroblasts or HUVECs) and organization (e.g., cardiospheres) of the heart. These approaches yield functional tissues but fall short in terms of physiological and structural relevance, as well as cell and ECM complexity.

4.1.2. Self-assembly recapitulation

Self-assembling organoids are those where cell aggregates undergo differentiation and organization into an organ-like structure with minimal external intervention. They typically require stem cells (either PSCs or adult) with high differentiation potential and addition of specific developmental signals. Good examples of this category of organoids are brain organoids¹⁷, intestinal organoids²⁹, and kidney organoids³⁴ to name a few. Self-assembling heart organoid generation has only been reported from PSCs (either iPSCs or ESCs). Self-assembling heart organoids are expected to form cardiac cell lineages and acquire morphology and function of the heart without directed formation such as cell type co-culture, structural confinement, or

scaffold support. It is important to note that some "self-assembling" organoid protocols do include the addition of other cell types at a later stage of development, such as epicardial or epicardial progenitor cells in an effort to model developmental processes (such as the generation of the proepicardial organ during heart formation). The self-assembling technique described in this dissertation relies on a single, three-step protocol without the need for the addition of other cell types, to generate the complex fetal-like heart features. This chapter focuses on the self-assembly capabilities of the heart organoids, demonstrating their organization, cardiac cell type complexity, ECM composition, vascular formation, and functionality.

4.2. RESULTS

4.2.1. Transcriptomic analysis

To characterize the developmental steps and molecular identity of the cellular populations present in hHOs, RNA-Sequencing (RNA-Seq) transcriptomic analysis was performed throughout hHO formation. hHOs were collected for RNA-Seq at different time points (day 0 through day 19) of differentiation (Figure 24). Unsupervised K-means clustering analysis revealed organoids progressed through three main developmental stages: day 0-day 1, associated with pluripotency and early mesoderm commitment; day 3-day 7, associated with early cardiac development; and day 9-day 19, associated with fetal heart maturation (Figure 24Figure 32). Gene ontology biological process analysis identified important genetic circuitry driving cardiovascular development and heart formation (Figure 24). To compare cardiac development in hHOs to that of previously existing methods, RNA-Seq was performed on monolayer iPSCderived cardiac differentiating cells using previously established protocols³. Furthermore, the RNA-Seq results were compared to publicly available datasets from previously reported monolayer cardiac differentiation protocols and human fetal heart tissue (gestational age days 57-67)¹³⁶. In all instances, hHO cardiac development transcription factor expression regulating first and second heart field specification (FHF, SHF, respectively) was similar to that observed in monolayer PSC-derived cardiac differentiation and corresponded well to that observed in fetal heart tissue (Figure 25). Gene expression profiles showed hHOs had higher cardiac cell lineage complexity than cells that underwent monolayer differentiation, especially in the epicardial, endothelial, endocardial, and cardiac fibroblast populations (Figure 26Figure 27). These data suggest a significant enrichment in the structural and cellular complexity of our hHOs, thus bringing them in line with fetal hearts and further away from monolayer-based differentiation. This was

confirmed by extending our gene expression analysis to look at several widespread critical gene clusters involved in classic cardiac function, including conductance, contractile function, calcium handling, and cardiac metabolism, among others (Figure 28). Of special interest, expression of heart-specific extracellular matrix genes was high in hHOs and fetal hearts but completely absent in monolayer differentiation protocols (Figure 28, Figure 29). Markers for pluripotency were not found in hHOs beyond day 1 (Figure 30). Principal component analysis showed a clear progression in development in the hHOs from day 0 to 19 (Figure 31). Taken together, these data suggest that hHO expression profiles are similar to those of fetal hearts, and their global transcriptomes are closer to those of fetal hearts than monolayer protocols, as determined by hierarchical clustering (Figure 28). Lastly, the time-course RNA sequencing analysis supports the involvement of endogenous morphogen production discussed in section 3.2.1 as it revealed the morphogens and their respective receptors expressed in our organoids between day 0 and 19 of differentiation (Figure 32).

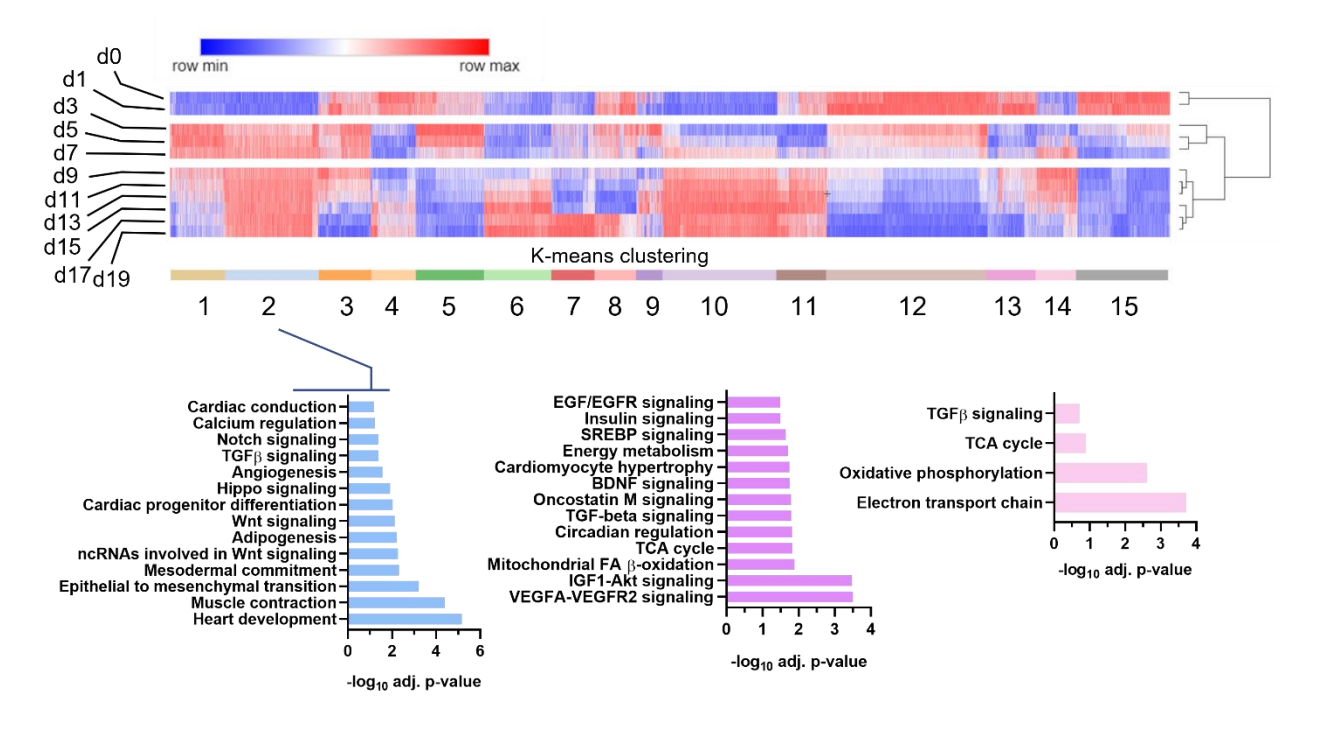


Figure 24. K-means cluster analysis of heart organoid transcriptomes by RNA-Seq. Clusters strongly associated with fetal heart development (e.g., 2, 10, and 14) appear from day 9 onwards. Pathway enrichment analysis is provided below for representative cardiac-specific clusters.

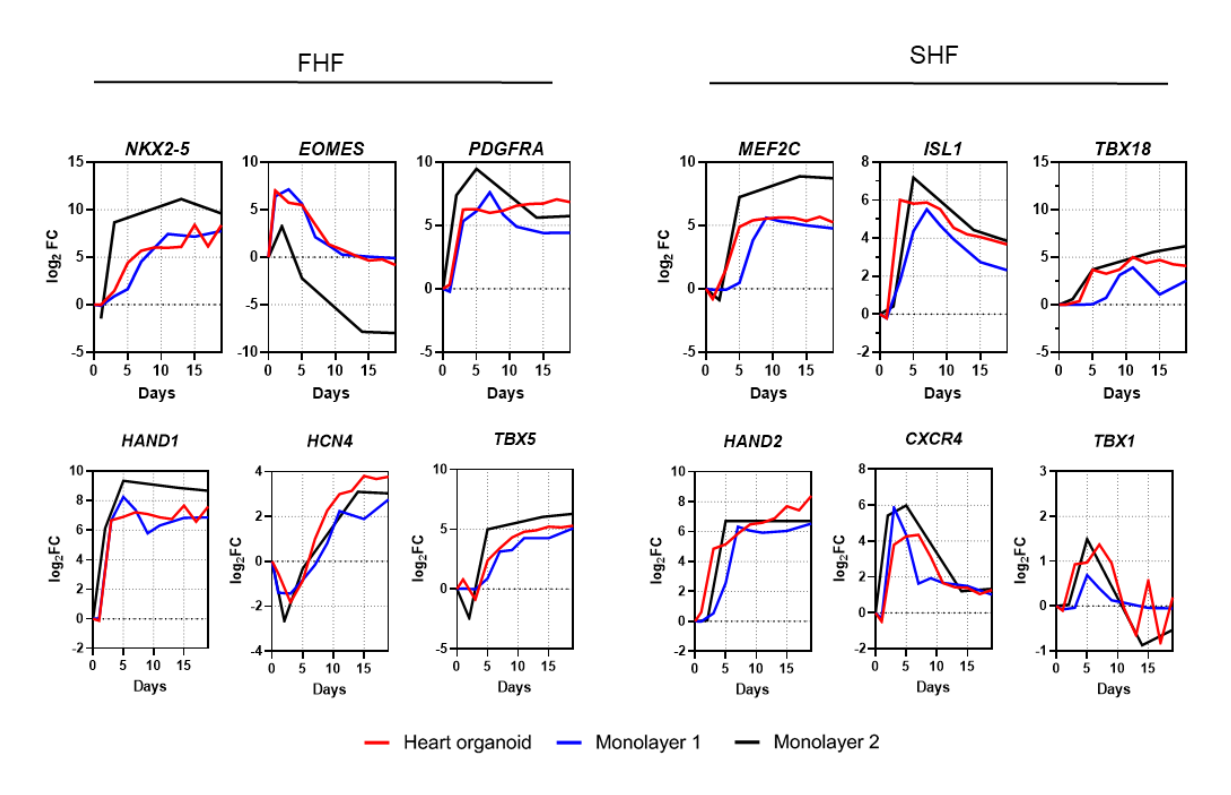


Figure 25. Heart field gene expression analysis from bulk RNA-Seq (log2 fold-change vs. day 0) of first and second heart field markers over heart organoid differentiation process (FHF, SHF respectively), showing that organoids can follow the developmental stages in a similar manner to monolayer cardiomyocytes differentiation protocols.

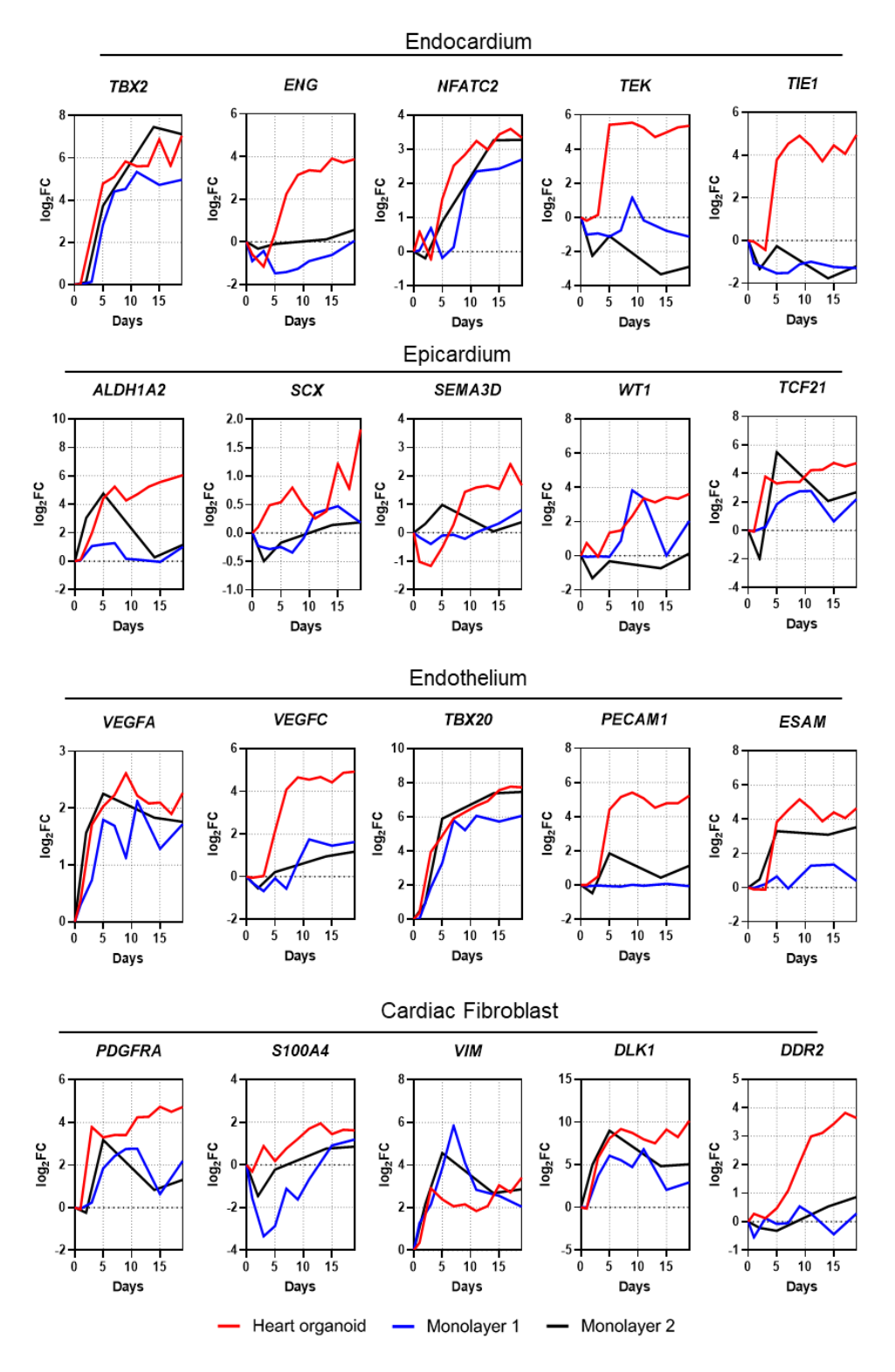


Figure 26. Cell specific gene expression analysis from bulk RNA-Seq (log2 fold-change vs. day 0) for cardiac cell type populations in heart organoids, including epicardial cells, fibroblasts, endocardial cells, and endothelium, showing the capacity of organoids to give rise to cardiac cell types that were not directly induced and that are not present in monolayer differentiation.

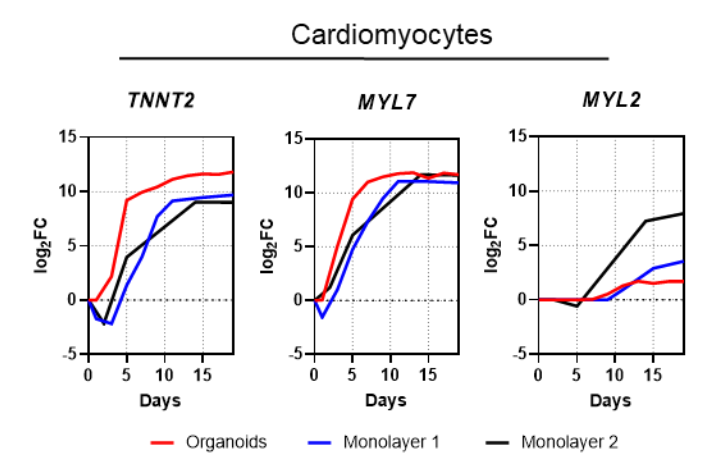


Figure 27. Cardiomyocyte gene expression analysis from bulk RNA-Seq (log2 fold-change vs. day 0) for cardiomyocyte markers in organoids, and 2 separate cardiomyocyte monolayer differentiation protocols.

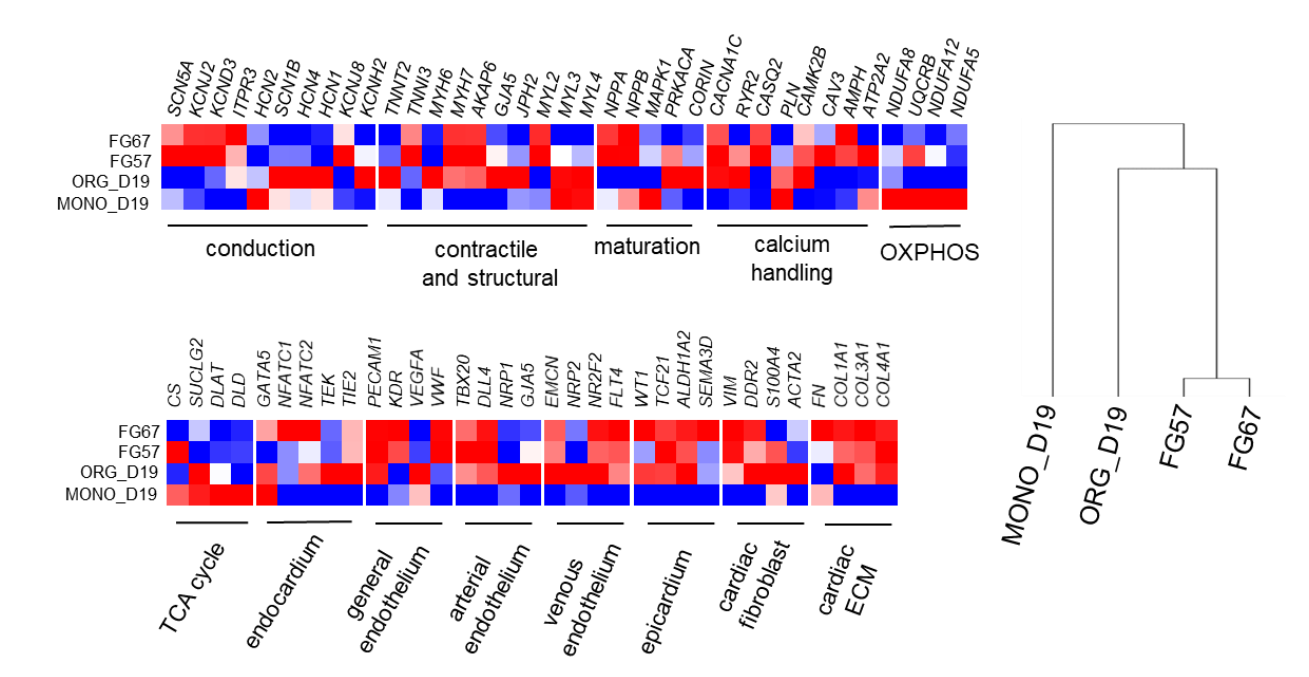


Figure 28. Heatmap of key genes comparing organoids, monolayers and fetal tissue. (**left**) Normalized comparison of key genes involved in cardiac function across heart organoids, monolayer differentiation methods, and fetal hearts at gestational day 57–67¹³⁶, from bulk RNA-Seq data. (**right**) Hierarchical clustering analysis of heart organoids, monolayer differentiation, and fetal hearts. FG57/67, showing that organoids more closely resemble fetal heart tissue compared with cardiomyocyte monolayers: fetal gestation day 57/67, FHF: first heart field, MONO_D19: monolayer cardiomyocytes at day 19 of differentiation, ORG_D19: human heart organoids at day 19 of differentiation, OXPHOS: oxidative phosphorylation. Heatmap colors are relative intensity representing gene expression.

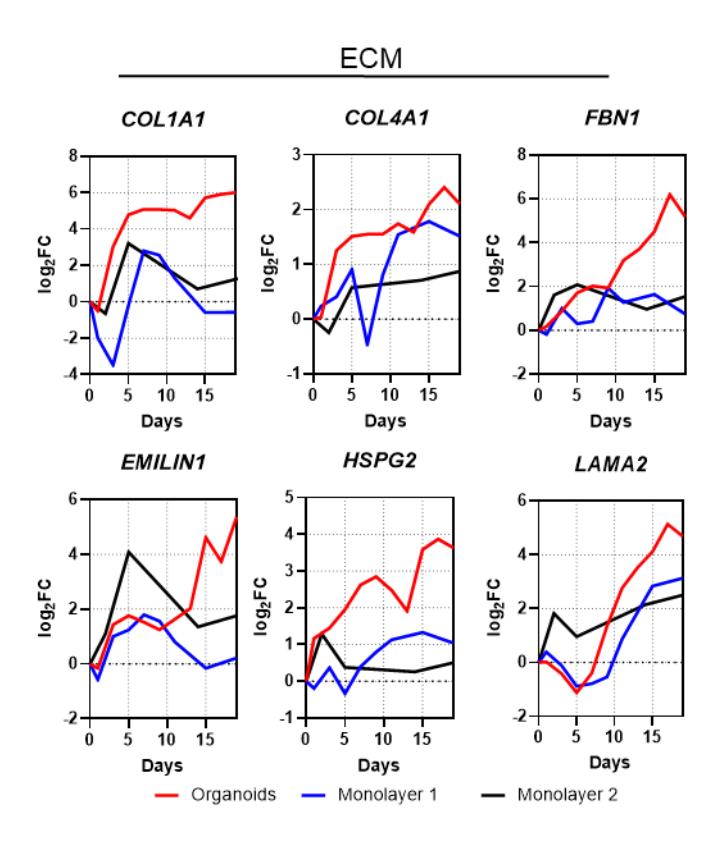


Figure 29. ECM gene expression analysis from bulk RNA-Seq (log2 fold-change vs. D0) for ECM protein-coding genes that are present in cardiac tissue, showing that organoids are better at giving rise to ECM proteins compared to monolayer cardiomyocytes. ECM: extracellular matrix.

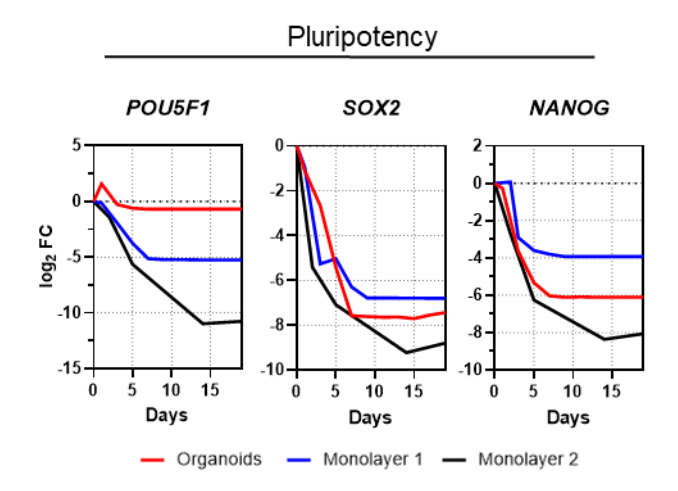


Figure 30. Pluripotency gene expression analysis from Bulk RNA-Seq (log2 fold-change vs. D0) for pluripotency markers, indicating that the cells are committed and have moved away from pluripotency.

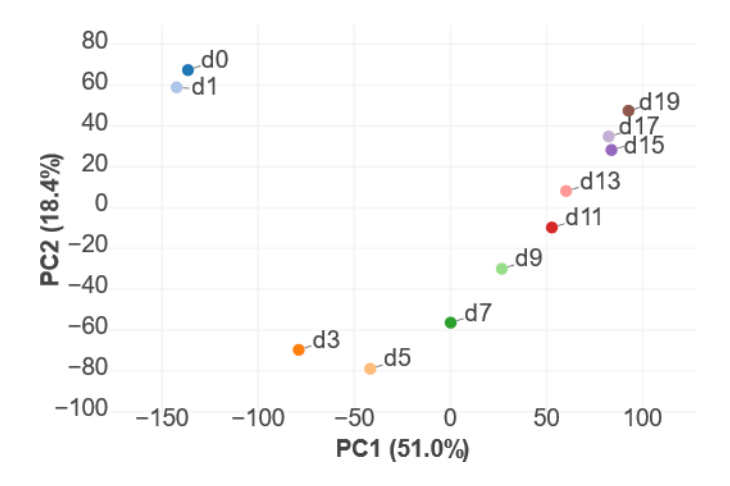


Figure 31. Principal component (PC) analysis of heart organoid differentiation over time from bulk RNA-Sequencing data, showing the progressive development of the organoids from day 0 to day 19 of differentiation.

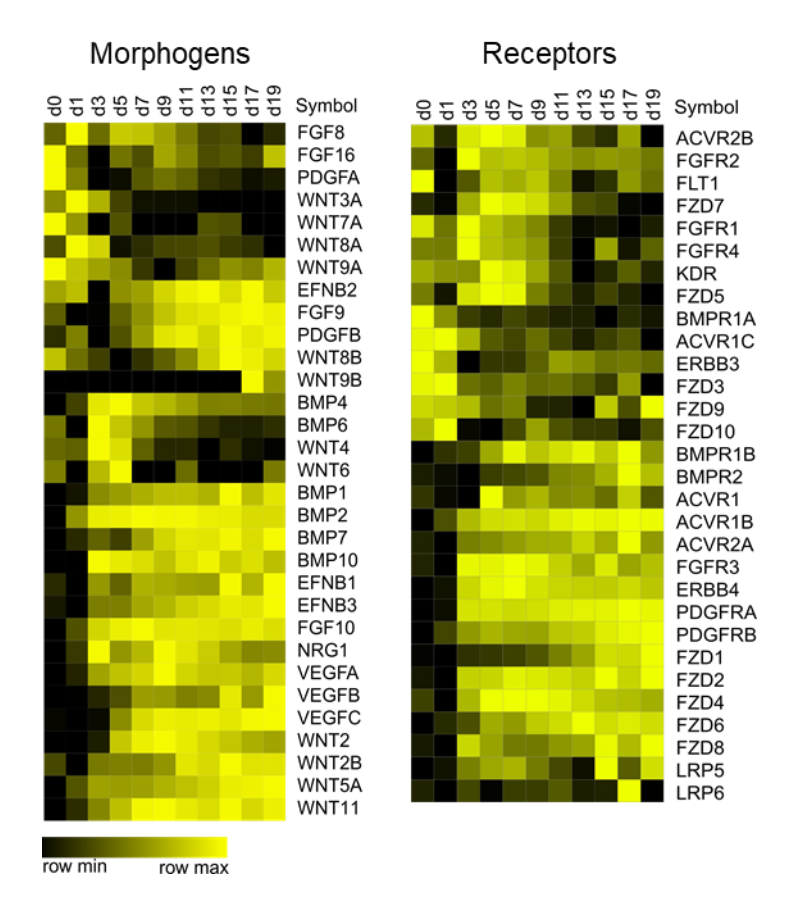


Figure 32. Morphogen and receptor expression levels as determined by RNA-Seq heatmaps in differentiating hHOs from day 0 to day 19. Heatmap colors are relative intensity representing gene expression.

4.2.2. Recapitulation of heart field development and atrioventricular specification

The first and second heart fields (FHF, SHF) are two cell populations found in the developing heart. Cells from the FHF contribute to the linear heart tube formation, followed by migrating cells belonging to the SHF that contribute to further expansion and chamber formation²⁰⁰. Evidence of cells representing both heart fields in our organoids were found. HAND1 (FHF) and HAND2 (SHF) are members of the Twist family of basic helix-loop-helix (bHLH) transcription factors that play key roles in the developing heart²⁰¹. Immunofluorescence of day 7 hHO cryosections showed well-differentiated regions of HAND1 and HAND2 (Figure 33) cells in the same organoid, suggesting that both FHF and SHF progenitors are present and segregated into their respective heart fields. FHF markers were observed as early as day 3 (prior to TNNT2 detection), confined to specific regions of the organoid, and reducing in expression around day 9 (Figure 34Figure 35). SHF markers appeared later in the process, only becoming prominent around day 7, and expressing throughout the organoid up to day 9 (Figure 34Figure 36). In human hearts, the left ventricle ultimately forms from FHF progenitors, and the atria form from SHF progenitors²⁰². Therefore, determining if the hHOs contain cardiomyocytes committed to either the atrial or ventricular lineages was the logical next step. Immunofluorescence for MYL2 (encodes myosin light chain-2, ventricular subtype) and MYL7 (encodes myosin light-chain 7, atrial subtype) in day 15 hHOs showed cardiomyocytes positive for both subtypes. The two different populations localized to different regions of the organoid and were in close proximity, which mirrors the expression pattern seen in human hearts (Figure 37Figure 38). Atrial cardiomyocytes made up most of the cell population (~48%) while ventricular cardiomyocytes made up about a fifth (~18%) of the total cells in the organoids at day 15 (Figure 38). The expression of HAND1, HAND2, and MYL7 transcripts was also observed throughout the differentiation protocol by RNA-Seg and was similar to that observed in human fetal hearts (Figure 25Figure 27). Taken together, these data suggest that the differentiation of our hHOs involves heart field formation, atrioventricular specification and chamber formation, all of which further emphasizes their recapitulation of human cardiac development.

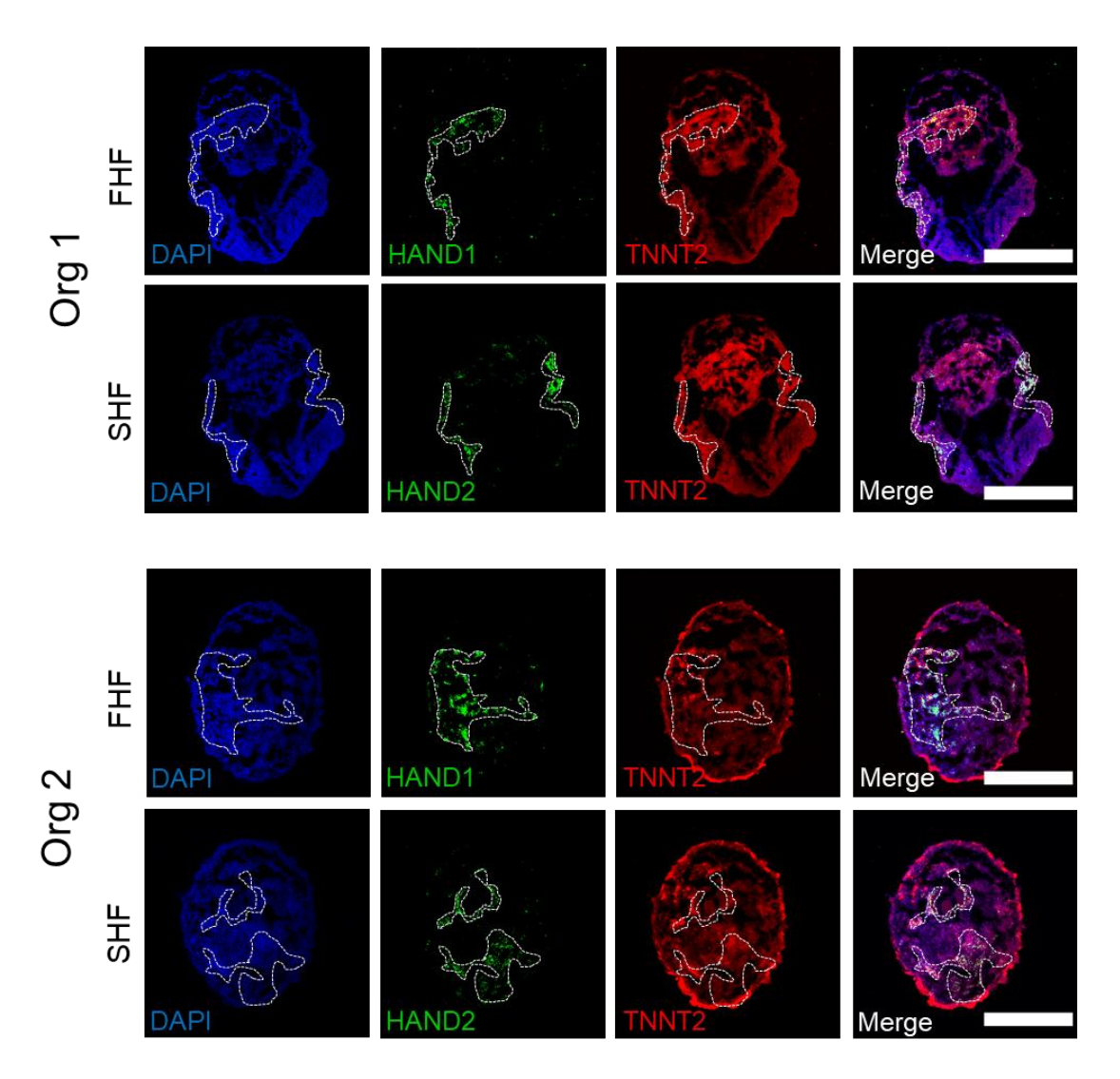


Figure 33. Regional formation of heart field markers. Confocal immunofluorescence images of two representative hHO cryosections on day 8 of differentiation showing robust HAND1 (FHF) and HAND2 (SHF) transcription factor expression (green) in different sections of the same organoid; TNNT2 (red), DAPI (blue); scale bar: $500 \, \mu m$, (n=12 organoids).

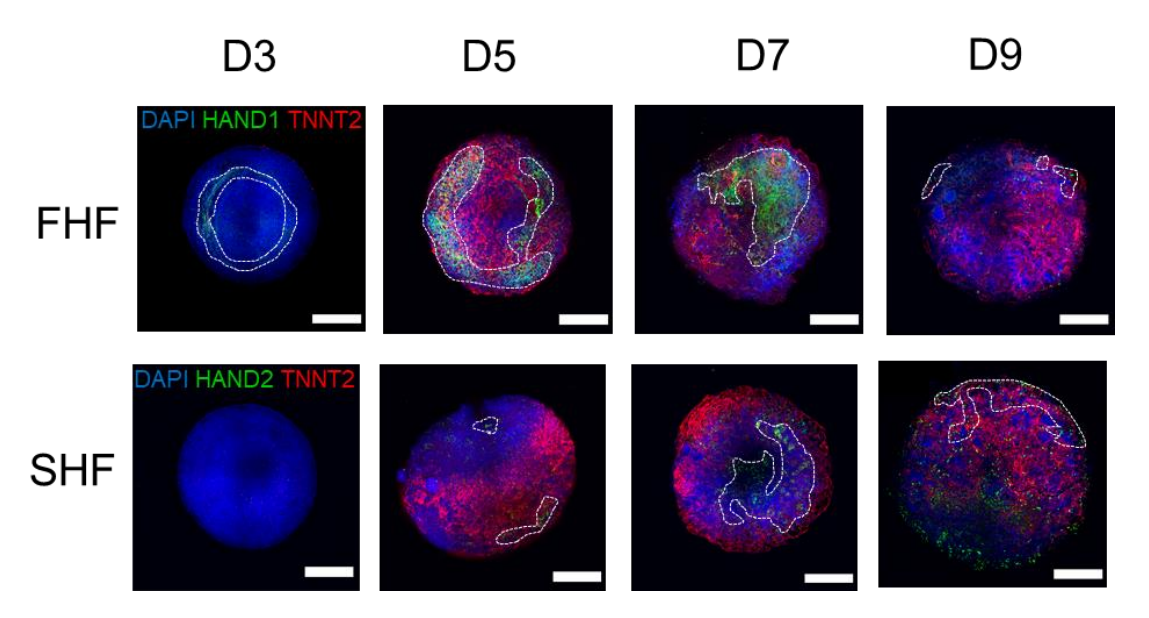


Figure 34. Heart field development in hHOs. Confocal images of day 3 to day 9 hHOs showing formation of FHF (HAND1, **left**) and SHF (HAND2, **right**), suggesting distinct regions of the two heart field populations in the organoids and showing the time dependent manner in which they develop; TNNT2 (red), DAPI (blue); scale bar: $500 \mu m$.

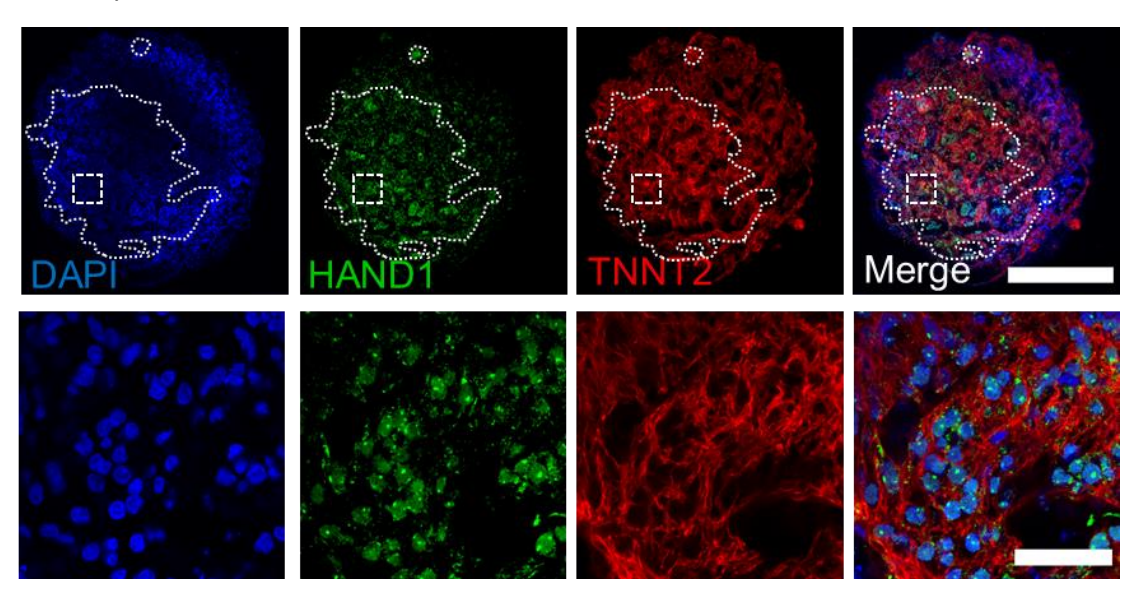


Figure 35. FHF markers expressed in cardiomyocytes. Confocal immunofluorescence images of hHOs at differentiation day 8 showing FHF marker HAND1 (green) in defined area of the hHO, DAPI (blue), TNNT2 (red); scale bars: $500 \ \mu m$, inset: $50 \ \mu m$.

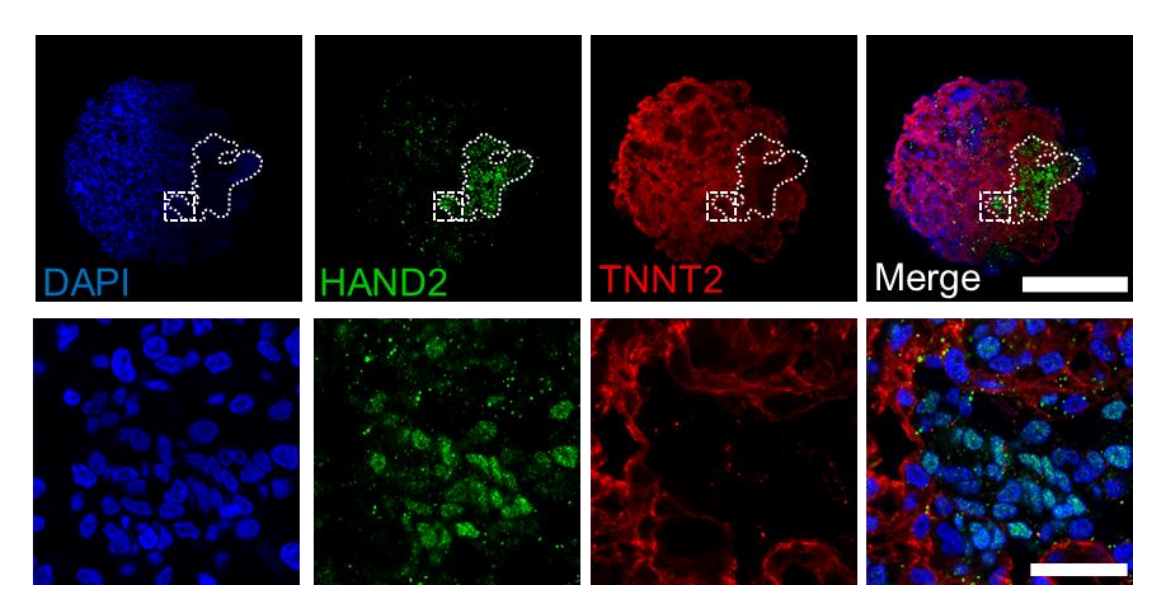


Figure 36. SHF markers expressed in non-myocyte cells. Confocal immunofluorescence images of hHOs at differentiation day 8 showing SHF marker HAND2 (green) in defined area of the hHO, indicating that SHF cells in the organoid can give rise to non-myocyte cell types; DAPI (blue), TNNT2 (red); scale bars: $500 \, \mu m$, inset: $50 \, \mu m$.

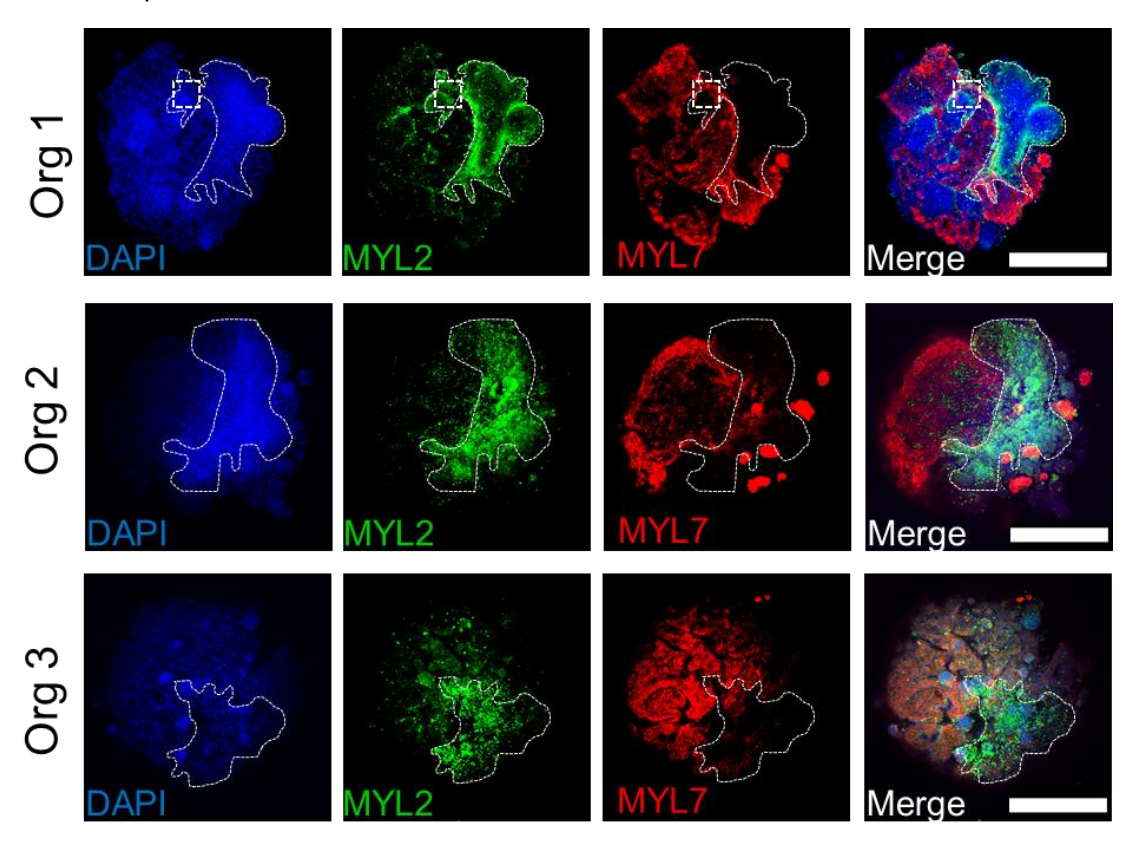


Figure 37. Atrioventricular cardiomyocyte specification in hHOs. Confocal immunofluorescence images of three representative day 15 hHOs containing well-differentiated ventricular (MYL2, green) and atrial (MYL7, red) regions, DAPI (blue); scale bar: 500 μm (n=10); inset shown in **Figure 38**.

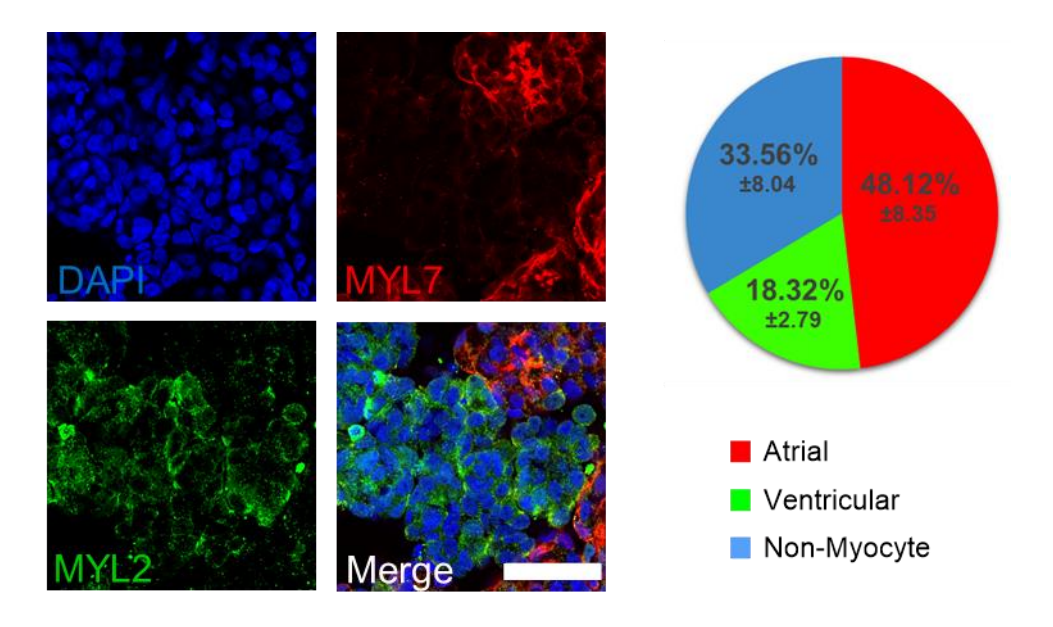


Figure 38. Atrioventricular composition in hHOs. (**left**) Confocal images showing inset images of organoid 1 from **Figure 37**; ventricular (MYL2, green) and atrial (MYL7, red) cardiomyocytes, DAPI (blue); scale bar: 50 μm. (**right**) Pie chart showing the percentage of atrial cardiomyocytes (MYL7+DAPI), ventricular cardiomyocytes (MYL2+DAPI), and non-myocyte cells (DAPI only); value = mean ± SD, (n=6 organoids).

4.2.3. Cell type composition

Results from the transcriptomic analysis (*4.2.1*, **Figure 24**) suggested that the second CHIR99021 exposure led to the formation of other mesenchymal lineages and higher complexity in hHOs due to induction of proepicardial organ formation. To evaluate this finding, immunofluorescence analysis was performed for secondary cardiac cell lineages. Confocal imaging confirmed the presence of cardiac fibroblasts positive for THY1 and VIM (**Figure 39**), similar to the composition of the fetal heart²⁰³. Immunofluorescence analysis for the endocardial marker NFATC1 (an endocardial specific cell marker⁸³) revealed the formation of endocardial layers, like the endocardial lining of heart chambers (**Figure 40**). Further imaging revealed a robust interconnected network of endothelial cells (PECAM1+), and vessel-like tube formation throughout the organoid assembling between day 11 and 13 (**Figure 41Figure 42**). Higher magnification images uncovered a complex web of endothelial cells adjacent to or embedded in myocardial tissue (**Figure 41**). These results strongly indicate that during hHO development, endothelial vascular structures emerge, adding a vascular network to the organoids. **Figure 43** shows a quantification of the contribution of the different cell cardiac populations to the organoids, with a composition of 12.49 ± 1.01% cardiac fibroblasts, 13.82 ± 1.54% endocardial cells, and 1.63 ± 0.21% endothelial cells. It should be noted that these non-myocyte cardiac cells were often intermixed within TNNT2+ myocyte regions (**Figure**

39Figure 42) as seen *in vivo*²⁰⁴. Lastly, extracellular matrix proteins common in cardiac tissue, such as collagen type 1, collagen type 4, and fibronectin, were all observed in our hHO model (**Figure 44**). Together, these observations depict a complex and sophisticated human heart organoid model with endocardial lined chambers within myocardial tissue, interspersed with cardiac fibroblasts and a network of endothelial cells, and complete with external epicardial tissue, features that are highly recapitulative of the developing human heart (**Figure 45**).

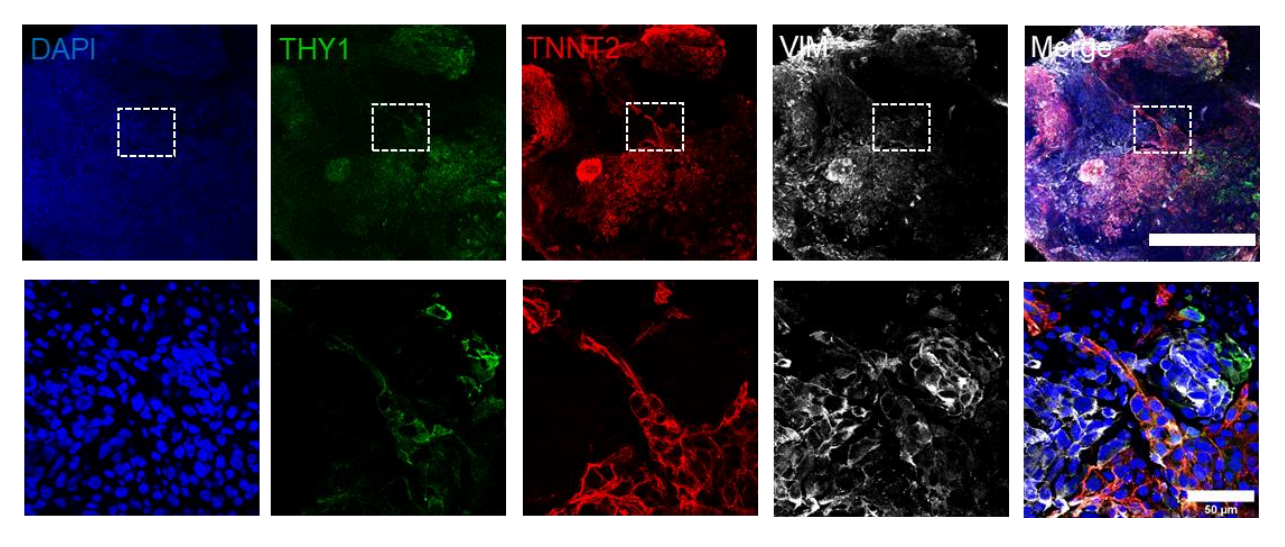


Figure 39. Cardiac fibroblast specification in hHOs. Confocal immunofluorescence showing cardiac fibroblast markers THY1 (green) and VIMENTIN (white) present throughout the hHOs, TNNT2 (red), DAPI (blue); scale bar: 500µm, inset: 50µm.

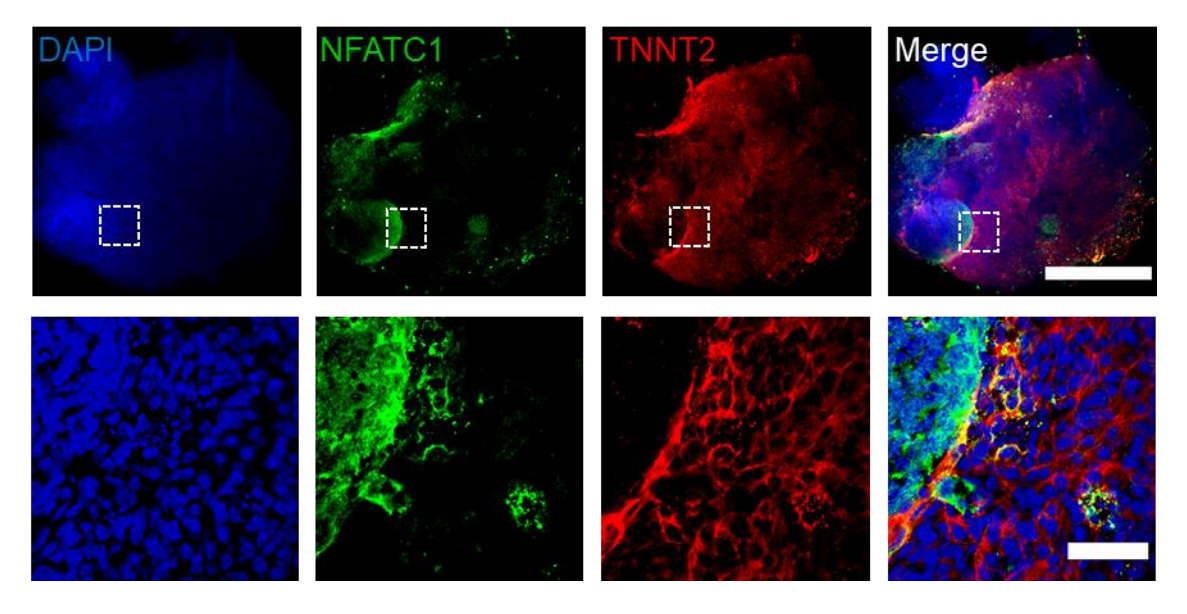


Figure 40. Endocardial specification in hHOs. Confocal immunofluorescence showing endocardial marker NFATC1 (green) highly expressed within chambers of TNNT2+ tissue (red); suggesting the formation of an endocardial lining within cardiac chamber; scale bar: 500µm, inset: 50µm.

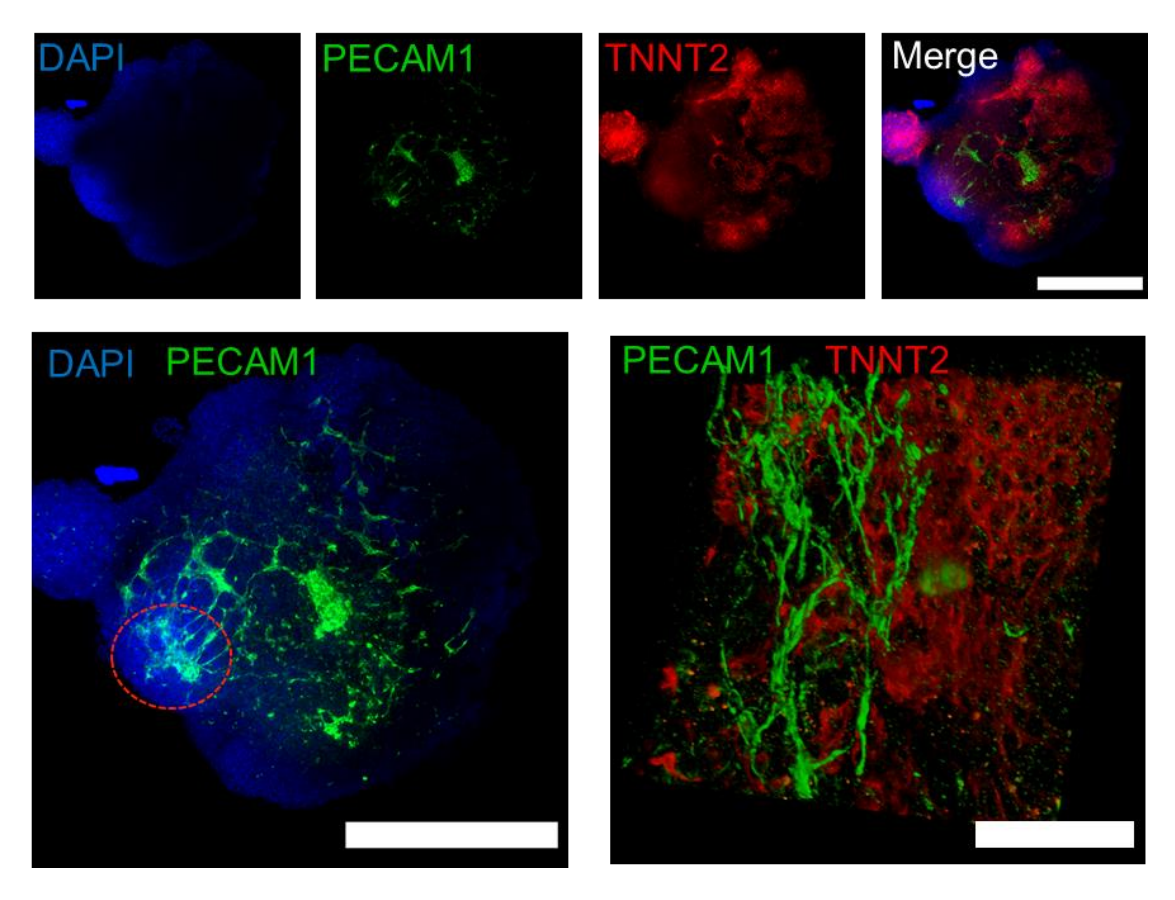


Figure 41. Endothelial specification and vascular network in hHOs. Confocal immunofluorescence showing endothelial marker PECAM1 (green) showing a defined network of vessels throughout the organoid and adjacent to TNNT2+ tissue (red), DAPI (blue); (**top**) showing a single confocal plane, (**bottom, left**) a maximum intensity projection to visualize the vascular network throughout the organoid, and (**bottom, right**) a high magnification 3D reconstruction showing tubular endothelial structures; red dotted circle in indicates area of high vascular branching.

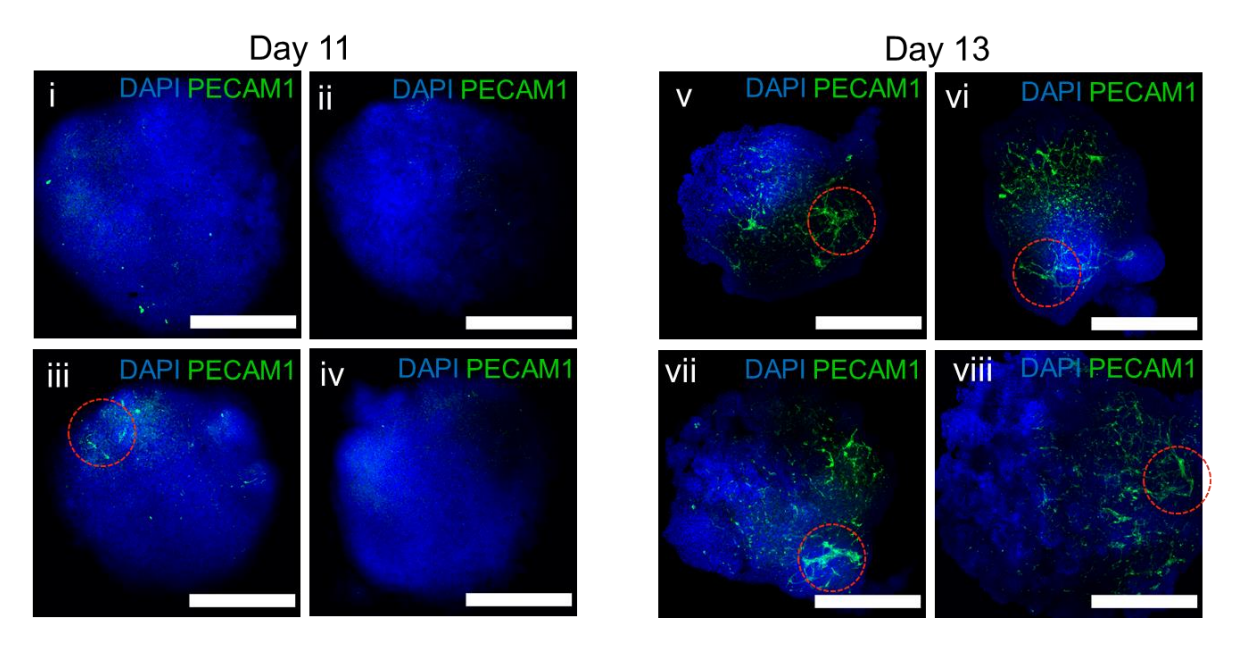


Figure 42. Emergence of a vascular network between day 11 and day 13 hHOs. Confocal immunofluorescence images of 8 hHOs (i-viii). Day 11 (i-iv) and day 13 (v-viii) organoids showing maximum intensity projections of PECAM1 (green) endothelial cells forming robust vascular-like network throughout the hHOs; red dotted circles indicate region of high vascular branching; DAPI (blue); scale bars: 500 μm.

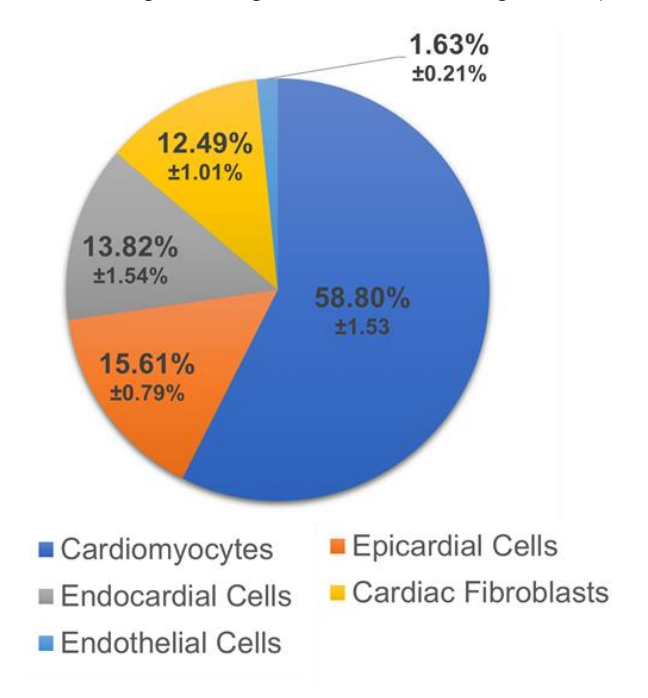


Figure 43. Pie chart of average cell composition in hHOs, calculated as the percentage cells with respective cell marker over all cells by nuclei counting using ImageJ.

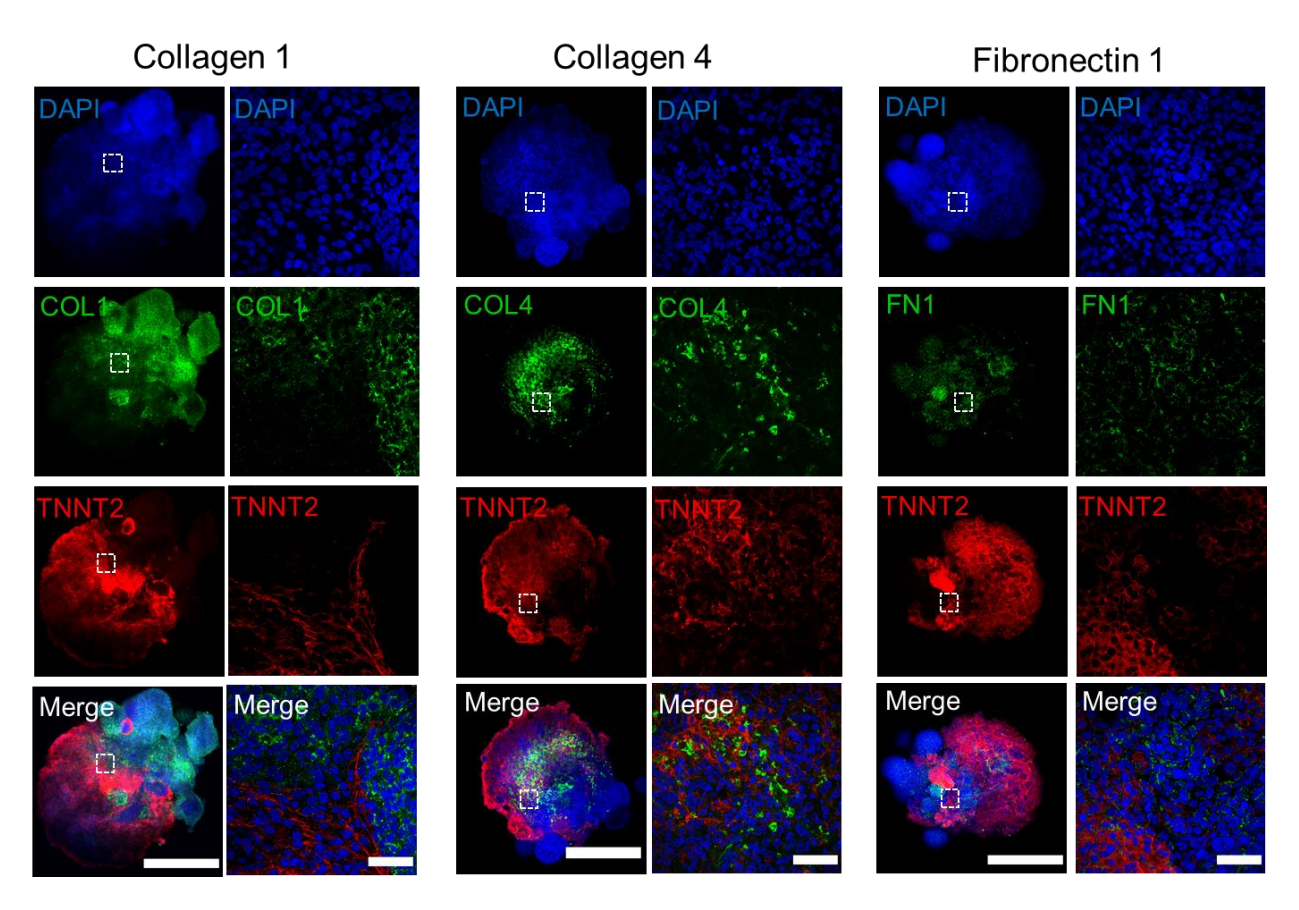


Figure 44. Presence of ECM proteins in day 15 organoids (green), showing collagen 1 (**left**), collagen 4 (**middle**), and fibronectin 1 (**right**); in green; scale bars: 500 μm, inset: 50 μm.

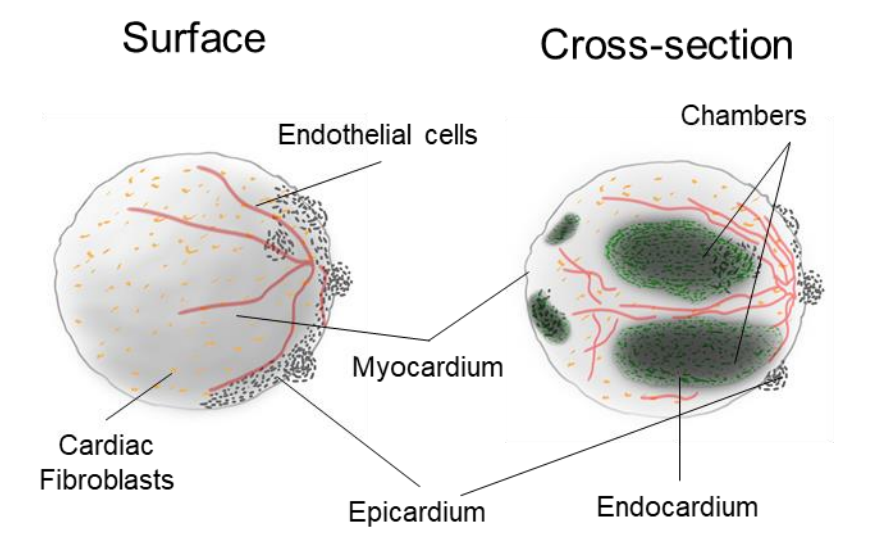


Figure 45. Updated sketch of hHO features showing surface (**left**) and cross-section (**right**) showing the organization of cell types and features of the hHOs (updated version of **Figure 21**). Key features in the organoid in addition to the myocardium body and epicardial clustering includes the development of a sophisticated vascular network throughout the organoid, interspersed cardiac fibroblasts within the body of the organoid, and internal cardiac chambers lined with endocardial cells.

4.2.4. BMP4 and Activin A: growth factor additives improve chamber formation and vascularization

The growth factors BMP4 and ActA have frequently been used as alternatives to small molecule-mediated Wnt signaling manipulation, since they are the endogenous morphogens that pattern the early embryonic cardiogenic mesoderm and determine heart field specification in vivo^{87,205-207}. It was hypothesized that BMP4 and ActA, in combination with our small molecule Wnt pathway activation/inhibition protocol, could synergistically improve the ability of hHOs to recapitulate cardiac development in vitro. The effect of BMP4 and Act A was tested, in the context of our optimized protocol, by adding the two morphogens at 1.25 ng/ml and 1 ng/ml, respectively⁸⁷, at differentiation day 0 for 24 hours in conjunction with 4 µM CHIR99021. No significant differences were found in the formation of myocardial (TNNT2+) or epicardial (WT1+/TJP1+) tissue between control and treated hHOs (Figure 46). However, significant differences in organoid size were observed as hHOs treated with growth factors were about 15% larger in diameter (Figure 46). This difference may correspond with increased chamber connectivity, as BMP4/ActA-treated hHOs had internal chambers-like cavities that were ~50% more interconnected with other chambers compared to control hHOs (Figure 47). Notably, immunofluorescence analysis of organoids treated with BMP4 and ActA showed a 160% increase in PECAM1+ cells too, indicating a significant effect on organoid vascularization (Figure 48). These results suggest improved structural organization in the developing organoids under BMP4/ActA, in agreement with previously reported differentiation methods using BMP4 and ActA alone⁸⁷.

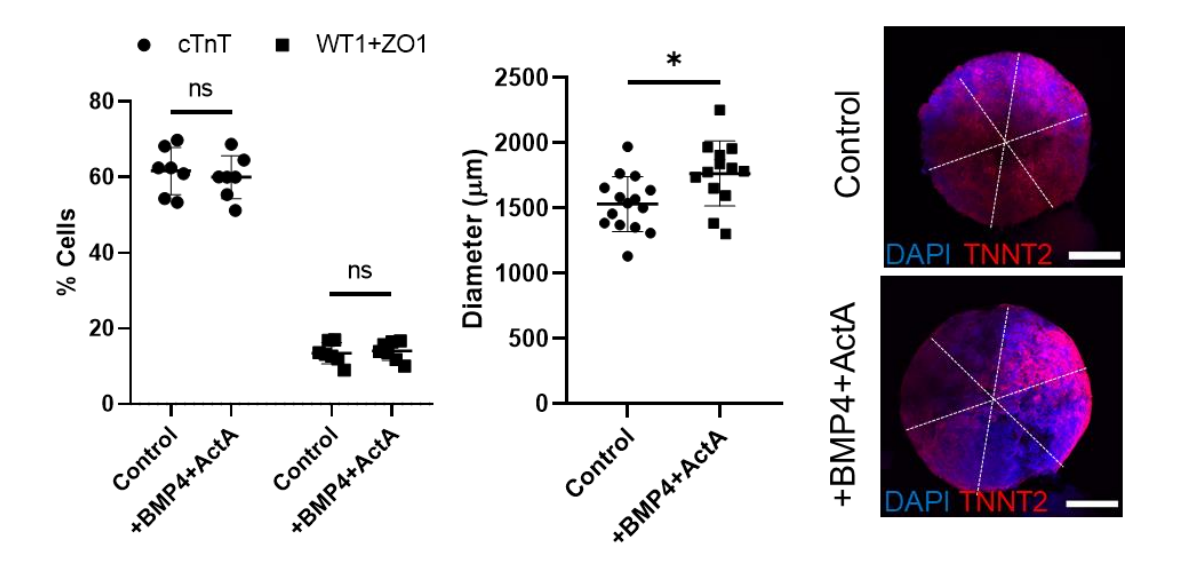


Figure 46. Effect of BMP4 and ActA on myocardial/epicardial formation and organoid size. Comparing hHOs differentiated with CHIR99021 alone (control) and with CHIR99021+BMP4+ActA. (**left**) Percent of cardiomyocyte and epicardial positive cells as a percentage of total DAPI+ nuclei (n=7 organoids per condition, value = mean ± SD, 2-way ANOVA Sidak's multiple comparisons test, ns: p= 0.76 for TNNT2 and p=0.97 for WT1+TJP1) and (**middle**), organoid diameter, (n=13 organoids per condition, value = mean ± SD, two-tailed, unpaired t-test, *p=0.012). (**right**) Dashed lines showing the diameter of a control and +BMP4+ActA organoid image averaged to determine the diameter.

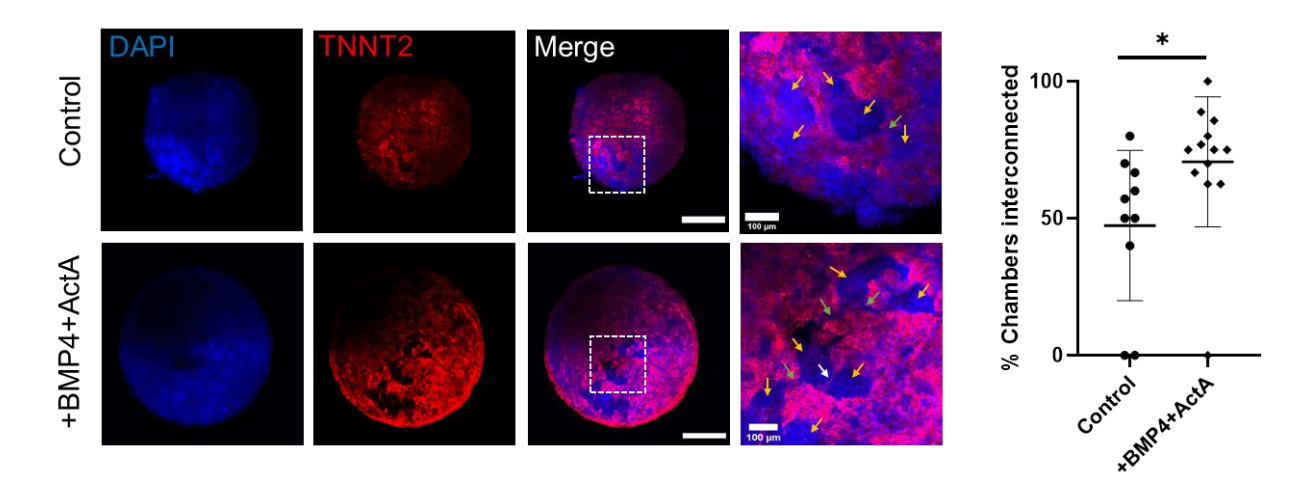


Figure 47. Effect of BMP4 and ActA on chamber formation (**left**) Immunofluorescence images of hHOs showing interconnected chambers (yellow arrows), TNNT2+ filaments (white arrows), and channels connecting chambers (green arrows), DAPI (blue), TNNT2 (red), scale bar: $500\mu m$, inset: $100 \mu m$. (**right**) Interconnectivity of chambers measured by their separation by thin TNNT2+ filaments or by thin channels showing clear connection (n=10 organoids per condition, value = mean \pm SD, two-tailed, unpaired t-test, *p=0.041).

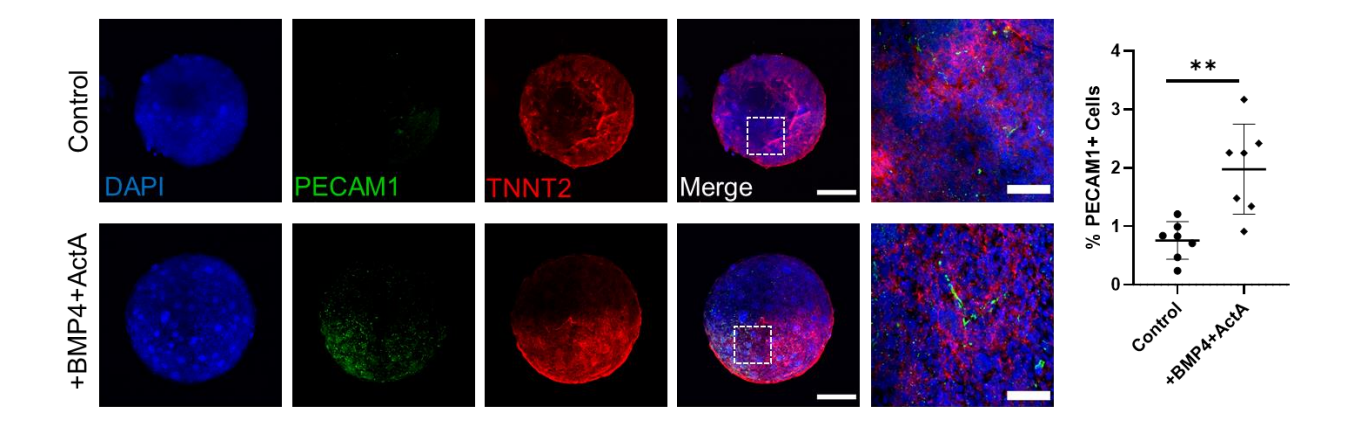


Figure 48. Effect of BMP4 and ActA on vascularization. (**left**) Immunofluorescence images of hHOs showing DAPI (blue), PECAM1 tissue (green), and TNNT2 tissue (red), scale bar: 500μm, inset: 50μm (n=12). (**right**) PECAM1+ cells as a percentage of total DAPI+ nuclei, (n=7 organoids per condition, value = mean ± SD, two-tailed, unpaired t-test, **p=0.0023).

4.2.5. Heart organoids exhibit functional and structural features of the developing human heart

Traditional imaging methods, such as confocal imaging, are poorly suited for the study of the complex 3D structures of the size present in hHOs. Thus, OCT was employed to characterize chamber properties using minimally invasive means, thus preserving chamber physical and morphological properties. OCT showed clear chamber spaces within day 15 hHOs (**Figure 49Figure 50**). 3D reconstruction of the internal hHO topology revealed a high degree of interconnectivity between these chambers, revealing 4–6 chambers near the center of the organoid ranging from 5.5e⁻⁴ mm³ to 1.3e⁻² mm³ (**Figure 51**). Given the relatively large size of our heart organoids (up to 1 mm in diameter, ~0.45 mm³), it was necessary to verify whether these chambers could be attributed to internal cell death. A transgenic hiPSC line expressing FlipGFP, a non-fluorescent engineered GFP variant that turns fluorescent upon effector caspase activation and is thus a reporter for apoptosis²⁰⁸, was created. FlipGFP organoids in control conditions exhibited no fluorescence indicating that there is no significant programmed cell death (**Figure 52**). Doxorubicin-treated hHOs were used as a positive control for apoptosis (**Figure 52**), with evident signs of cell death.

Ultrastructural analysis of hHOs showed similar features to those found in early human fetal hearts, with well-defined sarcomeres surrounded by mitochondria, gap junctions and the presence of tubular structures reminiscent of T-tubules (**Figure 53**), also confirmed by immunofluorescence staining with WGA (**Figure**

54). Electrophysiological activity to determine the hHO functionality was measured in two distinct ways. First, utilizing a multi-electrode array (MEA) (**Figure 8**), robust beating and normal electrophysiological activity with well-defined action potential waves reminiscent of QRS complexes, T and P waves, and regular action potentials across multiple organoids, were detected (**Figure 55**). Second, live calcium imaging in whole organoids to determine calcium activity. hHOs were generated from an iPSC line expressing the rapid calcium indicator GCaMP6f^{127,128}, and imaged fluorescence variation over time as a result of calcium entry and exit from the cells. hHOs presented strong regular calcium waves typical of cardiac muscle and in agreement with our electrophysiology data (**Figure 56**).

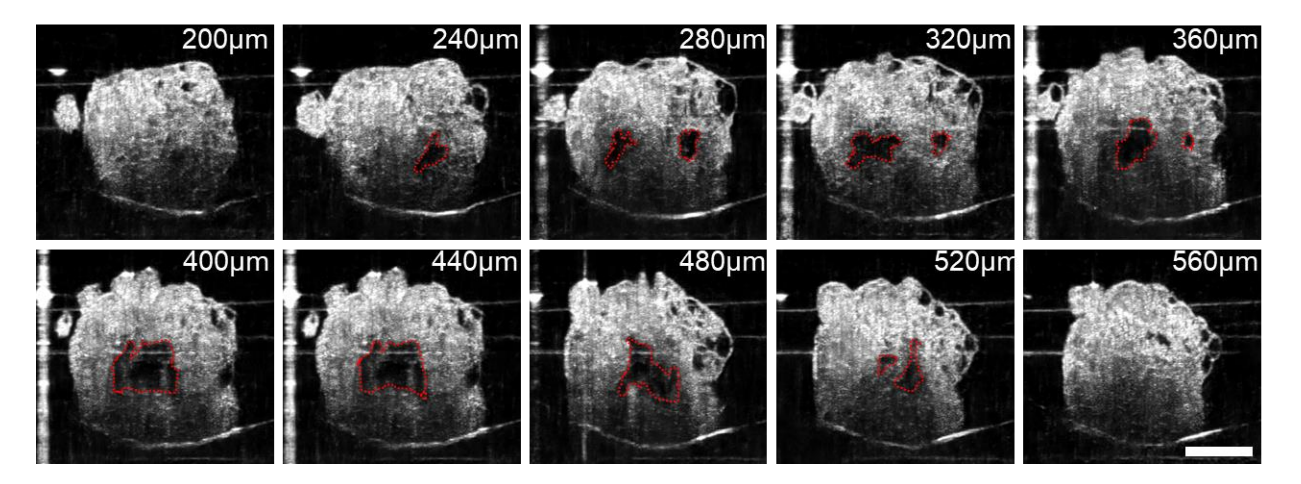


Figure 49. Optical coherence tomography images showing cross-sections through a day 15 organoid, revealing chambers that open and close as images slice through the organoid; scale bar: 500μm. OCT images were acquired by the Zhou Lab.

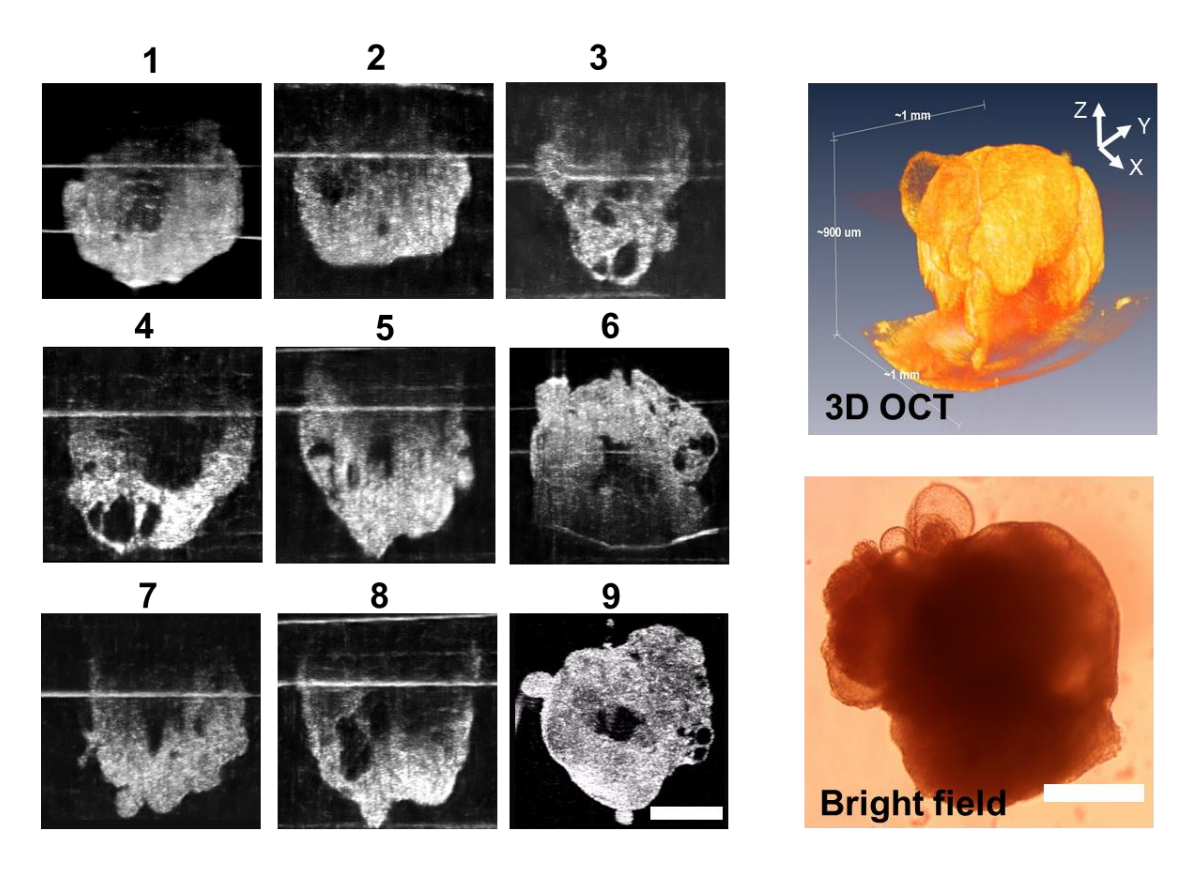


Figure 50. OCT images showing cross-sections of the center of 9 different organoids (**left**), revealing central chambers. 3D reconstruction of OCT images and bright field image of hHO (**right**); scale bars: 500 μ m. OCT images were acquired by the Zhou Lab.

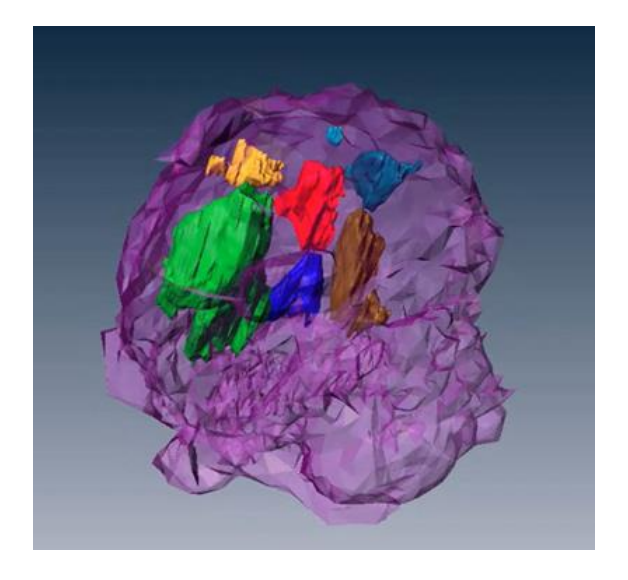


Figure 51. 3D reconstruction of chambers observed via OCT imaging, where magenta depicts the body of the organoid and all other colors represent chambers. OCT images were acquired by the Zhou Lab.

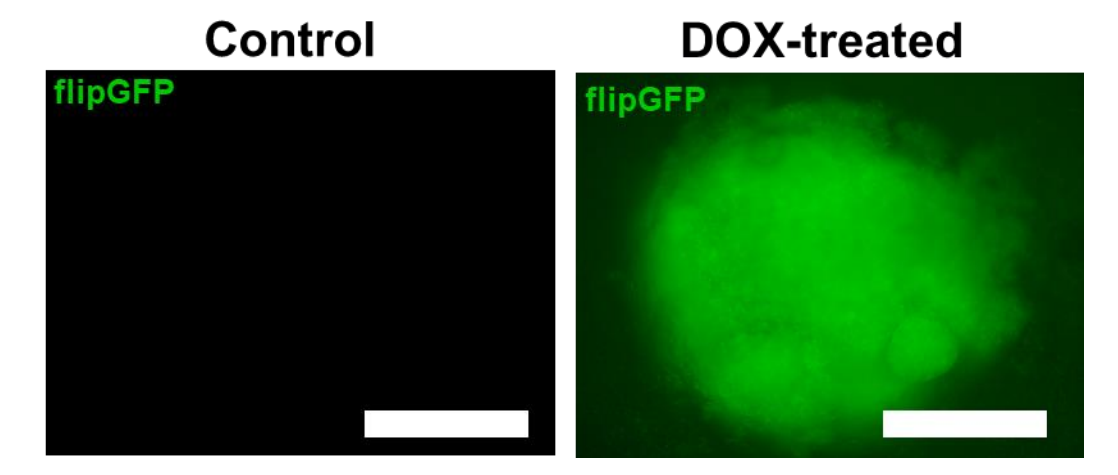


Figure 52. Immunofluorescence images of organoids derived from a FlipGFP transgenic iPSC line L1 showing no apoptosis in control hHOs (**left**) and high apoptosis in hHOs treated with 5 μM Doxorubicin (DOX) (**right**); scale bar: 500μm. Cell line and organoids were created by Brett Volmert (Aguirre Lab).

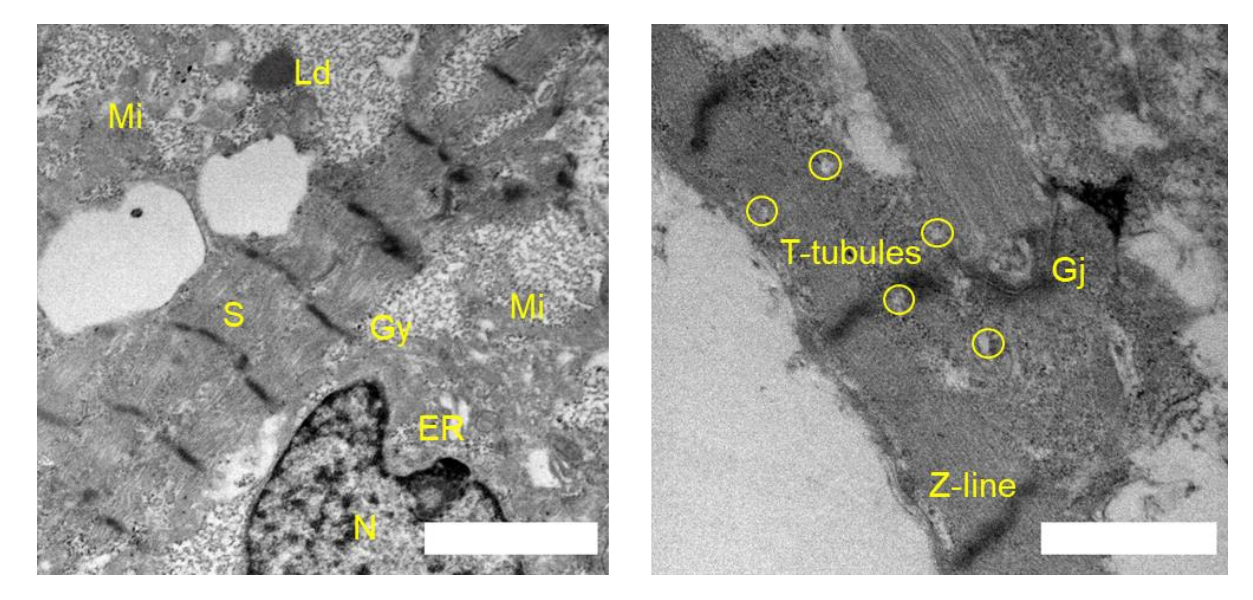


Figure 53. Transmission Electron Microscopy (TEM) images of hHOs showing endoplasmic reticulum (ER), gap junctions (Gj), glycogen granules (Gy), lipid droplets (Ld), mitochondria (Mi), nucleus (N), and sarcomeres (S); scale bars: 2 μ m (**left**), 1 μ m (**right**). TEM images were acquired by Natalia Pajares (Chatzistavrou Lab).

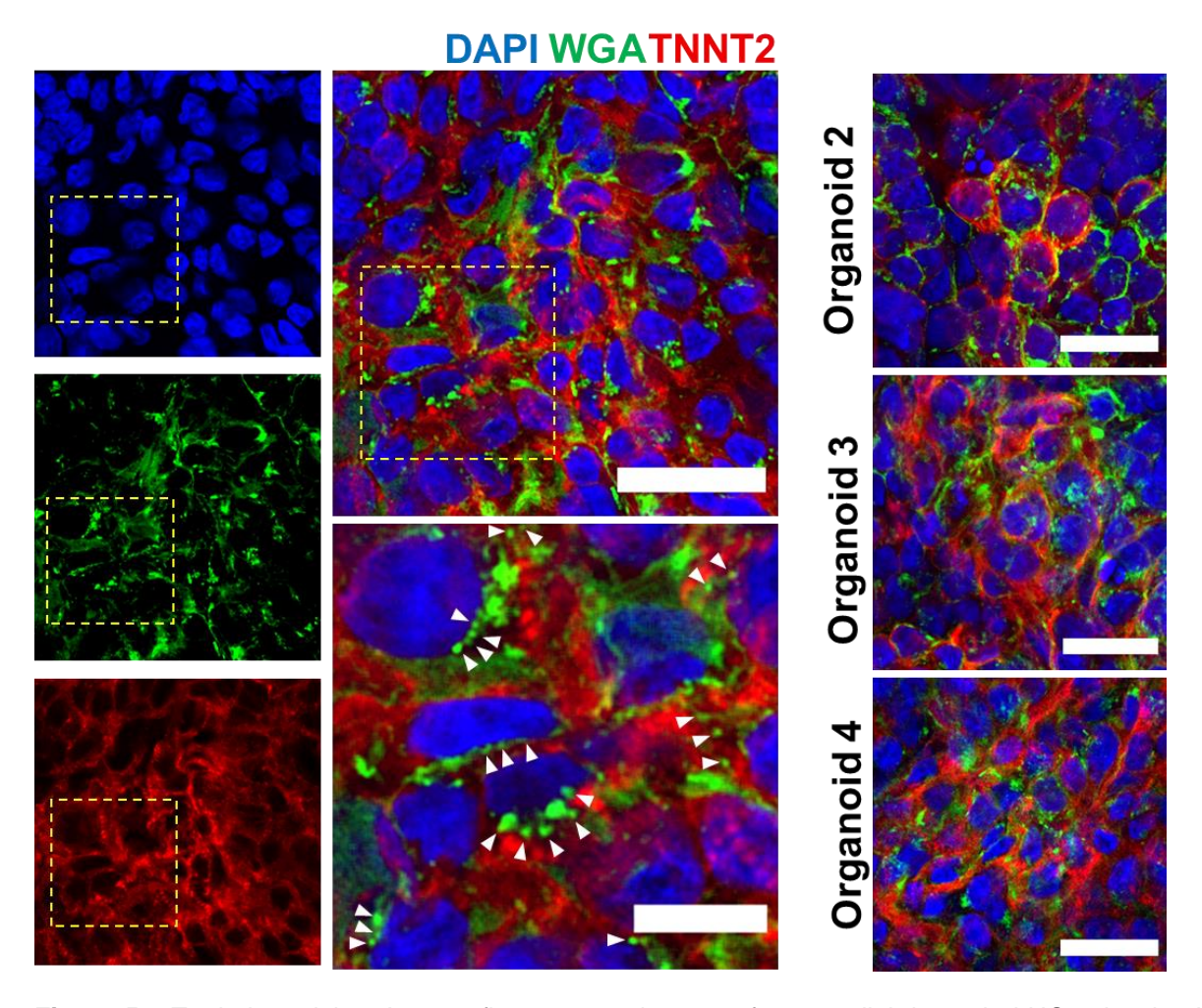


Figure 54. T-tubule staining. Immunofluorescence images of myocardial tissue in hHOs showing WGA staining of T-tubule-like structures (green); white arrowheads indicate representative T-tubule-like structures between cardiomyocytes; scale bar: $50 \mu m$, inset: $20 \mu m$.

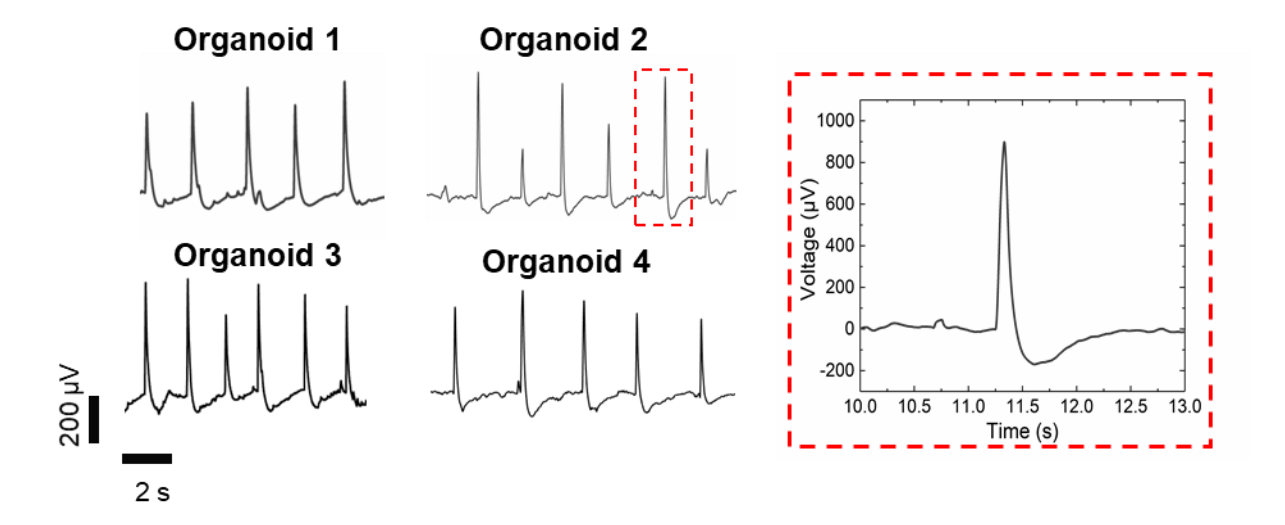


Figure 55. Electrophysiology recordings of 4 organoids on microelectrode array spanning 15 seconds and a representative action potential wave (inset). MEA recordings were conducted in collaboration with Weyang (Li Lab).

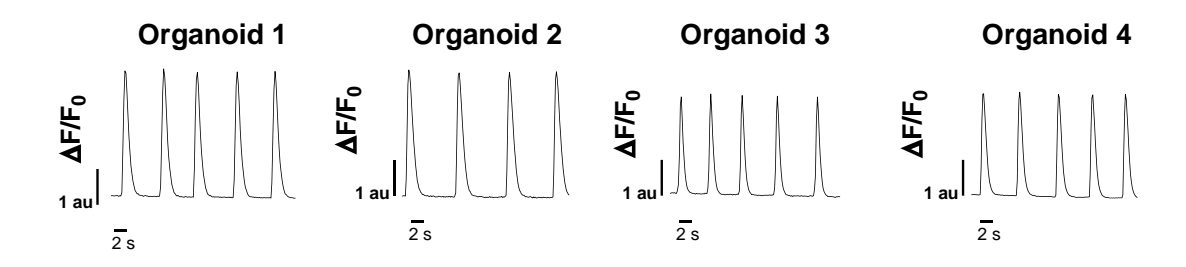


Figure 56. Ca2+ transients in 4 representative hHOs after two weeks of differentiation. Organoids exhibited consistent and reproducible calcium transient recordings.

4.3. DISCUSSION

The human heart is a complex, consisting of a multitude of tissue and cell types organized in organized into functional structures. Modeling the human heart *in vitro* requires the recapitulation of the cell type composition, general structure and functionality of the heart in order to faithful study it's development and associated diseases and disorders. This chapter explores the advanced features if the hHO model generated by the optimized protocol described in chapter 2. The non-myocyte or epicardial cells within the organoids comprised of 14% endocardial cells, 12% cardiac fibroblasts, and 1.6% endothelial cells and shows robust beating throughout the entire structure within a week from differentiation initiation and up to at least 8 weeks in culture (longer culture times were not attempted). The organization and specification of these cell types may be related to HAND transcription factor expression, as HAND1 and HAND2 lineagederived cells contribute to the developing myocardium, epicardium, endocardium, and vasculature^{201,209}

²¹¹. The fact that both FHF and SHF HAND markers are present suggests that they could play a role in the development of the structural and cell type complexity seen in our hHOs. When compared with existing cardiomyocyte monolayer differentiation methods, hHOs showed higher expression of genes associated with conduction, contractile function, calcium handling, and various cardiac cell populations, which better resemble gene expression data retrieved from human fetal hearts. The depiction of a complex transcriptome highly recapitulative of human fetal heart tissue further strengthens the potential use of hHOs as models of human heart development.

Together with the use of small-molecule inhibitors that manipulate canonical Wnt signaling pathways, successful cardiomyocyte differentiation has been achieved in the past using morphogens such as BMP4 and ActA^{137,212}. These growth factors lead to the induction of cardiac mesoderm in the embryo²¹³ and established differentiation protocols using them show effective differentiation to various cardiac mesoderm progenitors^{213–215}. Recently, gradient exposures to specific concentrations of BMP4 and ActA have been studied in the specification of first and second heart field formation⁸⁷. The addition of these growth factors to the initial CHIR99021 exposure in our hHO differentiation protocol led to improved morphological features, such as increased chamber interconnectivity and vascularization.

Immunofluorescence analysis of our hHOs revealed the presence of cardiac fibroblast markers including the membrane glycoprotein THY1, which is involved in cell-cell and cell-matrix adhesion^{216,217}, and the intermediate filament protein Vimentin, typically seen in cells of mesenchymal lineage²¹⁷. Other cardiac fibroblast markers were found in the hHOs via RNA-Sequencing analysis, including *DDR2* which plays an important role in EMT²¹⁶, and the FHF marker *PDGFRa* which is also crucial for vascularization during development²¹⁷. These data provide a strong indication of the increased complexity of our hHO system and its close resemblance to fetal heart tissue. It should be noted that while our immunofluorescence and bulk RNA-Sequencing data suggest the presence of the cardiac cell types described above, these techniques may not fully capture the heterogeneity of our organoids. In recent years, significant advances have been made in single-cell and single-organoid "omics" technologies^{218–220} as well as the ability to image 3D engineered tissues with unprecedented quality and resolution^{221–224}. Further studies employing these techniques significantly add more detail and information to the cell type compositions as will be discussed in the next chapter.

An acute limitation of many organoid systems is a lack of a functional vascular network to facilitate the exchange of nutrients and removal of waste material, as they instead rely solely on diffusion^{225–227}. Several vascularized organoids have been described in the literature modeling the brain²²⁷, kidney²²⁸, and blood vessel¹⁸², however, none have been described in cardiac organoids. In these studies, various techniques are used to induce vascularization including implantations in mice⁴, culturing the organoids under flow²²⁸, and embedding endothelial cells in a Matrigel/collagen matrix, and inducing their migration¹⁸² to create a vascular network. Remarkably, formation of vascular structures in the optimized final protocol for hHOs was observed without any additional steps. Furthermore, a point of high vascular branching was detected, which merits future exploration into developmental point of origin in heart vascularization.

In addition to endothelial structures, spontaneous hHO reorganization into interconnected chambers was observed, a powerful 3D feature that recapitulates fetal-like organogenesis. Previous studies of microchamber formation in vitro utilized micropatterning of hPSCs into a confined area to generate 3D cardiac microchambers with cell-free regions, a myofibroblast perimeter, and nascent trabeculae 156. Other reports have produced 3D bio-printed hPSC-laden scaffolds and differentiated them to beating cardiac microtissues with two chambers²²⁹. While the structures generated in these studies showed some fetal-like formation of cardiac microchambers, they lacked endocardial tissue²³⁰, a crucial player in heart maturation and morphogenesis²³¹. The hHOs reported here form multiple chambers lined with NFATC1+ endocardial cells which are interconnected as seen in the OCT cross-sectional imaging. Expression of specific ECM genes in the hHOs resembling the fetal heart matrix, such as COL1A1, COL4A1, COL5A2, FBN1, EMILIN1, HSPG2, and LAMA2 (Figure 29) might be an important factor in chamber organization, as ECM components have been shown to mediate the formation of chambered mouse cardiac organoids88. Therefore, the expression of these genes in our hHOs deserves further examination in the future. The chambers may also specify further into atrial-like and ventricular-like regions, as cardiomyocytes from both lineages are seen in separate regions in our hHOs. The data described here demonstrates a complex and highly sophisticated model of the human fetal heart organoids, mimicking the formation and organization of the in vivo organ, in a reproducible and high-throughput generation method that is highly amendable to disease and developmental studies. Therefore, the utilization of these organoids in modeling the etiology

of congenital heart defects as a result of pregestational diabetes provides an imperative example for the modeling of diseases affecting early-stage heart development, as will be discussed in the following chapter.

5. CHAPTER 5: AIM 3: CHARACTERIZING THE MOLECULAR PATHOLOGY OF PREGESTATIONAL DIABETES IN THE HUMAN HEART

5.1. INTRODUCTION

5.1.1. Pregestational diabetes-associated congenital heart disease

The connection that exists between PGD and the risk of CHD in the embryo/fetus has been described in both clinical observations ^{9,101–103}, animal studies ^{99,105–107,111–113}., and *in vitro* research^{114–116}. Nevertheless, the underlying mechanism in which PGD is associated with CHD remains unknown^{232–236}. PGD is an immense risk factor for CHD in newborns, going from ~1% in the normal population up to 12% for diabetic mothers²³⁶ (a 12-fold increase). Furthermore, the prevalence of diabetic-related CHDs is only going to increase in upcoming decades due to the ongoing worldwide type 2 diabetes (T2D) epidemic^{97,237}. Thus, PGD-induced CHD is a critical health problem for which preventive and therapeutic interventions are critically needed.

5.1.2. The effects of PGD on the developing heart

Very little is known about the effects of PGD on early heart development^{237–241}. Clinical evidence suggests lipid metabolism, and in particular omega-3 bioactive lipids^{242–245}, might be critically dysregulated processes. Animal studies hint at potential mechanisms of action, such as ROS production, mitochondrial stress, and transcription factors dysregulation ^{99,105–107,111–113}. *In vitro* CM research also explored the dysregulation in gene expression, focusing on hypertrophic markers^{114–116}. Yet a key understanding of how PGD affects the onset of CHD in the human fetal heart still eludes clinical, animal and 2D *in vitro* studies due to limited access to early stages of development, cross-species differences, and lack of complex features, respectively.

5.1.3. Treatments, preventatives, and models of pregestational diabetes

Human pluripotent stem cells (hPSCs), including hESCs and hiPSCs, have the capability to self-organize into three-dimensional (3D) organoids resembling embryo-like tissue patterns *in vitro*. Although organoid models have been described for a broad range of tissues, progress in the cardiovascular field has been limited. Recent studies of cardiac microtissues or organoids have improved on prior heart muscle engineering approaches^{91,166,246}. The protocol described in this dissertation demonstrated the capacity of hiPSC-derived cardiac organoids to model the developing human heart. As proof of concept of the utility of

this system, hHOs are used to model the effects of PGD on cardiac development. Diabetes affects a large sector of the female population of reproductive age and comes associated with significant epidemiological evidence linking it to CHD during the first trimester of pregnancy, but little understanding of the underlying mechanisms exists, especially in humans.

5.1.4. hHO modeling of PGD associated CHD

Chapters 2 and 3 describe the first self-assembling human heart organoid generated by a single protocol, faithfully recapitulating early human cardiac development. This model holds great promise for modeling aspects of human CHD that cannot be studied *in vivo*, such as PGD-induced CHD. This chapter hypothesizes that chronic fetal heart exposure to increased levels of glucose and insulin (two hallmarks of T2D) leads to abnormal metabolic and developmental signals altering the course of early fetal heart development. By discovering novel molecular and cellular roles for PGD in human cardiovascular development, this dissertation brings forward a potentially transformative paradigm toward understanding, preventing, and treating a class of congenital heart disorders that constitute a significant medical problem. To model PGD, hHOs were cultured in modified conditions to reflect reported physiological levels of glucose and insulin in healthy mothers (3.5 mM glucose, 170 pM insulin, normoglycemic hHOs or NHOs¹⁶¹), and reported diabetic conditions for females with type I and type II pregestational diabetes (11.1 mM glucose and 1.14 nM insulin, pregestational diabetes hHOs or PGDHOs^{161,162}).

5.2. RESULTS

5.2.1. Pregestational diabetes affecting organoid structure, organization, and ultrastructure NHOs and PGDHOs showed significant morphological differences as early as day 4 of differentiation. NHOs were slower to grow and exhibited patterning and elongation between days 4 and 8, while PGDHOs remained spherical throughout the two-week period (Figure 57). PGDHOs were also significantly larger after 1 week of differentiation (Figure 58), suggesting macrosomia, a common outcome of diabetic mother's newborns²⁴⁷. TEM imaging revealed PGDHOs had a reduced number of mitochondria surrounding sarcomeres and a significantly higher number of lipid droplets, suggesting dysfunctional lipid metabolism and a more glycolytic profile (Figure 59Figure 60). Further mitochondrial staining using the molecular probe Mitotracker, revealed an increase in mitochondrial swelling in PGDHOs compared to control (Figure 61Figure 62), hinting at mitochondrial dysfunction as a result of the diabetic conditions. Furthermore,

staining for the reactive oxygen species (ROS) molecular probe CellROX Green, revealed an increase in the cellular ROS if PGDHOs compared with controls (**Figure 63**), a phenotype that has been previously described in murine PGD models^{113,248}. Immunofluorescence imaging for myocardial and epicardial markers revealed a drastic difference in the morphological organization as PGDHOs contained epicardial tissue surrounded by myocardial tissue, whereas NHOs contained epicardial tissue on top of or beside myocardial tissue as physiologically expected (**Figure 64**).

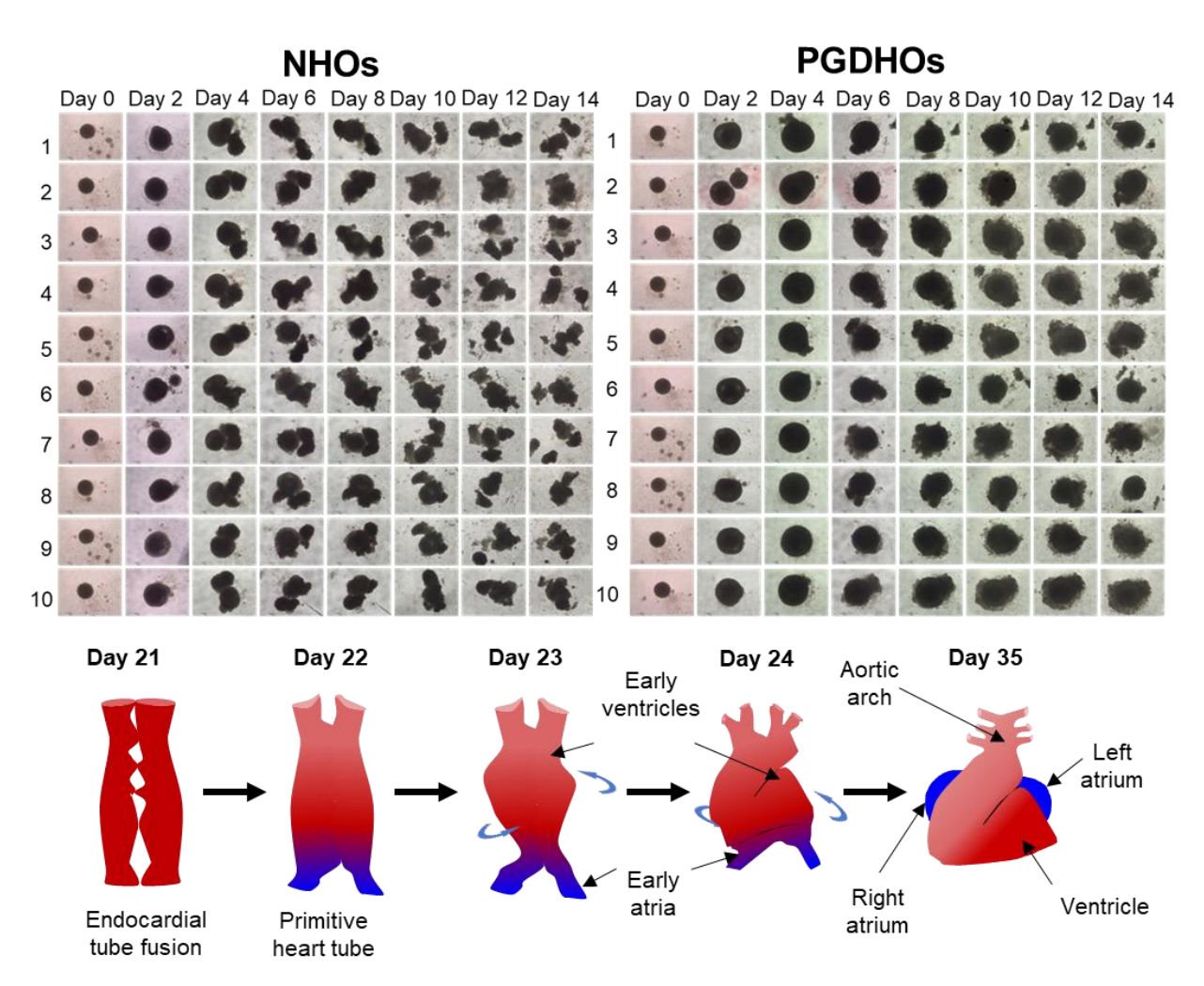


Figure 57. Developmental dysregulation of PGDHOs. (**top**) Brightfield images following the development of 10 hHOs under normal glycemic conditions (NHOs, **left**) and under diabetic conditions (PGDHOs, **right**) over two weeks of differentiation, showing a trend in structural formations of the organoids between the two conditions, and the lack of elongation and possible looping under diabetic conditions. (**bottom**) Schematic of heart tube formation and looping into the four chambers of the heart.

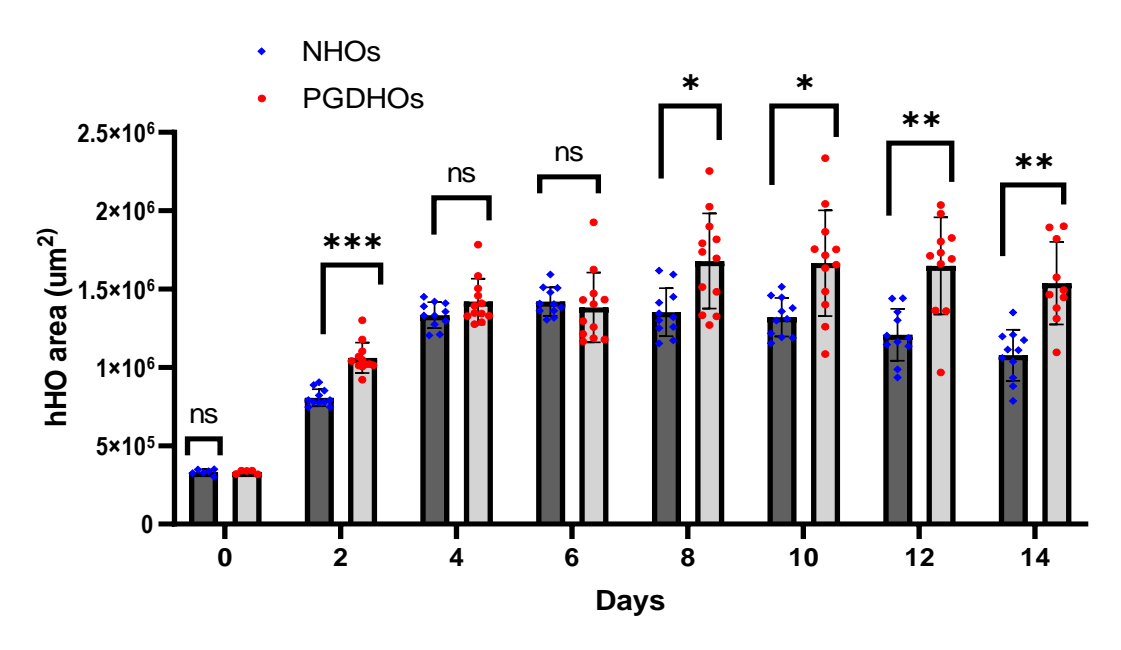


Figure 58. Increased size of PGDHOs. Area of hHOs under a light microscope over the first two weeks of differentiation (value = mean \pm SD; n=12; 2-way ANOVA Sidak's multiple comparisons test, exact p-values: day 0: p>0.99, day 2: p=0.017, day 4: p=0.94, day 6: p=0.99, day 8: p=0.0008, day 10: p=0.0003, days 12 and 14: p<0.0001).

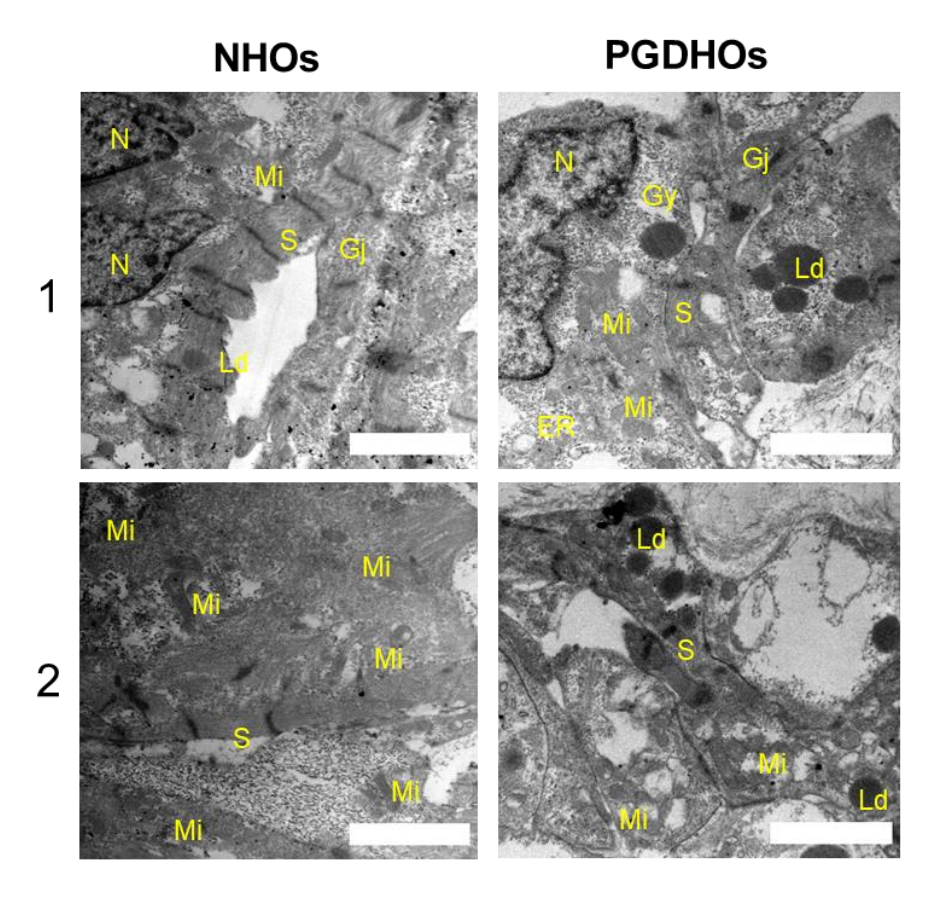


Figure 59. Ultrastructural analysis by TEM of NHOs and PGDHOs showing endoplasmic reticulum (ER), gap junctions (Gj), glycogen granules (Gy), lipid droplets (Ld), mitochondria (Mi), nucleus (N), and sarcomeres (S); scale bars: 2µm.

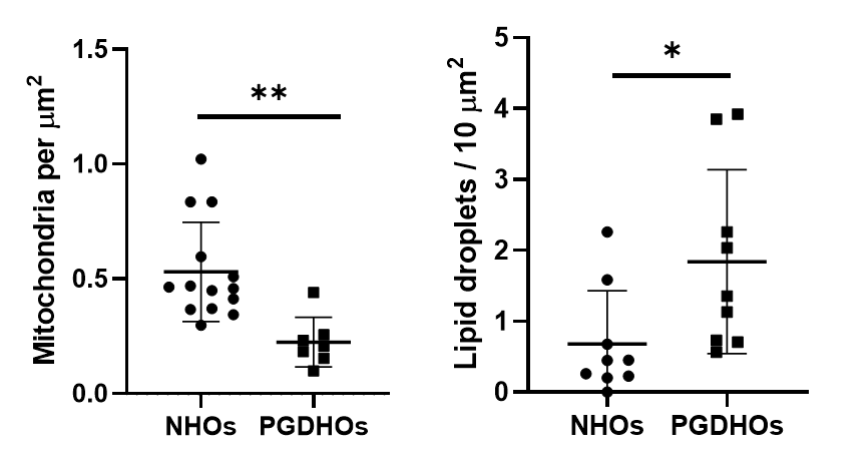


Figure 60. Decrease mitochondrial and increased lipid droplet count in PGDHOs. (**left**) Number of Mitochondria per μ m2 as seen in TEM images of NHOs and PGDHOs (value = mean \pm SD, n=6, two-tailed, unpaired t-test, **p=0.0024). (**right**) Quantification of lipid droplets per 10 μ m²; value = mean \pm SD; n=9, two-tailed, unpaired t-test, *p=0.033.

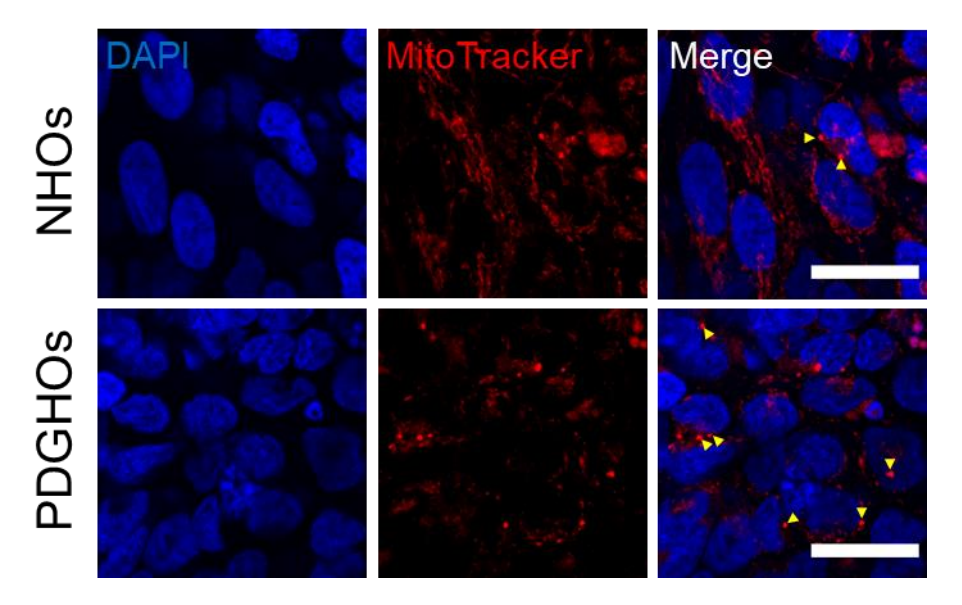


Figure 61. Mitochondrial swelling fluorescent images. High magnification fluorescence microscopy of mitochondria stained with MitoTracker (red) and DAPI (blue), in healthy (**top**) and diabetic (**bottom**) organoids. Arrowheads indicate swollen mitochondria. Scale bar: 25 µm (n=5 organoids per condition).

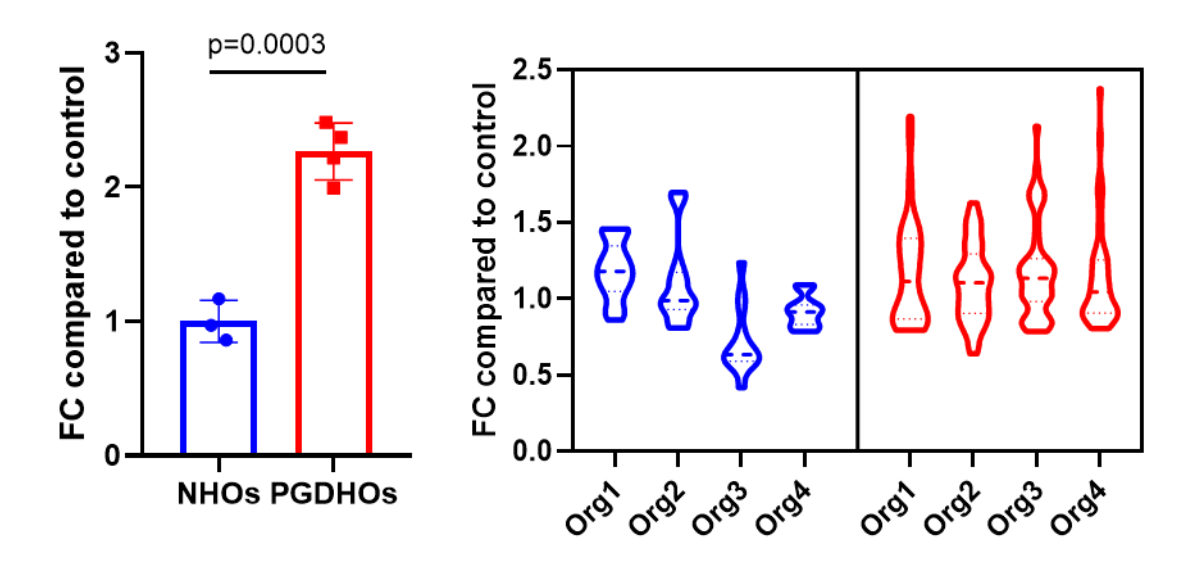


Figure 62. Mitochondrial swelling quantification showing fold change per organoid (**left**) and swollen mitochondrial width distribution (**right**), indicating mitochondrial dysregulation in response to diabetic condition during organoid development. Mean ± SD, n=4 (NHOs) and n=4 (PGDHOs). Org = organoid.

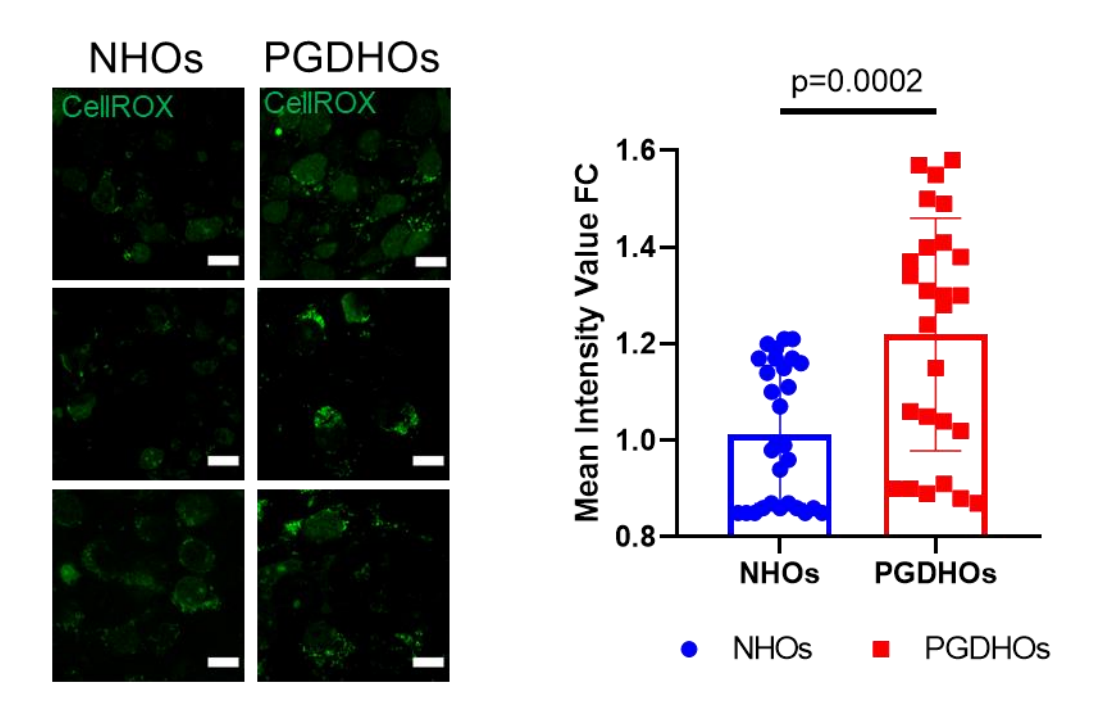


Figure 63. Reactive oxygen species in NHOs and PGDHOs. (**left**) Immunofluorescence images of representative live NHOs and PGDHOs stained with the reactive oxygen species molecular probe CellROX Green, and (right) fold change mean intensity value of z-plane images form NHOs (n=29 z-plane images from 3 organoids) and from PGDHOs (n=26 z-plane images from 4 organoids). Value = mean \pm SD, unpaired t test; scale bar: 10 μ m.

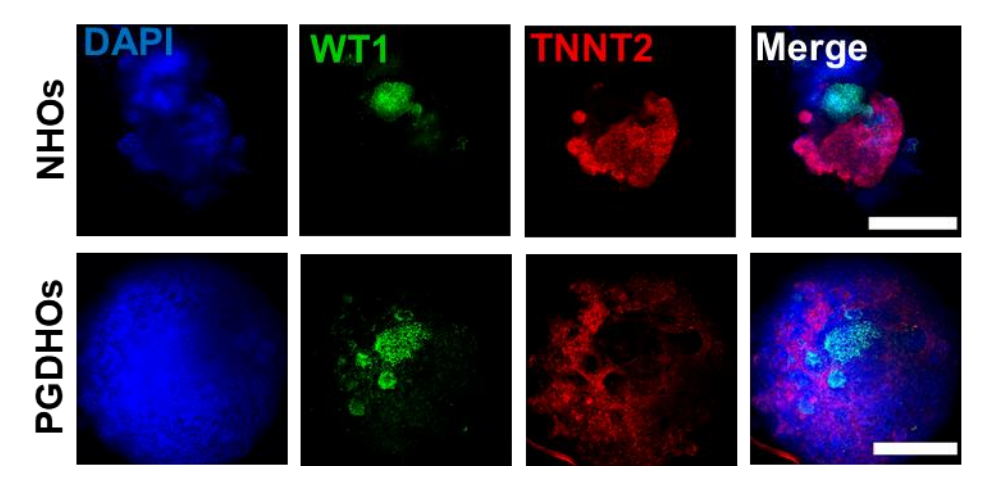


Figure 64. Myocardial and epicardial organization in NHOs and PGDHOs. Confocal immunofluorescence images at differentiation day 15 for cardiac (TNNT2, red) and epicardial (WT1, green) formation, scale bar: 500µm.

5.2.2. Pathological atrioventricular specification and vascular formation

Compared with normal glycemic conditions, diabetic hHOs showed decreased MYL2+ ventricular CMs and enlarged MYL7+ atrial cardiomyocyte regions, indicative of structural defects such as those observed in CHD (**Figure 65**). Furthermore, the PGDHOs showed less defined separation between the areas of

ventricular and atrial CMs compared with the NHO controls. Furthermore, while the formation of a vascular network emerged in hHOs under both the control and diabetic conditions, a drastic difference in the organization was observed. The marker PECAM1 revealed a sophisticated plexus of vascular endothelial tissue covering large portions of the control NHOs (**Figure 66**). Vascularization in PGDHOs appeared less organized and not as far-reaching compared to NHOs, showing regions of PECAM1 staining and large congregations of vessels as opposed to a more mesh-like organization that was characteristic in the NHOs (**Figure 66**).

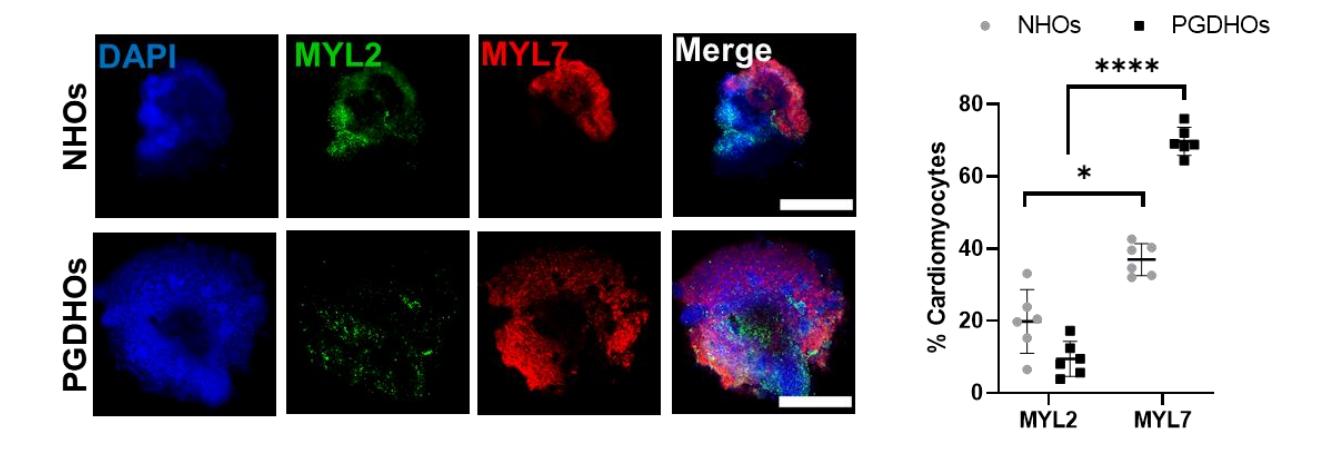


Figure 65. Atrioventricular organization in NHOs and PGDHOs. (**left**) Confocal imaging for ventricular (MYL2, green) and atrial (MYL7, red) chamber formation under normal and diabetic-like conditions, scale bar: 500μm. (**right**) Percentage area of MYL2+ and MYL7+ regions in NHOs and PGDHOs showing ventricular and atrial cardiomyocytes markers, respectively (value = mean ± SD, n=4, 2-way ANOVA Sidak's multiple comparisons test). *p=0.012, *****p<0.0001, otherwise ns: no significance).

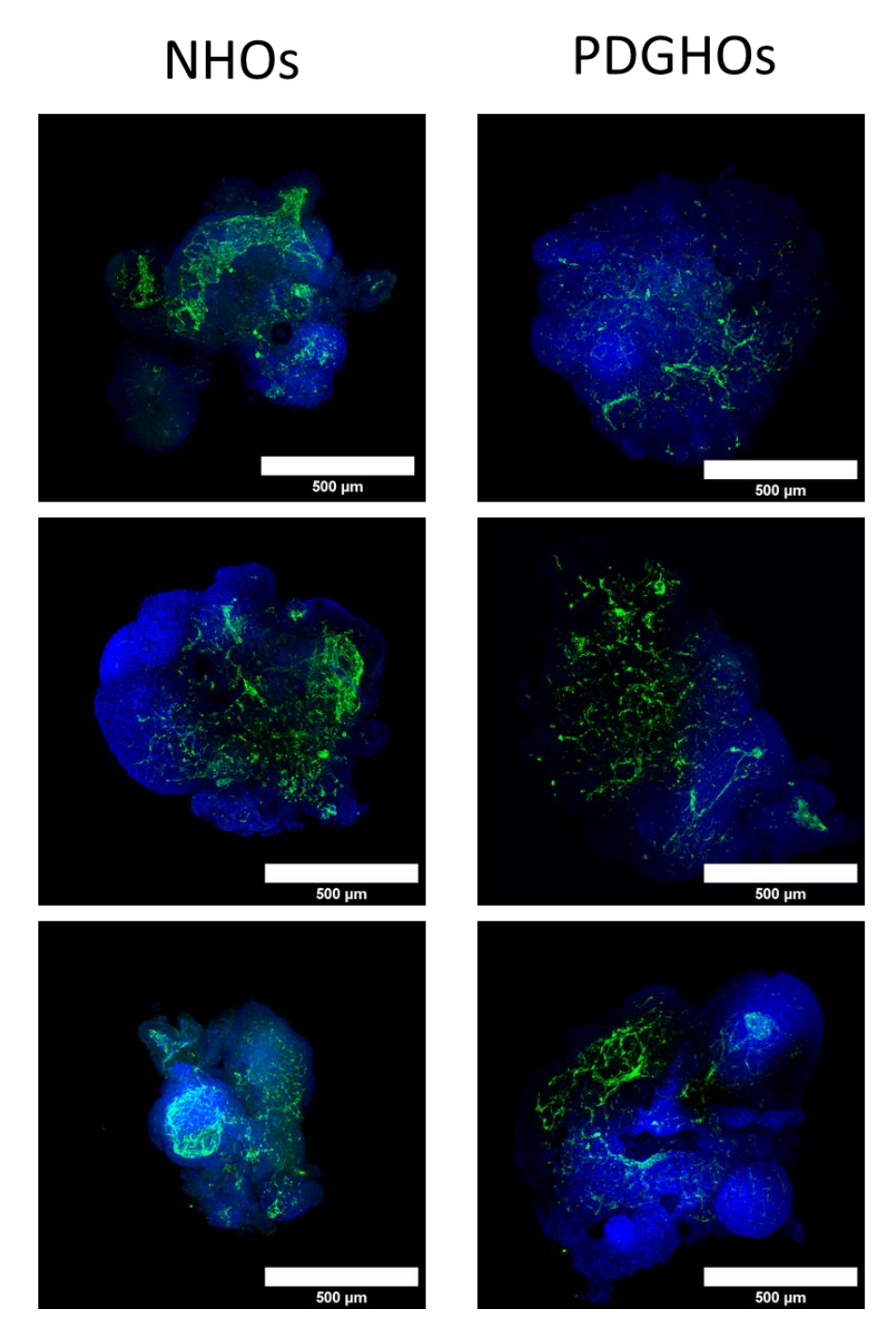


Figure 66. Vascular self-assembly in NHOs and PGDHOs. Maximum intensity projection confocal immunofluorescence images showing endothelial marker PECAM1 (green) showing a defined network of vessels throughout the control NHOs (**left**) and diabetic PGDHOs (**right**) organoids. Scale bar: 500 μm.

5.2.3. Functional analysis of PGDHOs show increased arrythmias and decreased beat frequency in response to PGD

Electrophysiological analysis was performed as discussed in section <u>4.2.5</u>, using both direct recordings on an MEA (**Figure 67**) and showed an irregular frequency of action potentials in PGDHOs suggesting arrhythmic events (**Figure 67**). To validate the recordings from the MEA, calcium transient analysis by live organoid imaging was conducted. The beating frequency of the control organoids was about 120 beats per minute (bpm) compared to about 60 bpm in the diabetic organoids (**Figure 68**). Fetal heart rate can range from 110 to over 160 bpm²⁴⁹, with slower fetal heart rate long known to be associated with poor pregnancy outcomes²⁵⁰.

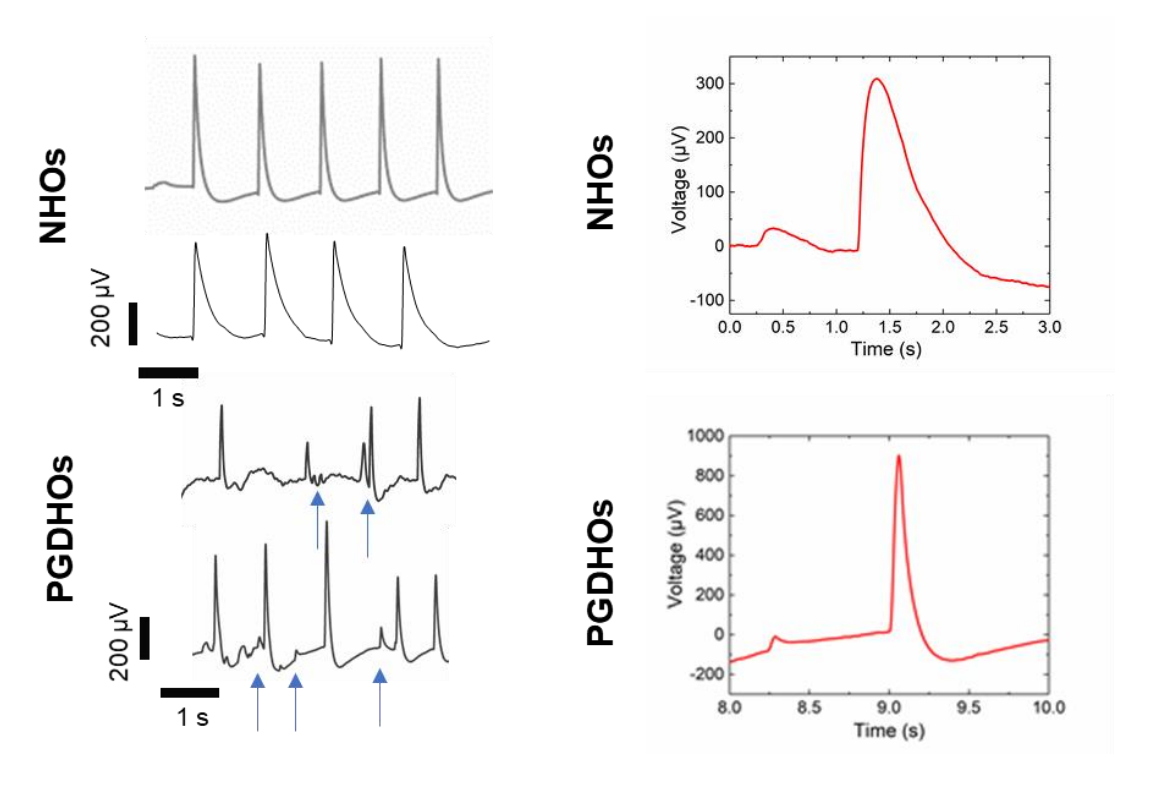


Figure 67. Electrophysiology performed on NHOs and PGDHOs at 15 days. Direct recordings of organoid electrophysiology on MEA. Arrows indicate arrhythmic events, and representative MEA electrophysiology action potential wave of normal vs. diabetic organoids. MEA recordings were conducted in collaboration with Weyang (Li Lab).

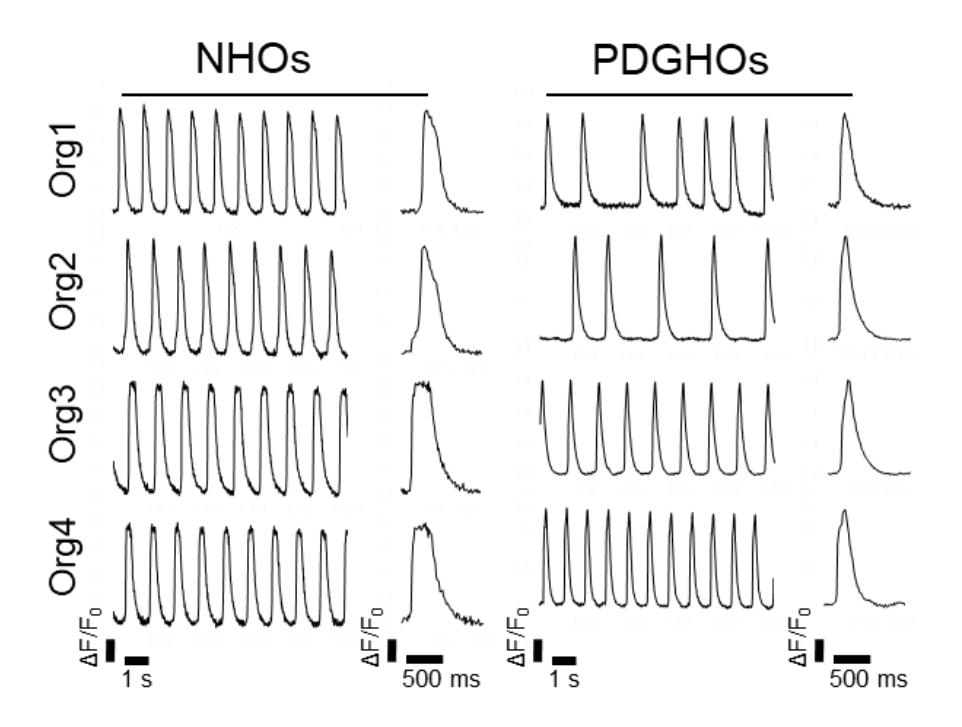


Figure 68. Ca2+ transients in 4 NHOs (**left**) and 4 PGDHOs (**right**), showing representative recordings. Calcium transients in healthy organoids are consistent and reproducible, while organoids grown under diabetic conditions exhibited irregular calcium transients. Org = organoid.

5.2.4. Single cell RNA-Seq identifies diverse cellular response to pregestational diabetes in organoids

To explore the cellular discrepancies that arise as a result of hHO differentiation and development under diabetic conditions, single-cell RNA-Sequencing (scRNA-Seq) was performed. 4 organoids from each condition were dissociated into a single-cell suspension and pooled prior to sequencing. *k*-mean clustering revealed 6 distinct cell lineage populations in both NHOs and PGDHOs, presented using t-distributed stochastic neighbor embedding (t-SNE) dimension reduction (**Figure 69**). These include a cluster of CMs, immature CMs, cardiac fibroblasts, epicardial cells, and endothelial cells. A notable decrease in the number of cells in the CMs and immature CMs clusters can be seen in the PGDHOs, while the number of cells in the epicardial cluster increases by over 800% (**Figure 69**,**Figure 70**), hinting at dysregulation of cardiomyocyte differentiation and at epicardial activation, often associated with response to injury and regeneration²⁵¹. **Figure 71**, presents t-SNE plots of key genes expressed by these clusters. The largest of the cluster was that of cardiac fibroblasts (representing ~39% and ~42% in NHOs and PGDHOs, respectively), which were characterized by genes including *THY1*, *COL1A1*, and *COL3A1*. Gene ontology

(GO) analysis of each cluster is presented in **Figure 72**, showing the similarities between clusters from NHOs and PGDHOs, with highly influential genes shown in larger font.

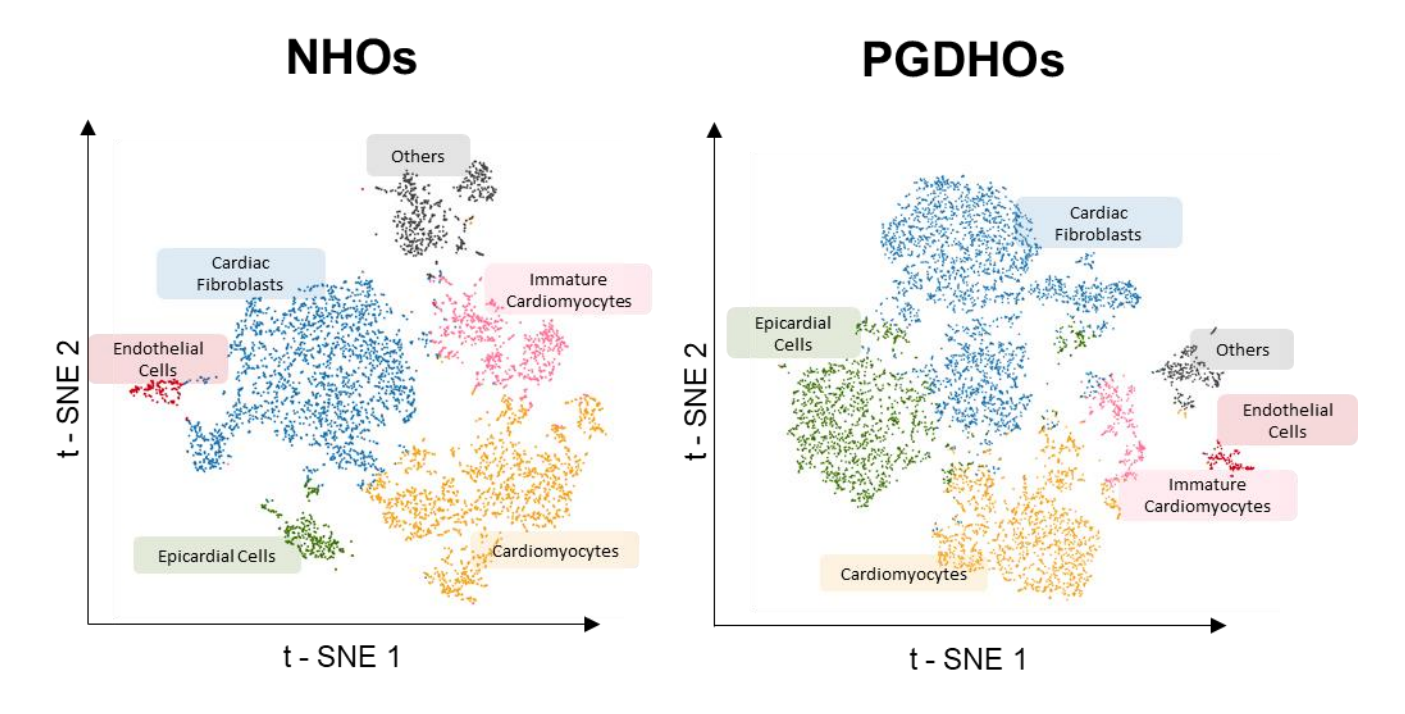


Figure 69. scRNA-Seq shows complex cardiac lineage clustering in healthy and diabetic organoids at day 15. t-SNE plots showing 5,951 cells from 4 pooled dissociated NHO organoids (**left**) and 7,463 cells from 4 pooled dissociated PGDHO organoids (**right**), colored by automatic k-mean clustering. Each cluster was named based on the expression of key genes in the respective cell populations. Library preparation and sequencing was conducted by the MSU Genomics Core.

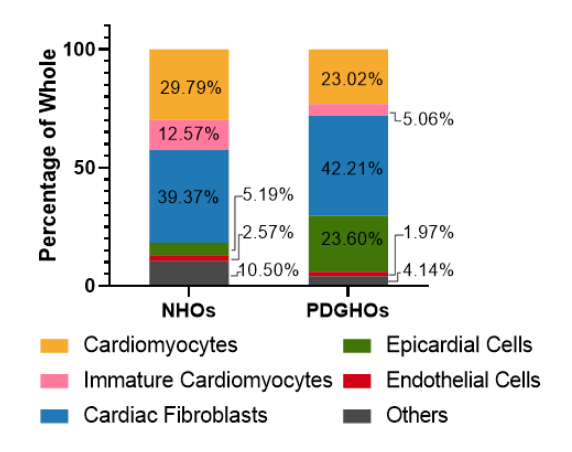


Figure 70. Percentage of respective cell clusters from healthy and diabetic organoid cell populations. Single cell sequencing data revealed some differences in the cell type compositions that resulted from organoids grown under healthy vs diabetic conditions.

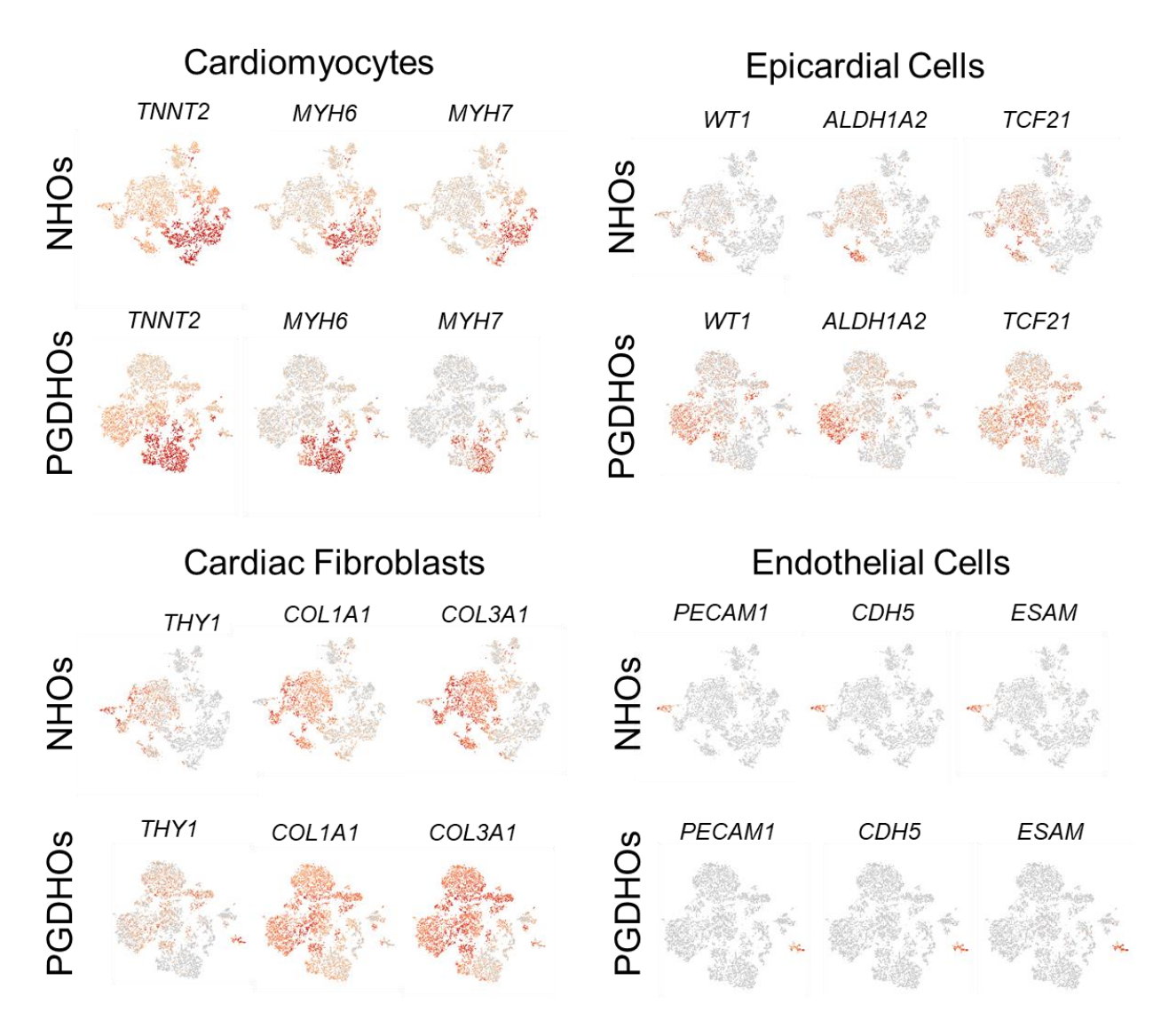


Figure 71. Relative expression of genes of interest across clusters shown in the NHOs t-SNE (**top**) and in the PGDHOs t-SNA (**bottom**) plots. These show some of the key features observed in clusters that define main cell type populations in the organoids.

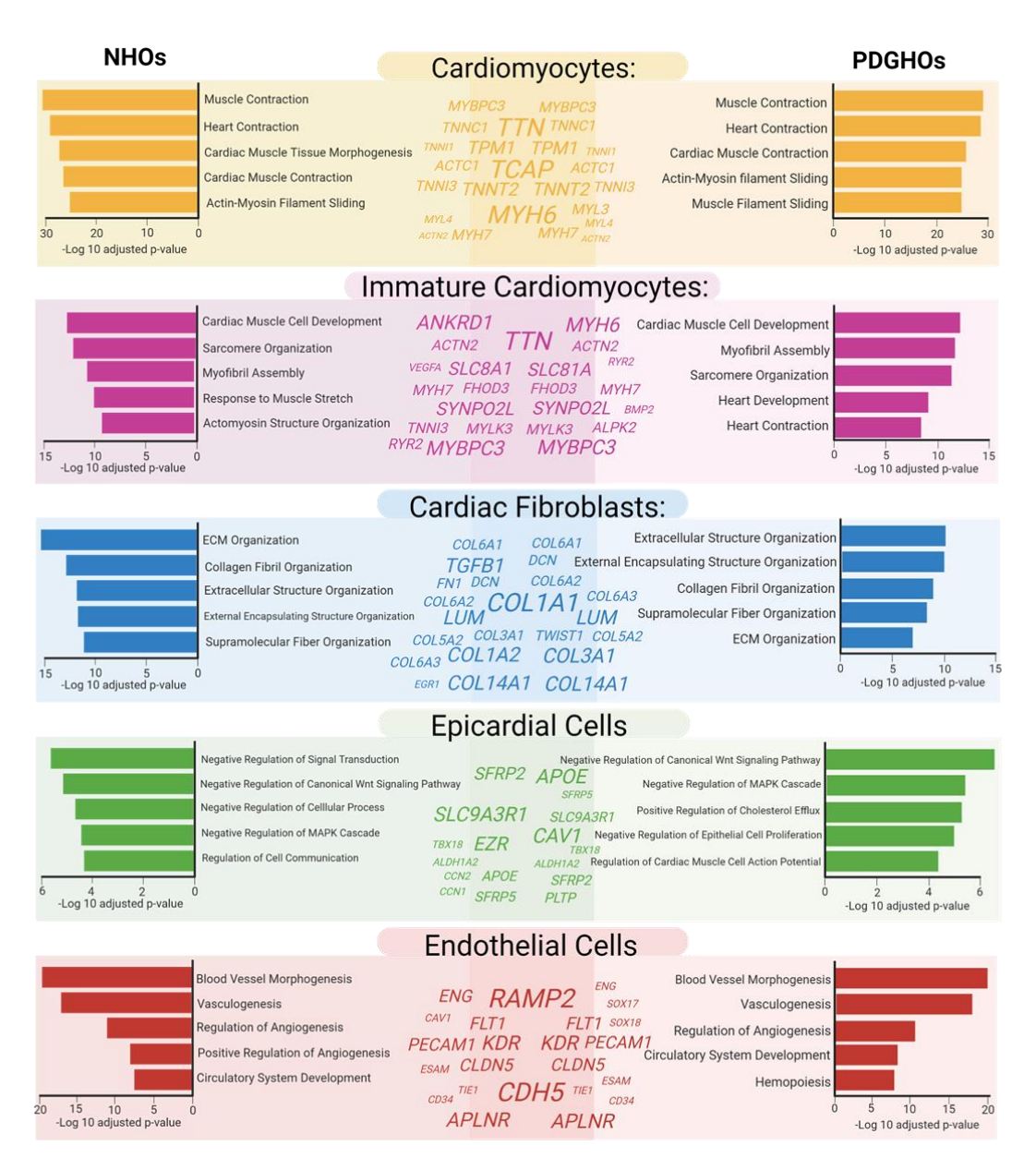


Figure 72. Gene ontology analysis of biological processes associated significantly expressed genes in respective clusters showing NHOs ontology on the left and PGDHOs ontology on the right. Genes that most influence the gene ontology appear larger, with genes on the left side and right side of the center line being associated with NHOs and PGDHOs, respectively.

5.2.5. Pregestational diabetic conditions trigger molecular responses underlying the risk of CHD

To better understand the transcriptomic differences between NHOs grown in healthy conditions and PGDHOs grown in diabetic conditions, differentially expressed genes (DEG) for the clusters in (**Figure 69**), were identified and analyzed with GO. Key differences in GO were revealed from DEGs of all clusters and can be used for further investigation into potential mechanisms behind PGD-CHD and investigation into

targeted therapeutics (Figure 73). For example, bioinformatics analysis revealed 379 DEGs in the CM cluster, 223 and 156 significantly expressed genes distinct to NHOs and PGDHOs, respectively. GO for upregulated DEGs showed a focus on mitochondrial respiration and ATP synthesis in NHOs, while downregulated DEGs were associated with vessel morphogenesis, cell differentiation, and proliferation. In contrast, GO DEGs in PGDHOs revealed upregulation of genes related to negative regulation of metabolic processes and differentiation of non-myocytes, and downregulation of translation processes and protein targeting to the ER. These hint at developmental issues in CMs of PGDHOs related to protein translation and ER function. DEG analysis revealed 373, 289, and 315 significantly expressed DEG for the cardiac fibroblasts, epicardial and endothelial cell clusters, respectively (Figure 73). No significantly expressed DEGs were found in the immature CMs cluster, likely due to the heterogeneous nature of the cluster and variability of progenitor stages of CM development. qPCR was performed on NHOs and PGDHOs every other day between days 0 and days 14, looking at expressions of key transcription factors (HAND1, HAND2, GATA4, GATA5, NKX2-5, and TBX5) and well as two glucose transporters (SLC2A1 and SLC2A4)(Figure 74). NHOs displayed a clear transition in the expression of the FHF marker HAND1 which was highly expressed between days 2 and 8, and the expression of the SHF marker HAND2 which was highly expressed from days 8 onwards. Both heart field markers were downregulated in PGDHOs compared to NHOs at most critical time points. GATA4, NKX2-5, and TBX5 all showed overexpression in the PGDHOs which was not present in their control counterparts, the first two showing an early overexpression on day 6 and the latter showing an overexpression on days 12 and 14. NHOs show a clear transition between the glucose transporter SLC2A1 (highly expressed in the fetal heart) and the glucose transporter SLC2A4 (highly expressed in the adult heart), between days 6 and 8, corresponding to the switch to media with insulin as seen in the differentiation protocol (Figure 10). On the other hand, PGDHOs show downregulation of SLC2A1 in the early days of differentiation, hinting and possible dysfunction in glycolysis (Figure 74). To visualize the discrepancies in the cell population arising from the two heart fields, t-SNE plots for key FHF markers (HAND1, HCN4, TBX5) and key SHF markers (HAND1, ISL1, TBX1) were overlayed for NHOs and PGDHOs (Figure 75). Interestingly, cell populations from NHOs that showed expression of FHF markers cells were predominantly in the CM and immature CM clusters while many of the SHF marker-expressing cells appeared throughout the clusters in myocyte and non-myocyte cell populations. This observation is in agreement with the precardiac organoids derived from mouse ESCs demonstrating the development of non-myocyte cells from SHF progenitor cells²⁵². The expression profile in the PGDHO t-SNE plot was less clear-cut, with both FHF and SHF markers being expressed in most clusters, suggesting a dysfunction in early heart field differentiation and lineage specification.

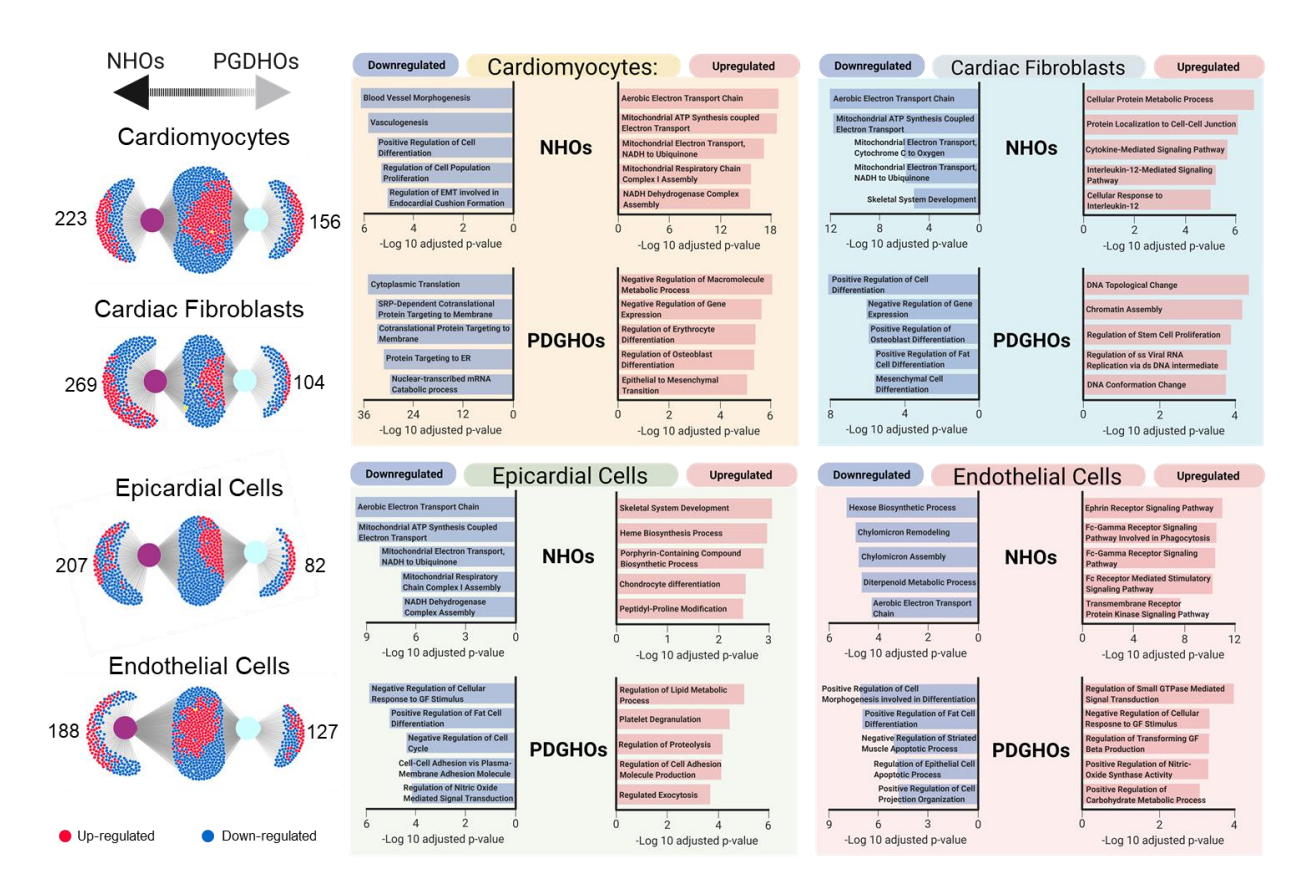


Figure 73. Differentially expressed genes from clusters and their corresponding ontology. Showing significantly upregulated genes (red) and significantly downregulated genes (blue). Genes expressed exclusively in NHOs or PGDHOs are shown on the left or right, respectively, with genes that are expressed in both appearing in the middle. Corresponding gene ontology graphs are on the right for each cluster's downregulated (blue, **left**) and upregulated (red, **right**) for NHOs (**top**) and PGDHOs (**bottom**).

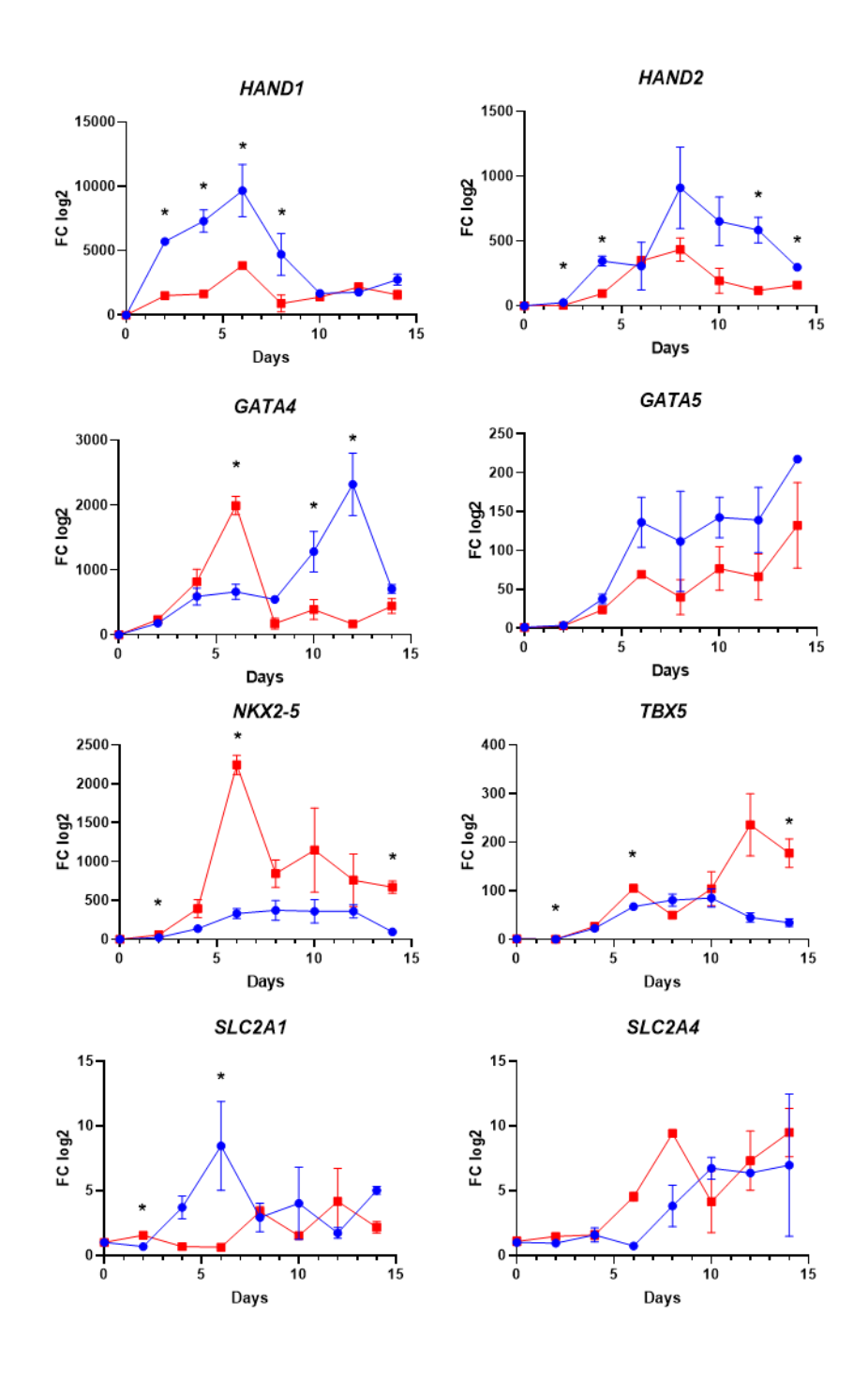


Figure 74. qRT-PCR gene expression of key transcription factors and glucose transporters that are central to cardiac development and glucose metabolism between days 0 and 14. Fold change is compared to day 0 EBs. Blue and red lines represent NHO and PGDHO gene expression, respectively. Each datapoint represents 3 replicates of 3-4 pooled organoids for each time point per condition (n=9-12 organoids per timepoint per condition). Value = mean \pm SEM. *p<0.05.

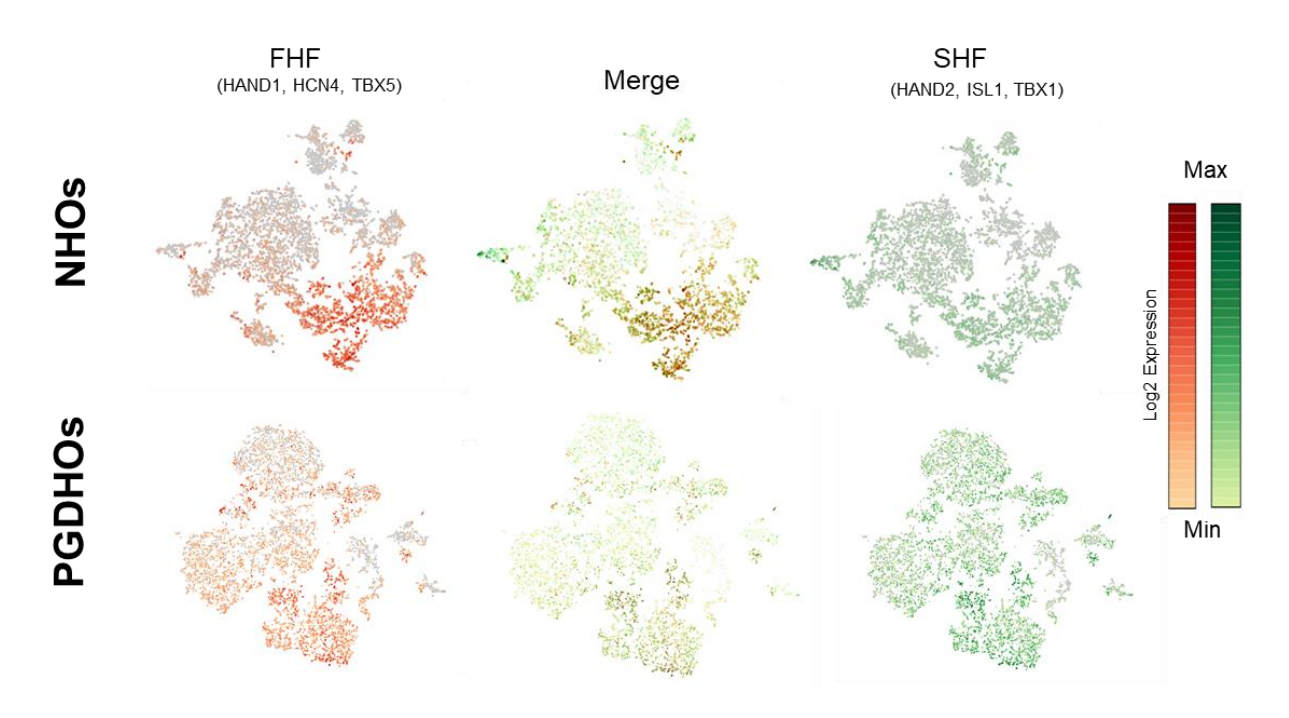


Figure 75. Heart field t-SNE plots showing FHF markers (**left**), SHF markers (**right**), and an overlay of both heart field markers (**center**), for NHOs (**top**) and PGDHOs (**bottom**). Gene expression is shown as relative Log2 fold change.

5.2.6. Metabolomics analysis reveal disparities in glycolysis and fatty acid concentrations in PGDHOs

To achieve a full picture of the effect of diabetic conditions on developing human heart organoids, the metabolic profile of PGDHOs was compared to that of NHOs. Firstly, metabolic assays for glycolysis and oxygen consumption revealed decreased oxygen consumption rate in day 15 PGDHOs and increased glycolysis when compared to cells dissociated from NHOs (Figure 76). By day 15 the hHOs are expected to transition from a glycolysis-based metabolism to a more mature oxidative phosphorylation-based metabolism, as is suggested by the glucose transporter qPCR plots for NHOs (Figure 74). High Performance Liquid Chromatography Mass Spectrometry (HPLC-MS) metabolomic profiling revealed insightful discrepancies between PGDHOs and NHOs (Figure 77). Given the well contained nature of the organoids – with individual organoids in a single well without exogenous sources of lipids aside from essential fatty acids (linoleic and linolenic acid) – all other fatty acids present are therefore synthesized by the organoids to be used in intracellular signaling for to be secreted into the media. This data revealed that the hyperglycemic and hyperinsulinic condition resulted in a lipid imbalance in the very long chain fatty acids (VLCFA), which have been previously shown to be instrumental during heart development 135,253,254.

Furthermore, a closer look at omega-3 polyunsaturated fatty acids (PUFA) suggests that PGDHOs experience ER stress (**Figure 78**) which may be a result or the cause of the VLCFA imbalance. To further explore the mechanism of ER stress as a result of the diabetic conditions, hHOs were co-stained with CellROX Green and ERTracker Red, and revealed that the increase in reactive oxygen species previously discussed (**Figure 63**) is localized to the ER (**Figure 79**). ER stress has not been described in animal models and may be a human-specific phenotype, constituting a potential target for therapeutics.

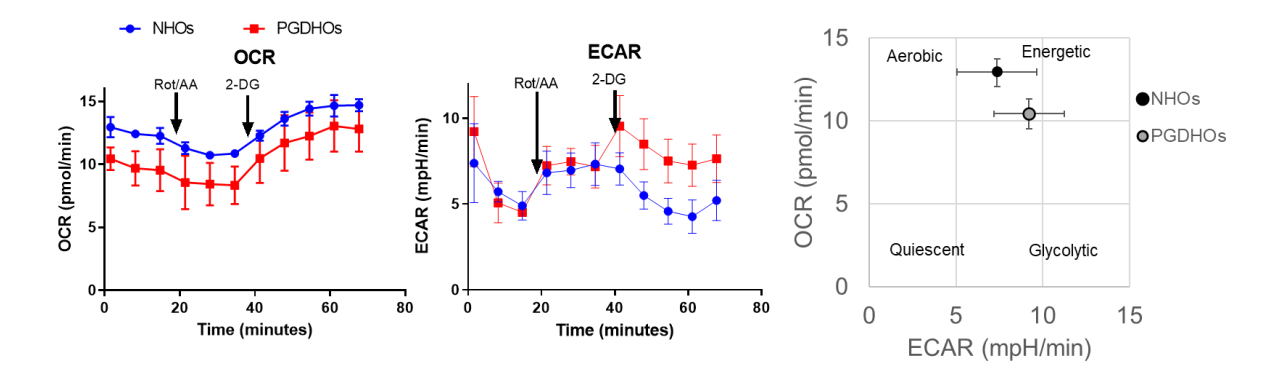


Figure 76. Seahorse analysis for (**left**) oxygen consumption rate (OCR), and (**middle**) extracellular acidification rate (ECAR) of normal and diabetic hHOs (Value = mean \pm s.d; n=3 organoids per condition). (**right**) Seahorse energy map of normal and diabetic-like organoids (value = mean \pm s.d, n=6). 2-DG: 2-deoxy-D-glucose, ECAR: extracellular acidification rate, NHOs: normal heart organoids, OCR: oxygen consumption rate, PGDHOs: pregestational diabetes heart organoids, Rot/AA: Rotenone and Antimycin A.

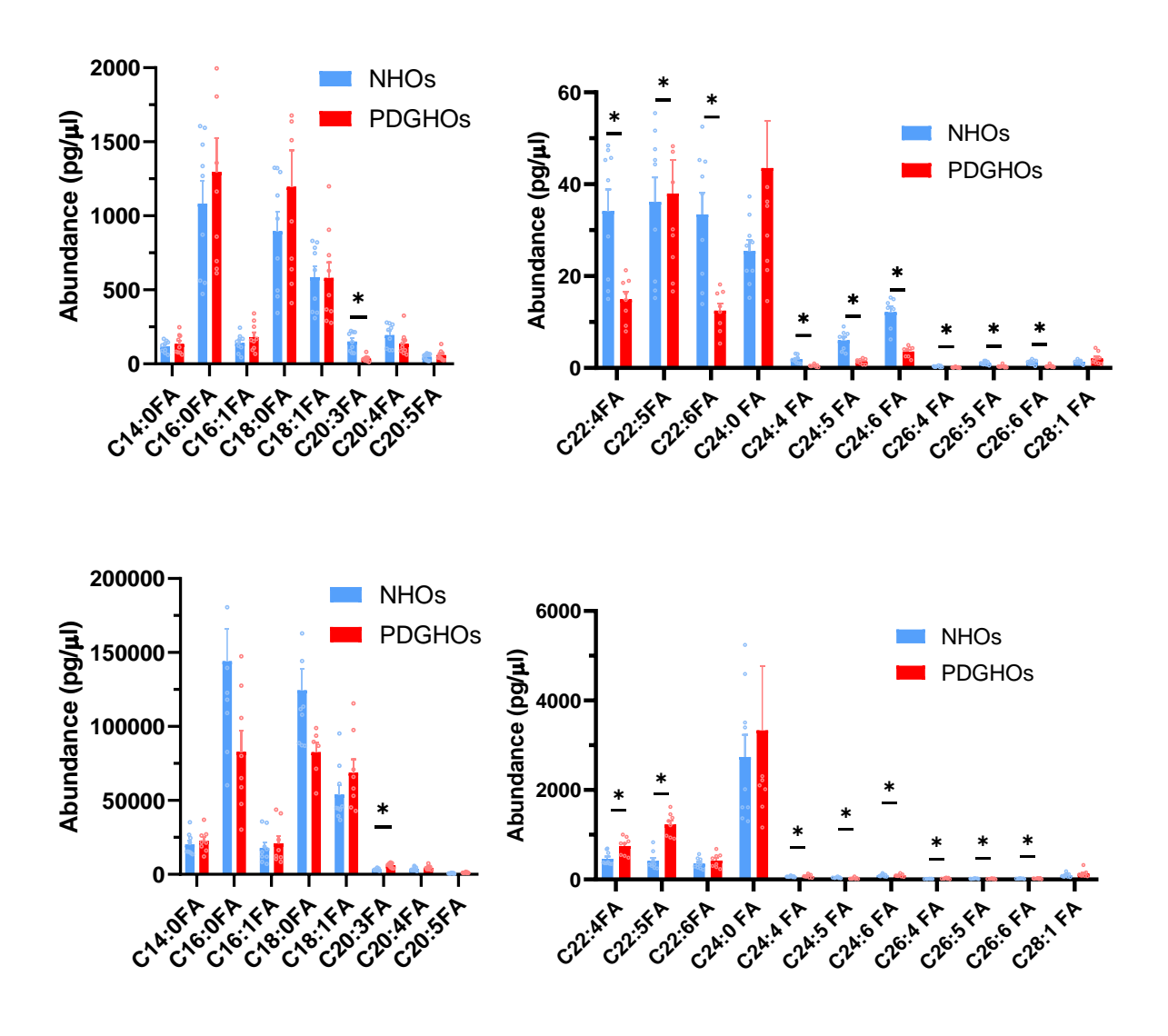


Figure 77. HPLC-MS metabolomic analysis of long chain fatty acids (LCFA; **left**) and very long chain fatty acids (VLCFA; **right**) concentrations from day 15 media (**top**) and day 15 organoids (**bottom**) comparing NHOs (blue) and PGDHOs (red). (n=9 organoids per condition, value = mean ± SD, multiple unpaired t-tests, *p<0.05).

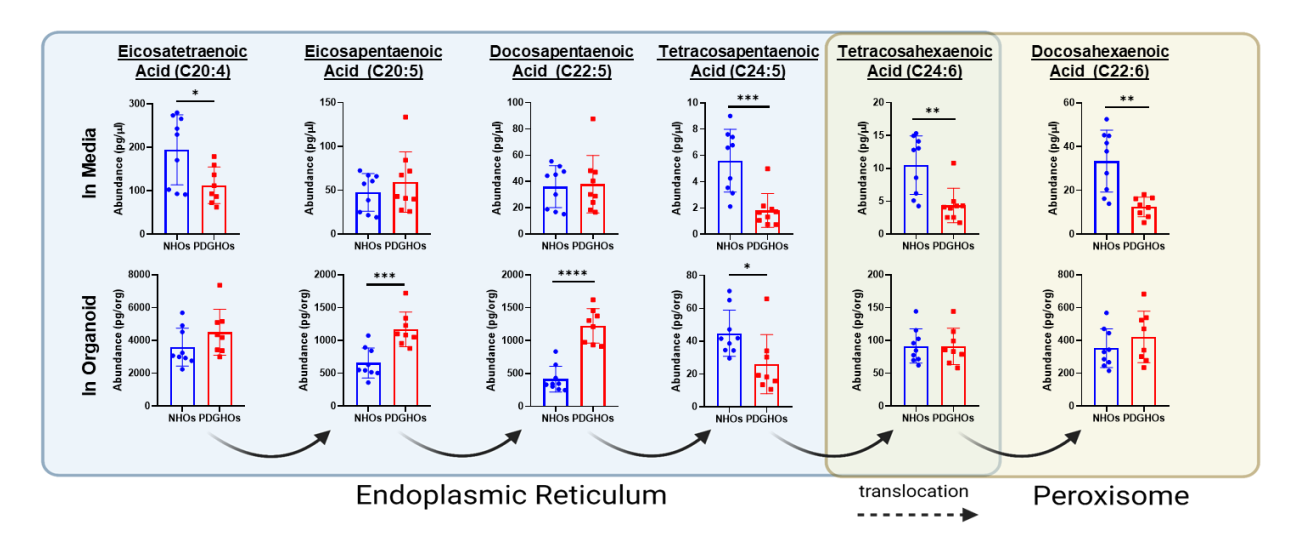


Figure 78. Concentrations of omega-3 polyunsaturated fatty acids (PUFA) from day 15 organoids and their corresponding media in control (NHOs) and diabetic (PGDHOs) conditions, extracted from the LC-MS data in **Figure 77**, showing dysregulation in abundance between the two conditions. These omega-3 PUFA are synthesized by a series of enzymatic desaturation and elongations taking place in the ER and the peroxisome. (n=9 organoids per condition, value = mean \pm SD, multiple unpaired t-tests, *p<0.05, **p<0.01, ****p<0.001).

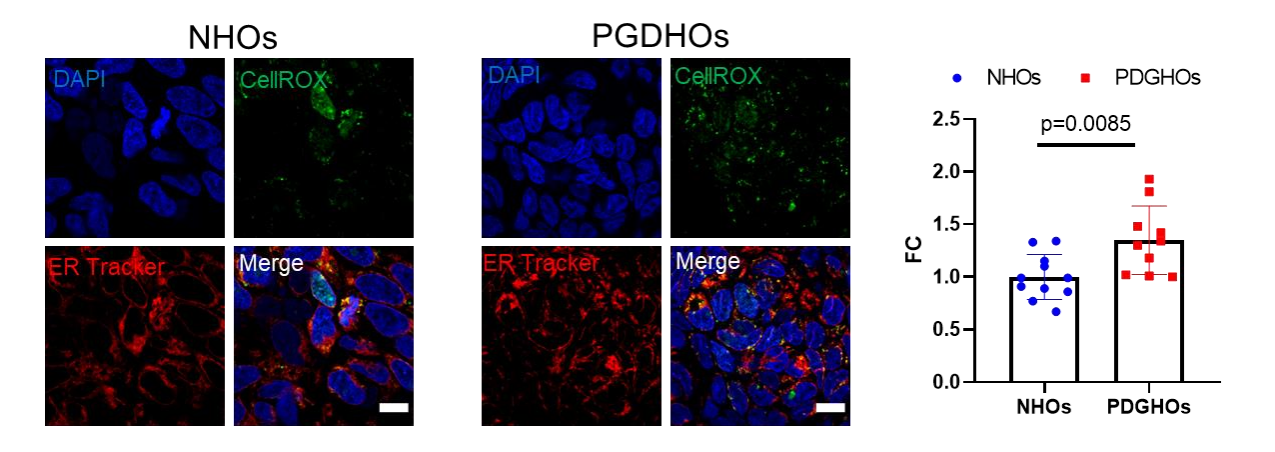


Figure 79. Localization of reactive oxygen species in the ER. Immunofluorescence images of representative NHOs (**left**) and PGDHOs (**center**) showing localization of reactive oxygen species marked by CellROX (green) in the ER of PGDHOs marked by ER Tracker (red); DAPI nuclear stain (blue); scale bar: 10 μ m. (**right**) Fold change compared to NHOs of measured relative percentage of ROS in the ER (n=10 organoids per condition; value = mean \pm SD, unpaired t test).

5.3. DISCUSSION

This chapter describes in detail how to utilize the heart organoid technology described in previous chapters for the study of PGD-CHD in humans, bridging the gap between rodent studies and the true human fetus. First, embryoid bodies (EBs) from hiPSCs are generated in individual wells allowing for independent samples. Then, cardiac mesoderm and subsequent epicardial specification are induced under healthy and

diabetic conditions, facilitating a platform to model the effects of pregestational diabetes in the developing human heart (**Figure 3**). Finally, several avenues of analyses of the fetal-like cardiac organoids highlighting characteristics features of congenital heart defects caused by the hyperglycemic and hyperinsulinemic environment are presented.

To model the effects of PGD, hHO culture conditions were modified to reflect reported physiological levels of glucose and insulin in normal mothers (3.5 mM glucose, 170 pM insulin, normoglycemic hHOs or NHOs), and reported diabetic conditions for females with type I and type II pregestational diabetes (11.1 mM glucose and 1.14 nM insulin, pregestational diabetes hHOs or PGDHOs)^{161,162}. Maternal diabetes is one of the most common causes of newborn CHD (up to 12% of newborns from diabetic mothers have some form of CHD²³⁶), yet the ability to study the etiology of these disorders in humans is greatly limited due to inaccessibility to human fetal hearts at crucial stages of development. The effects of PGD on CHD has been studied extensively in animal models, identifying many contributing factors including the dysregulation of lipid metabolism^{255,256}, an increase in oxidative stress^{113,248,257}, and dysregulation of key transcription factors related to heart development^{99,105–107,111–113}. However, the extent of the ability of these animal models to properly recapitulate human PGD-CHD abnormalities is limited by cross-species differences. hHOs provide the necessary platform on which to investigate the underlying mechanisms between the association of PGD and CHD in humans.

Using healthy and diabetic levels of glucose and insulin in the differentiation media, hHOs demonstrate the effects of diabetic conditions on the developmental process of the fetal heart model. Organoids developing in healthy conditions displayed active structural changes including patterning, while hHOs in diabetic conditions developed larger in size reminiscent of macrosomia. The larger size of diabetic hHOs also suggests potential signs of cardiac hypertrophy, a hallmark of maternal PGD²⁵⁸. Evident differences were noted with regards to the mitochondria of PGDHOs, revealing a decrease in number and an increase in swelling, in addition to an accumulation of lipid droplets, signifying apparent disfunction in metabolic processes. Furthermore, an increase in reactive oxygen species was observed on a cellular level in live imaging of PGDHOs compared to NHOs. Key structural abnormalities were observed in the PGDHOs, including disorganization of myocardial, epicardial, and endothelial tissue, as well as disruption of atrioventricular specification and organization, hinting at disfunction in early developmental stages. These

structural abnormalities, along with the enlarged size of the organoids may also correspond to the arrhythmias and reduction in beat frequency apparent in the electrophysiology recordings. These impairments in structural/developmental organization, lipid metabolism, and mitochondrial dysfunction in PGDHOs are consistent with expected phenotypes found in PGD-induced CHD in animal models^{113,248,257,259}.

Single-cell transcriptomics provides a valuable tool to investigate cell-specific disparities between healthy and diabetic hearts, which has yet to be explored in human tissue and has only very recently been explored in animal models²⁶⁰. Single-cell RNA-Sequencing (scRNA-Seq) was performed on day 15 PGDHOs and NHOs, revealing clear differences in cardiac lineage specifications including a reduction of cardiomyocytes and a significant expansion of epicardial tissue. As these organoids recapitulate the human fetal heart, such differences will likely result in severe malformations later in development. Gene ontology analysis showed general consistency between the clusters from the PGDHOs and NHOs, nevertheless, closer investigations into the differentially expressed genes (DEGs) from the different clusters revealed interesting findings. All the clusters revealed at least 289 significant DEGs, the highest number being attributed to the cardiomyocyte clusters with 379 DEGs. This demonstrates the distinct effects that pregestational diabetes has on specific cell populations and emphasizes the necessity for a complex model of the heart such as this organoid platform. NHO cardiomyocytes showed a focus on mitochondrial respiration and energy synthesis, suggesting that these are disrupted in the PGDHO cardiomyocytes, and may correspond to the mitochondrial dysfunction observed earlier. Mouse models of PGD has shown dysregulation of transcription factors key to heart development, including GATA4, GATA5, TBX5, and NKX2-5^{99,105–107,111–113}. Time course qPCR analysis of PGDHOs and NHOs revealed disparities in the regulation of GATA4, NKX2-5, and TBX5 at different time points throughout development, highlighting the importance observing the etiology of developmental disorders at different stages of development. Moreover, the specification of the FHF and subsequent SHF are crucial in the development and organization of the heart, and the observed downregulation of heart field markers in PGDHOs likely contributes to the structural malformation and under-representation of cardiomyocytes compared to NHOs. Similarly, the downregulation of the glucose transporter SLC2A1 during the early stages of differentiation corresponds suggests disruption in glycolysis may prove to be crucial in the observed metabolic disfunction.

The metabolic profiles of the PGDHOs revealed a clear dysregulation of VLCFA, especially with regards to omega-3 fatty polyunsaturated fatty acids (PUFA). The synthesis of these PUFA mostly takes place in the ER, and, along with the observed ROS that localizes in the ER, suggested an increase ER stress in response to the hyperglycemic and hyperinsulinemic conditions in PGDHOs. This ER stress may hint at a potential underlying mechanism in which PGD increases the risk of CHD, and thus can be used as a target for therapeutic approaches.

In the past few years, 3D human cardiac tissues have been used to model genetic and non-genetic conditions (myocardial infarction, drug cardiotoxicity)^{224,261}. This chapter provides evidence that heart organoids can be valuable models to study CHD in pregestational diabetes-like conditions. Taken together, the data suggest significant molecular and metabolic perturbations between NHOs and PGDHOs consistent with previous studies on PGD suggesting increased oxidative and ER stress, cardiomyopathy, and altered lipid profiles^{113,241,262}, constituting a significant step forward towards modeling metabolic disorders in human organoids.

6. CHAPTER 6: CONCLUSION AND FUTURE DIRECTIONS

6.1. CONCLUSION

Cardiovascular diseases, including congenital heart defects, are a leading cause of death worldwide and constitute a major burden on patients, their families, and on the healthcare system as a whole. Nevertheless, access to human heart tissue, especially at the early stages of development, is often inaccessible resulting in the need to investigate diseases in animal models or *in vitro* cell culture models. These models, however, are greatly limited due to cross-species differences and the lack of complexity of traditional *in vitro* models. There is an urgent need for complex *in vitro* models that closely resemble the human heart.

Recently, 3D organoids derived from human stem cells have emerged, modeling complex tissues and organoids including the brain, intestine, liver, and more. Human heart organoids have been lagging behind other organs. This dissertation describes a highly reproducible and high-throughput human heart organoid generation method relying on self-assembly triggered by developmental cues. The self-assembling hHOs are generated by plating ~10,000 human PSCs per well in 96-well plates, the most cells per aggregate among the reported articles. Using a three-step WNT pathway activation/inhibition/activation, they guided mesodermal induction on days 0-1, cardiogenic mesoderm induction on days 2-4, and a quick, hour-long induction on day 7 to induce proepicardial organ formation. Heart organoids displayed physiologically representative stages of development, showing FHF and SHF markers throughout the protocol as well as the formation of both atrial and ventricular cardiomyocytes (atrioventricular specification). The resulting cardiac organoids had a complex cellular make-up, which included myocardial tissue with interspersed cardiac fibroblasts, epicardial clusters near the outer surface, internal chambers lined with endocardial tissue, and spontaneously forming vasculature. RNA-Sequencing revealed that these organoids closely resemble fetal heart tissue and are much more representative of their in vivo counterparts than in monolayer models. Functional electrophysiological features were observed and describe several hallmarks of tissue maturation, such as the presence of t-tubules, organized mitochondria, and oxidative metabolism. The method described presents a better model of the human heart compared with animal models and traditional in vitro models is the recapitulation and close resemblance to the fetal human heart. It further prevails over other heart organoid methods recently described due to the sophisticated complexity, physiological-like

self-assembly, and the simplicity of the single protocol nature of the derivation method, negating the need for complex multi-protocol organoid assembly.

As proof of concept for the utilitarian aspect of this organoid platform, the modeling of a congenital heart disorder is demonstrated, exploring associations between pregestational diabetes and the risk of congenital heart defects in human tissue. Pregestational diabetes organoids showed notable structural, metabolic, and functional differences between organoids cultured in healthy versus diabetic conditions. These results unmistakably illustrate the capacity of these organoids to be used to model features of pregestational diabetes-induced congenital heart disease that are unique to humans and might thus constitute useful models for the study of the molecular pathology of congenital heart disease in humans in the future.

6.2. LIMITATIONS

Although our technology offers exciting opportunities to model human congenital heart disease *in vitro*, significant limitations still exist. First, organoids tend to deviate from their normal developmental pathway as a function of time, becoming less relevant the longer they are cultured. Second, their ability to recapitulate heart development is still limited when compared to other existing models, such as mice, even though they have the significant advantage of being human in origin rather than a surrogate animal model. Other limitations of organoid work include a microenvironment which is sometimes lacking, particularly as the organoids age and real organs get more complex. Protocols for organoid generation and quality control are not globally standardized, affecting reproducibility, and their production and maintenance are relatively expensive compared to traditional cell lines or animal models. Lastly, the cells and tissues present in these organoids are immature and fetal in nature, and, therefore, future studies into the maturation of self-assembled heart organoids will be necessary for modeling the adult human heart to explore associated diseases and toxicity studies.

6.3. IMPLICATIONS AND FUTURE DIRECTIONS

Human organoid cultures present several advantages over animal models: first and foremost, they constitute a human model, and are more readily accessible than mouse fetuses. Organoids can be easily followed over time *in vitro*, and culture conditions can be tailored to specific purposes. They can also be systematically produced in large quantities for high-throughput or high-content screenings. The project described herein fills the gap in CHD modeling and the importance of generating simple and easily scalable

in vitro models of the fetal heart and utilizing them in modeling diseases affecting the developing human heart. The human heart organoid platform described here accurately recapitulates the functional and structural features of the fetal human heart. iPSCs provide the ultimate source for capturing the essence of human development and genetic diseases outside of clinical work. The data suggest highly efficient hHOs from multiple iPSC and ESC cell lines in a rapid and scalable way. The emergence of self-organizing tissues such as endothelial vascularization and endocardial chamber formation merit more in-depth investigation in future studies. For example, further studies into the functionality of the observed vascular tissue will be necessary, particularly to determine the maturity of the vessels, their levels of connectivity, and if they closely resemble coronary vasculature. This latter feature would open the door to modeling coronary vasculature pathologies that arise due to CVD and metabolic disorders.

Lastly, this research deepens the understanding of *in vitro* PSC-derived cardiac developmental models and expands on the currently poorly understood association between pregestational diabetes and congenital heart defects in humans. Furthermore, the ability to identify human phenotypes and cell-type-specific responses to pregestational diabetes allows the use of these hHOs in the screening of therapeutic targets to help mediate the observed dysfunctions, dysregulations, and deformities. Lastly, this model of the fetal human heart is not limited to PGD and can be used for other diseases affecting the developing human heart such as Danon Disease and other generic or environmentally caused disorders. There is a large room for improvement in the technology, particularly in trying to better recapitulate morphological and anatomical features and inducing the formation of effective vascular networks that can provide nutrients. Nevertheless, it has the potential for highly efficient and scalable therapeutic screening capabilities for developmental and environmentally affected heart diseases and to revolutionize the future of cardiovascular development, maturation, and pharmacological modeling.

REFERENCES

- 1. Virani, S. S. *et al.* Heart Disease and Stroke Statistics—2020 Update: A Report From the American Heart Association. *Circulation* **141**, (2020).
- 2. Hoffman, J. I. E. & Kaplan, S. The incidence of congenital heart disease. *J Am Coll Cardiol* **39**, 1890–1900 (2002).
- 3. Gilboa, S. M. *et al.* Congenital Heart Defects in the United States. *Circulation* **134**, 101–109 (2016).
- 4. Pierpont, M. E. *et al.* Genetic Basis for Congenital Heart Defects: Current Knowledge. *Circulation* **115**, 3015–3038 (2007).
- 5. Marelli, A. J. *et al.* Lifetime Prevalence of Congenital Heart Disease in the General Population From 2000 to 2010. *Circulation* **130**, 749–756 (2014).
- 6. Oster, M. E. *et al.* Temporal Trends in Survival Among Infants With Critical Congenital Heart Defects. *PEDIATRICS* **131**, e1502–e1508 (2013).
- 7. Navaratnam, D. *et al.* Exercise-Induced Systemic Venous Hypertension in the Fontan Circulation. *The American Journal of Cardiology* **117**, 1667–1671 (2016).
- 8. Gilboa, S. M. *et al.* Congenital Heart Defects in the United States. *Circulation* **134**, 101–109 (2016).
- 9. Correa, A. Pregestational Diabetes Mellitus and Congenital Heart Defects. *Circulation* **133**, 2219–2221 (2016).
- 10. Smedts, H. P. M. *et al.* Maternal intake of fat, riboflavin and nicotinamide and the risk of having offspring with congenital heart defects. *European Journal of Nutrition* **47**, 357–365 (2008).
- 11. Bredenoord, A. L., Clevers, H. & Knoblich, J. A. Human tissues in a dish: The research and ethical implications of organoid technology. *Science* (1979) **355**, eaaf9414 (2017).
- 12. Dunn, K. K. & Palecek, S. P. Engineering scalable manufacturing of high-quality stem cell-derived cardiomyocytes for cardiac tissue repair. *Frontiers in Medicine* **5**, (2018).
- 13. Burridge, P. W. *et al.* Chemically defined generation of human cardiomyocytes. *Nature Methods* **11**, 855–860 (2014).
- 14. Kurian, L. *et al.* Identification of Novel Long Noncoding RNAs Underlying Vertebrate Cardiovascular Development. *Circulation* **131**, 1278–1290 (2015).
- 15. Lancaster, M. A. *et al.* Cerebral organoids model human brain development and microcephaly. *Nature* **501**, 373–9 (2013).
- 16. Quadrato, G. *et al.* Cell diversity and network dynamics in photosensitive human brain organoids. *Nature* **545**, 48–53 (2017).
- 17. Mansour, A. A. *et al.* An in vivo model of functional and vascularized human brain organoids. *Nature Biotechnology* **36**, 432–441 (2018).
- 18. Pham, M. T. *et al.* Generation of human vascularized brain organoids. *Neuroreport* **29**, 588–593 (2018).
- 19. Dye, B. R. *et al.* In vitro generation of human pluripotent stem cell derived lung organoids. *Elife* **4**, e05098 (2015).
- 20. Porotto, M. *et al.* Authentic Modeling of Human Respiratory Virus Infection in Human Pluripotent Stem Cell-Derived Lung Organoids. *mBio* **10**, (2019).

- 21. Salahudeen, A. A. *et al.* Progenitor identification and SARS-CoV-2 infection in human distal lung organoids. *Nature* **588**, 670–675 (2020).
- 22. Vyas, D. *et al.* Self-assembled liver organoids recapitulate hepatobiliary organogenesis in vitro. *Hepatology* **67**, 750–761 (2018).
- 23. Wang, Y. *et al.* In situ differentiation and generation of functional liver organoids from human iPSCs in a 3D perfusable chip system. *Lab on a Chip* **18**, 3606–3616 (2018).
- 24. Mun, S. J. *et al.* Generation of expandable human pluripotent stem cell-derived hepatocyte-like liver organoids. *Journal of Hepatology* **71**, 970–985 (2019).
- 25. Broutier, L. *et al.* Culture and establishment of self-renewing human and mouse adult liver and pancreas 3D organoids and their genetic manipulation. *Nature Protocols* **11**, 1724–43 (2016).
- 26. Dossena, M. *et al.* Standardized GMP-compliant scalable production of human pancreas organoids. *Stem Cell Research & Therapy* **11**, 94 (2020).
- 27. Georgakopoulos, N. *et al.* Long-term expansion, genomic stability and in vivo safety of adult human pancreas organoids. *BMC Developmental Biology* **20**, 4 (2020).
- 28. Spence, J. R. *et al.* Directed differentiation of human pluripotent stem cells into intestinal tissue in vitro. *Nature* **470**, 105–9 (2011).
- 29. Serra, D. *et al.* Self-organization and symmetry breaking in intestinal organoid development. *Nature* **569**, 66–72 (2019).
- 30. Mithal, A. *et al.* Generation of mesenchyme free intestinal organoids from human induced pluripotent stem cells. *Nature Communications* **11**, 1–15 (2020).
- 31. Crespo, M. *et al.* Colonic organoids derived from human induced pluripotent stem cells for modeling colorectal cancer and drug testing. *Nature Medicine* **23**, 878–884 (2017).
- 32. Múnera, J. O. *et al.* Differentiation of Human Pluripotent Stem Cells into Colonic Organoids via Transient Activation of BMP Signaling. *Cell Stem Cell* **21**, 51–64 (2017).
- 33. Michels, B. E. *et al.* Human colon organoids reveal distinct physiologic and oncogenic Wnt responses. *The Journal of Experimental Medicine* **216**, 704–720 (2019).
- 34. Takasato, M. *et al.* Kidney organoids from human iPS cells contain multiple lineages and model human nephrogenesis. *Nature* **526**, 564–8 (2015).
- 35. Homan, K. A. *et al.* Flow-enhanced vascularization and maturation of kidney organoids in vitro. *Nature Methods* **16**, 255–262 (2019).
- 36. Uchimura, K., Wu, H., Yoshimura, Y. & Humphreys, B. D. Human Pluripotent Stem Cell-Derived Kidney Organoids with Improved Collecting Duct Maturation and Injury Modeling. *Cell Reports* **33**, 108514 (2020).
- 37. Corrò, C., Novellasdemunt, L. & Li, V. S. W. A brief history of organoids. *American Journal of Physiology Cell Physiology* **319**, C151–C165 (2020).
- 38. Ronaldson-Bouchard, K. *et al.* Advanced maturation of human cardiac tissue grown from pluripotent stem cells. *Nature* **556**, 239–243 (2018).
- 39. Keung, W. *et al.* Human Cardiac Ventricular-Like Organoid Chambers and Tissue Strips From Pluripotent Stem Cells as a Two-Tiered Assay for Inotropic Responses. *Clinical Pharmacology and Therapeutics* **106**, 402–414 (2019).
- 40. Oltolina, F. *et al.* Human Cardiac Progenitor Spheroids Exhibit Enhanced Engraftment Potential. *PloS One* **10**, e0137999 (2015).

- 41. Figtree, G. A., Bubb, K. J., Tang, O., Kizana, E. & Gentile, C. Vascularized Cardiac Spheroids as Novel 3D in vitro Models to Study Cardiac Fibrosis. *Cells, Tissues, Organs* **204**, 191–198 (2017).
- 42. Freedman, B. S. *et al.* Modelling kidney disease with CRISPR-mutant kidney organoids derived from human pluripotent epiblast spheroids. *Nature Communications* **6**, 8715 (2015).
- 43. Kim, T. Y. *et al.* Directed fusion of cardiac spheroids into larger heterocellular microtissues enables investigation of cardiac action potential propagation via cardiac fibroblasts. *PloS One* **13**, e0196714 (2018).
- 44. Bursac, N. *et al.* Cardiac muscle tissue engineering: toward an in vitro model for electrophysiological studies. *The American Journal of Physiology* **277**, H433-44 (1999).
- 45. Zimmermann, W. H. *et al.* Three-dimensional engineered heart tissue from neonatal rat cardiac myocytes. *Biotechnology and Bioengineering* **68**, 106–14 (2000).
- 46. Kelm, J. M. & Fussenegger, M. Microscale tissue engineering using gravity-enforced cell assembly. *Trends in Biotechnology* **22**, 195–202 (2004).
- 47. Guo, X.-M. *et al.* Creation of engineered cardiac tissue in vitro from mouse embryonic stem cells. *Circulation* **113**, 2229–37 (2006).
- 48. Radisic, M. *et al.* Optical mapping of impulse propagation in engineered cardiac tissue. *Tissue Engineering Part A* **15**, 851–60 (2009).
- 49. de Lange, W. J. *et al.* Neonatal mouse-derived engineered cardiac tissue: a novel model system for studying genetic heart disease. *Circulation Research* **109**, 8–19 (2011).
- 50. Liau, B., Christoforou, N., Leong, K. W. & Bursac, N. Pluripotent stem cell-derived cardiac tissue patch with advanced structure and function. *Biomaterials* **32**, 9180–7 (2011).
- 51. Figtree, G. A., Bubb, K. J., Tang, O., Kizana, E. & Gentile, C. Vascularized Cardiac Spheroids as Novel 3D in vitro Models to Study Cardiac Fibrosis. *Cells, Tissues, Organs* **204**, 191–198 (2017).
- 52. Kim, T. Y. *et al.* Directed fusion of cardiac spheroids into larger heterocellular microtissues enables investigation of cardiac action potential propagation via cardiac fibroblasts. *PloS One* **13**, e0196714 (2018).
- 53. Khademhosseini, A. *et al.* Microfluidic patterning for fabrication of contractile cardiac organoids. *Biomedical Microdevices* **9**, 149–57 (2007).
- 54. Boudou, T. *et al.* A microfabricated platform to measure and manipulate the mechanics of engineered cardiac microtissues. *Tissue Engineering Part A* **18**, 910–9 (2012).
- 55. Oltolina, F. *et al.* Human Cardiac Progenitor Spheroids Exhibit Enhanced Engraftment Potential. *PloS One* **10**, e0137999 (2015).
- 56. Tiburcy, M. *et al.* Defined Engineered Human Myocardium With Advanced Maturation for Applications in Heart Failure Modeling and Repair. *Circulation* **135**, 1832–1847 (2017).
- 57. Mills, R. J. *et al.* Functional screening in human cardiac organoids reveals a metabolic mechanism for cardiomyocyte cell cycle arrest. *Proc Natl Acad Sci U S A* **114**, E8372–E8381 (2017).
- 58. Zhao, Y. *et al.* A Platform for Generation of Chamber-Specific Cardiac Tissues and Disease Modeling. *Cell* **176**, 913–927 (2019).
- 59. Kupfer, M. E. *et al.* In Situ Expansion, Differentiation, and Electromechanical Coupling of Human Cardiac Muscle in a 3D Bioprinted, Chambered Organoid. *Circulation Research* **127**, 207–224 (2020).
- 60. Gunti, S., Hoke, A. T. K., Vu, K. P. & London, N. R. Organoid and Spheroid Tumor Models: Techniques and Applications. *Cancers (Basel)* **13**, 1–17 (2021).

- 61. Lee, J. *et al.* In vitro generation of functional murine heart organoids via FGF4 and extracellular matrix. *Nature Communications* **11**, 4283 (2020).
- 62. Drakhlis, L. *et al.* Human heart-forming organoids recapitulate early heart and foregut development. *Nat Biotechnol* **39**, 737–746 (2021).
- 63. Lewis-Israeli, Y. *et al.* Self-assembling human heart organoids for the modeling of cardiac development and congenital heart disease. *Nature Communications*.
- 64. Hofbauer, P. *et al.* Cardioids reveal self-organizing principles of human cardiogenesis. *Cell* **184**, 3299–3317 (2021).
- 65. Mills, R. J. *et al.* Drug Screening in Human PSC-Cardiac Organoids Identifies Pro-proliferative Compounds Acting via the Mevalonate Pathway. *Cell Stem Cell* **24**, 895–907 (2019).
- 66. Buhaescu, I. & Izzedine, H. Mevalonate pathway: a review of clinical and therapeutical implications. *Clinical Biochemistry* **40**, 575–84 (2007).
- 67. Mills, R. J. *et al.* BET inhibition blocks inflammation-induced cardiac dysfunction and SARS-CoV-2 infection. *Cell* **184**, 2167-2182.e22 (2021).
- 68. Voges, H. K. *et al.* Development of a human cardiac organoid injury model reveals innate regenerative potential. *Development* **144**, 1118–1127 (2017).
- 69. Nunes, S. S. *et al.* Biowire: a platform for maturation of human pluripotent stem cell-derived cardiomyocytes. *Nature Methods* **10**, 781–7 (2013).
- 70. Sun, X. & Nunes, S. S. Maturation of Human Stem Cell-derived Cardiomyocytes in Biowires Using Electrical Stimulation. *Journal of Visualized Experiments* 55373 (2017) doi:10.3791/55373.
- 71. Leonard, A. *et al.* Afterload promotes maturation of human induced pluripotent stem cell derived cardiomyocytes in engineered heart tissues. *Journal of Molecular and Cellular Cardiology* **118**, 147–158 (2018).
- 72. Lu, K. *et al.* Progressive stretch enhances growth and maturation of 3D stem-cell-derived myocardium. *Theranostics* **11**, 6138–6153 (2021).
- 73. Li, R. A. *et al.* Bioengineering an electro-mechanically functional miniature ventricular heart chamber from human pluripotent stem cells. *Biomaterials* **163**, 116–127 (2018).
- 74. Varzideh, F. *et al.* Human cardiomyocytes undergo enhanced maturation in embryonic stem cell-derived organoid transplants. *Biomaterials* **192**, 537–550 (2019).
- 75. Takebe, T. *et al.* Vascularized and functional human liver from an iPSC-derived organ bud transplant. *Nature* **499**, 481–4 (2013).
- 76. Richards, D. J. *et al.* Human cardiac organoids for the modelling of myocardial infarction and drug cardiotoxicity. *Nature Biomedical Engineering* **4**, 446–462 (2020).
- 77. Richards, D. J. *et al.* Inspiration from heart development: Biomimetic development of functional human cardiac organoids. *Biomaterials* **142**, 112–123 (2017).
- 78. Silva, A. C. *et al.* Developmental co-emergence of cardiac and gut tissues modeled by human iPSC-derived organoids. *bioRxiv* 2020.04.30.071472 (2021) doi:10.1101/2020.04.30.071472.
- 79. Pinto, A. R. *et al.* Revisiting Cardiac Cellular Composition. *Circulation Research* **118**, 400–9 (2016).
- 80. Andersen, P. *et al.* Precardiac organoids form two heart fields via Bmp/Wnt signaling. *Nature Communications* **9**, 1–13 (2018).
- 81. Rossi, G. et al. Capturing Cardiogenesis in Gastruloids. Cell Stem Cell 28, (2020).

- 82. Lee, J. *et al.* In vitro generation of functional murine heart organoids via FGF4 and extracellular matrix. *Nature Communications* **11**, (2020).
- 83. Drakhlis, L. *et al.* Human heart-forming organoids recapitulate early heart and foregut development. *Nature Biotechnology* 1–10 doi:10.1038/s41587-021-00815-9.
- 84. Hofbauer, P. *et al.* Cardioids reveal self-organizing principles of human cardiogenesis. *Cell* (2021) doi:10.1016/j.cell.2021.04.034.
- 85. Rossi, G. et al. Capturing Cardiogenesis in Gastruloids. Cell Stem Cell 28, 230–240 (2021).
- 86. Lewis-Israeli, Y. R. *et al.* Self-assembling human heart organoids for the modeling of cardiac development and congenital heart disease. *Nature Communications* **12**, 5142 (2021).
- 87. Andersen, P. *et al.* Precardiac organoids form two heart fields via Bmp/Wnt signaling. *Nature Communications* **9**, 1–13 (2018).
- 88. Lee, J. *et al.* In vitro generation of functional murine heart organoids via FGF4 and extracellular matrix. *Nature Communications* **11**, 4283 (2020).
- 89. Andersen, P. et al. Precardiac organoids form two heart fields via Bmp/Wnt signaling. *Nature Communications* **9**, 3140 (2018).
- 90. Mjaatvedt, C. H. *et al.* The outflow tract of the heart is recruited from a novel heart-forming field. *Developmental Biology* **238**, 97–109 (2001).
- 91. Drakhlis, L. *et al.* Human heart-forming organoids recapitulate early heart and foregut development. *Nat Biotechnol* **39**, 737–746 (2021).
- 92. Lyons, I. *et al.* Myogenic and morphogenetic defects in the heart tubes of murine embryos lacking the homeo box gene Nkx2-5. *Genes & Development* **9**, 1654–66 (1995).
- 93. Baillie-Johnson, P., van den Brink, S. C., Balayo, T., Turner, D. A. & Martinez Arias, A. Generation of Aggregates of Mouse Embryonic Stem Cells that Show Symmetry Breaking, Polarization and Emergent Collective Behaviour In Vitro. *Journal of Visualized Experiments* 1–10 (2015) doi:10.3791/53252.
- 94. Zaidi, S. & Brueckner, M. Genetics and Genomics of Congenital Heart Disease. *Circulation Research* **120**, 923–940 (2017).
- 95. Øyen, N. *et al.* Prepregnancy Diabetes and Offspring Risk of Congenital Heart Disease. *Circulation* **133**, 2243–2253 (2016).
- 96. Centers for Disease Control and Prevention. *National Diabetes Statistics Report*. https://www.cdc.gov/diabetes/data/statistics-report/index.html (2020).
- 97. Cho, N. H. *et al.* IDF Diabetes Atlas: Global estimates of diabetes prevalence for 2017 and projections for 2045. *Diabetes Research and Clinical Practice* **138**, 271–281 (2018).
- 98. Basu, M. & Garg, V. Maternal hyperglycemia and fetal cardiac development: Clinical impact and underlying mechanisms. *Birth Defects Research* **110**, 1504–1516 (2018).
- 99. Ornoy, A., Reece, E. A., Pavlinkova, G., Kappen, C. & Miller, R. K. Effect of maternal diabetes on the embryo, fetus, and children: Congenital anomalies, genetic and epigenetic changes and developmental outcomes. *Birth Defects Research Part C: Embryo Today: Reviews* **105**, 53–72 (2015).
- 100. Tabib, A. *et al.* Cardiac malformations in fetuses of gestational and pre gestational diabetic mothers. *Iranian Journal of Pediatrics* **23**, 664–668 (2013).
- 101. Øyen, N. *et al.* Prepregnancy Diabetes and Offspring Risk of Congenital Heart Disease: A Nationwide Cohort Study. *Circulation* **133**, 2243–2253 (2016).

- 102. Hoang, T. T. *et al.* The congenital heart disease genetic network study: Cohort description. *PLoS ONE* **13**, 1–14 (2018).
- 103. Simeone, R. M. *et al.* Diabetes and Congenital Heart Defects. *American Journal of Preventive Medicine* **48**, 195–204 (2015).
- 104. Buchanan, M. D. T. A. & Kitzmiller, M. D. J. L. METABOLIC INTERACTIONS OF DIABETES AND PREGNANCY. *Annual Review of Medicine* **45**, 245–260 (1994).
- 105. Engineer, A. *et al.* Sapropterin Treatment Prevents Congenital Heart Defects Induced by Pregestational Diabetes Mellitus in Mice. *J Am Heart Assoc* **7**, (2018).
- 106. Lehtoranta, L. *et al.* Maternal hyperglycemia leads to fetal cardiac hyperplasia and dysfunction in a rat model. *American Journal of Physiology-Endocrinology and Metabolism* **305**, E611–E619 (2013).
- 107. Piddington, R., Joyce, J., Dhanasekaran, P. & Baker, L. Diabetes mellitus affects prostaglandin E2 levels in mouse embryos during neurulation. *Diabetologia* **39**, 915–920 (1996).
- 108. Gupta, A., Chacko, V. P., Schär, M., Akki, A. & Weiss, R. G. Impaired ATP Kinetics in Failing In Vivo Mouse Heart. *Circulation: Cardiovascular Imaging* **4**, 42–50 (2011).
- 109. Hamlin, R. L. & Altschuld, R. A. Extrapolation From Mouse to Man. *Circulation: Cardiovascular Imaging* **4**, 2–4 (2011).
- 110. Loiselle, D. S. & Gibbs, C. L. Species differences in cardiac energetics. *American Journal of Physiology-Heart and Circulatory Physiology* **237**, H90–H98 (1979).
- 111. Kumar, S. D., Dheen, S. T. & Tay, S. S. W. Maternal diabetes induces congenital heart defects in mice by altering the expression of genes involved in cardiovascular development. *Cardiovascular Diabetology* **6**, 34 (2007).
- 112. Kumar, S. D. *et al.* Zinc supplementation prevents cardiomyocyte apoptosis and congenital heart defects in embryos of diabetic mice. *Free Radical Biology and Medicine* **53**, 1595–1606 (2012).
- 113. Moazzen, H. *et al.* N-Acetylcysteine prevents congenital heart defects induced by pregestational diabetes. 1–13 (2014).
- 114. Drawnel, F. M. *et al.* Disease modeling and phenotypic drug screening for diabetic cardiomyopathy using human induced pluripotent stem cells. *Cell Reports* **9**, 810–820 (2014).
- 115. Geraets, I. M. E. *et al.* Human embryonic stem cell-derived cardiomyocytes as an in vitro model to study cardiac insulin resistance. *Biochimica et Biophysica Acta (BBA) Molecular Basis of Disease* **1864**, 1960–1967 (2018).
- 116. Ng, K.-M. *et al.* Empagliflozin Ammeliorates High Glucose Induced-Cardiac Dysfuntion in Human iPSC-Derived Cardiomyocytes. *Scientific Reports* **8**, 14872 (2018).
- 117. Kretzschmar, K. & Clevers, H. Organoids: Modeling Development and the Stem Cell Niche in a Dish. *Developmental Cell* **38**, 590–600 (2016).
- 118. Paşca, S. P. Assembling human brain organoids. Science (1979) 363, 126–127 (2019).
- 119. Rossi, G. et al. Capturing Cardiogenesis in Gastruloids. Cell Stem Cell 28, 230–240 (2021).
- 120. Sasai, Y. Next-generation regenerative medicine: Organogenesis from stem cells in 3D culture. *Cell Stem Cell* **12**, 520–530 (2013).
- 121. Weeber, F., Ooft, S. N., Dijkstra, K. K. & Voest, E. E. Tumor Organoids as a Pre-clinical Cancer Model for Drug Discovery. *Cell Chemical Biology* **24**, 1092–1100 (2017).
- 122. Lewis-Israeli, Y. R., Wasserman, A. H. & Aguirre, A. Heart Organoids and Engineered Heart Tissues: Novel Tools for Modeling Human Cardiac Biology and Disease. *Biomolecules* **11**, 1277 (2021).

- 123. Tuveson, D. & Clevers, H. Cancer modeling meets human organoid technology. *Science (1979)* **364**, 952–955 (2019).
- 124. Hofbauer, P. *et al.* Cardioids reveal self-organizing principles of human cardiogenesis. *Cell* **184**, 3299–3317 (2021).
- 125. Rossi, G. *et al.* Article Capturing Cardiogenesis in Gastruloids Article Capturing Cardiogenesis in Gastruloids. *Cell Stem Cell* **28**, 1–11 (2021).
- 126. Chan, C. *et al.* Repositioned Drugs for COVID-19—the Impact on Multiple Organs. *SN Comprehensive Clinical Medicine* **3**, 1484–1501 (2021).
- 127. Chen, T.-W. *et al.* Ultrasensitive fluorescent proteins for imaging neuronal activity. *Nature* **499**, 295–300 (2013).
- 128. Huebsch, N. *et al.* Automated Video-Based Analysis of Contractility and Calcium Flux in Human-Induced Pluripotent Stem Cell-Derived Cardiomyocytes Cultured over Different Spatial Scales. *Tissue Engineering Part C: Methods* **21**, 467–479 (2015).
- 129. Lian, X. *et al.* Directed cardiomyocyte differentiation from human pluripotent stem cells by modulating Wnt/β-catenin signaling under fully defined conditions. *Nature Protocols* **8**, 162–175 (2013).
- 130. Yang, X. *et al.* Fatty Acids Enhance the Maturation of Cardiomyocytes Derived from Human Pluripotent Stem Cells. *Stem Cell Reports* **13**, 657–668 (2019).
- 131. Dong, Z. *et al.* Optical coherence tomography image denoising using a generative adversarial network with speckle modulation. *Journal of Biophotonics* **13**, (2020).
- 132. van den Berge, K. *et al.* RNA Sequencing Data: Hitchhiker's Guide to Expression Analysis. *Annual Review of Biomedical Data Science* **2**, 139–173 (2019).
- 133. Yang, W., Fan, Q. H. & Li, W. A Fully Transparent, Flexible μECoG Array Based on Highly Conductive and Anti-reflective PEDOT:PSS-ITO-Ag-ITO Thin Films. in 2020 IEEE 15th International Conference on Nano/Micro Engineered and Molecular System (NEMS) 124–129 (IEEE, 2020). doi:10.1109/NEMS50311.2020.9265573.
- 134. PHC Eilers, H. B. Baseline correction with asymmetric least squares smoothing. *Leiden University Medical Centre Report* (2005).
- 135. Watrous, J. D. *et al.* Directed Non-targeted Mass Spectrometry and Chemical Networking for Discovery of Eicosanoids and Related Oxylipins. *Cell Chemical Biology* **26**, 433-442.e4 (2019).
- 136. Bertero, A. *et al.* Dynamics of genome reorganization during human cardiogenesis reveal an RBM20-dependent splicing factory. *Nature Communications* **10**, 1538 (2019).
- 137. Lian, X. *et al.* Robust cardiomyocyte differentiation from human pluripotent stem cells via temporal modulation of canonical Wnt signaling. *Proc Natl Acad Sci U S A* **109**, E1848–E1857 (2012).
- 138. Ronaldson-Bouchard, K. *et al.* Advanced maturation of human cardiac tissue grown from pluripotent stem cells. *Nature* **556**, 239–243 (2018).
- 139. Yang, X. *et al.* Fatty Acids Enhance the Maturation of Cardiomyocytes Derived from Human Pluripotent Stem Cells. *Stem Cell Reports* **13**, 657–668 (2019).
- 140. Sun, N. *et al.* Patient-specific induced pluripotent stem cells as a model for familial dilated cardiomyopathy. *Science Translational Medicine* **4**, 130ra47-130ra47 (2012).
- 141. Hashem, S. I. *et al.* Brief report: Oxidative stress mediates cardiomyocyte apoptosis in a human model of danon disease and heart failure. *Stem Cells* **33**, 2343–2350 (2015).

- 142. Panopoulos, A. D. *et al.* iPSCORE: A Resource of 222 iPSC Lines Enabling Functional Characterization of Genetic Variation across a Variety of Cell Types. *Stem Cell Reports* **8**, 1086–1100 (2017).
- 143. Stroud, M. J. *et al.* Luma is not essential for murine cardiac development and function. *Cardiovascular Research* **114**, 378–388 (2018).
- 144. Liang, P. et al. Drug screening using a library of human induced pluripotent stem cell-derived cardiomyocytes reveals disease-specific patterns of cardiotoxicity. *Circulation* **127**, 1677–1691 (2013).
- 145. Mills, R. J. *et al.* Functional screening in human cardiac organoids reveals a metabolic mechanism for cardiomyocyte cell cycle arrest. *Proc Natl Acad Sci U S A* **114**, E8372–E8381 (2017).
- 146. Osataphan, N., Phrommintikul, A., Chattipakorn, S. C. & Chattipakorn, N. Effects of doxorubicin-induced cardiotoxicity on cardiac mitochondrial dynamics and mitochondrial function: Insights for future interventions. *Journal of Cellular and Molecular Medicine* 1–24 (2020) doi:10.1111/jcmm.15305.
- 147. Braam, S. R. *et al.* Prediction of drug-induced cardiotoxicity using human embryonic stem cell-derived cardiomyocytes. *Stem Cell Research* **4**, 107–116 (2010).
- 148. Burridge, P. W. *et al.* Human induced pluripotent stem cell–derived cardiomyocytes recapitulate the predilection of breast cancer patients to doxorubicin-induced cardiotoxicity. *Nature Medicine* **22**, 547–556 (2016).
- 149. Kitani, T. *et al.* Human-Induced Pluripotent Stem Cell Model of Trastuzumab-Induced Cardiac Dysfunction in Patients With Breast Cancer. *Circulation* **139**, 2451–2465 (2019).
- 150. Mills, R. J. *et al.* Functional screening in human cardiac organoids reveals a metabolic mechanism for cardiomyocyte cell cycle arrest. *Proc Natl Acad Sci U S A* **114**, E8372–E8381 (2017).
- 151. Ronaldson-Bouchard, K. *et al.* Advanced maturation of human cardiac tissue grown from pluripotent stem cells. *Nature* **556**, 239–243 (2018).
- 152. Voges, H. K. *et al.* Development of a human cardiac organoid injury model reveals innate regenerative potential. *Development (Cambridge)* **144**, 1118–1127 (2017).
- 153. Wang, S. *et al.* Human neonatal thymus mesenchymal stem cells promote neovascularization and cardiac regeneration. *Stem Cells International* **2018**, (2018).
- 154. Skardal, A., Shupe, T. & Atala, A. Organoid-on-a-chip and body-on-a-chip systems for drug screening and disease modeling. *Drug Discovery Today* **21**, 1399–1411 (2016).
- 155. Trujillo, C. A. *et al.* Nested oscillatory dynamics in cortical organoids model early human brain network development. *bioRxiv* 358622 (2018) doi:10.1101/358622.
- 156. Ma, Z. *et al.* Self-organizing human cardiac microchambers mediated by geometric confinement. *Nature Communications* **6**, 1–10 (2015).
- 157. Bargehr, J. *et al.* Epicardial cells derived from human embryonic stem cells augment cardiomyocyte-driven heart regeneration. *Nature Biotechnology* **37**, 895–906 (2019).
- 158. Bao, X. *et al.* Long-term self-renewing human epicardial cells generated from pluripotent stem cells under defined xeno-free conditions. *Nature Biomedical Engineering* **1**, 1–12 (2017).
- 159. Zhou, P. & Pu, W. T. Recounting Cardiac Cellular Composition. *Circulation Research* **118**, 368–370 (2016).
- 160. Elliott, N. T. & Yuan, F. A review of three-dimensional in vitro tissue models for drug discovery and transport studies. *Journal of Pharmaceutical Sciences* **100**, 59–74 (2011).
- 161. Güemes, M., Rahman, S. A. & Hussain, K. What is a normal blood glucose? *Archives of Disease in Childhood* **101**, 569–574 (2016).

- 162. Diagnosis and Classification of Diabetes Mellitus. Diabetes Care 32, S62–S67 (2009).
- 163. Davis, D. R., Ruckdeschel Smith, R. & Marbán, E. Human cardiospheres are a source of stem cells with cardiomyogenic potential. *Stem Cells* **28**, 903–4 (2010).
- 164. Rossi, G. et al. Capturing Cardiogenesis in Gastruloids. Cell Stem Cell 28, 1–11 (2020).
- 165. Lee, J. *et al.* In vitro generation of functional murine heart organoids via FGF4 and extracellular matrix. *Nature Communications* **11**, 4283 (2020).
- 166. Hofbauer, P. *et al.* Cardioids reveal self-organizing principles of human cardiogenesis. *Cell* **184**, 3299–3317 (2021).
- 167. Bao, X. *et al.* Long-term self-renewing human epicardial cells generated from pluripotent stem cells under defined xeno-free conditions. *Nature Biomedical Engineering* **1**, 1–12 (2017).
- 168. Breckwoldt, K. *et al.* Differentiation of cardiomyocytes and generation of human engineered heart tissue. *Nature Protocols* **12**, 1177–1197 (2017).
- 169. Giacomelli, E., Mummery, C. L. & Bellin, M. Human heart disease: lessons from human pluripotent stem cell-derived cardiomyocytes. *Cellular and Molecular Life Sciences* **74**, 3711–3739 (2017).
- 170. Hoang, P., Wang, J., Conklin, B. R., Healy, K. E. & Ma, Z. Generation of spatial-patterned early-developing cardiac organoids using human pluripotent stem cells. *Nature Protocols* **13**, 723–737 (2018).
- 171. Lian, X. *et al.* Chemically defined, albumin-free human cardiomyocyte generation. *Nature Methods* **12**, 595–596 (2015).
- 172. Witty, A. D. *et al.* Generation of the epicardial lineage from human pluripotent stem cells. *Nature Biotechnology* **32**, 1026–1035 (2014).
- 173. Burridge, P. W., Keller, G., Gold, J. D. & Wu, J. C. Production of de novo cardiomyocytes: Human pluripotent stem cell differentiation and direct reprogramming. *Cell Stem Cell* **10**, 16–28 (2012).
- 174. Protze, S. I., Lee, J. H. & Keller, G. M. Human Pluripotent Stem Cell-Derived Cardiovascular Cells: From Developmental Biology to Therapeutic Applications. *Cell Stem Cell* **25**, 311–327 (2019).
- 175. Jackson, S. A., Schiesser, J., Stanley, E. G. & Elefanty, A. G. Differentiating Embryonic Stem Cells Pass through 'Temporal Windows' That Mark Responsiveness to Exogenous and Paracrine Mesendoderm Inducing Signals. *PLoS ONE* **5**, e10706 (2010).
- 176. Titmarsh, D. M. *et al.* Microbioreactor Arrays for Full Factorial Screening of Exogenous and Paracrine Factors in Human Embryonic Stem Cell Differentiation. *PLoS ONE* **7**, e52405 (2012).
- 177. Nishino, I. *et al.* Primary LAMP-2 deficiency causes X-linked vacoular cardiomyopathy and myopathy (Danon disease). *Nature* **406**, 906–910 (2000).
- 178. Hashem, S. I. *et al.* Brief report: Oxidative stress mediates cardiomyocyte apoptosis in a human model of danon disease and heart failure. *Stem Cells* **33**, 2343–2350 (2015).
- 179. Schutgens, F. & Clevers, H. Human Organoids: Tools for Understanding Biology and Treating Diseases. *Annual Review of Pathology: Mechanisms of Disease* **15**, 211–234 (2020).
- 180. Baker, L. A., Tiriac, H., Clevers, H. & Tuveson, D. A. Modeling pancreatic cancer with organoids. *Trends Cancer* **2**, 176–190 (2016).
- 181. Richards, D. J. *et al.* Human cardiac organoids for the modelling of myocardial infarction and drug cardiotoxicity. *Nature Biomedical Engineering* **4**, 446–462 (2020).
- 182. Wimmer, R. A. *et al.* Human blood vessel organoids as a model of diabetic vasculopathy. *Nature* **565**, 505–510 (2019).

- 183. Tsakmaki, A., Fonseca Pedro, P. & Bewick, G. A. Diabetes through a 3D lens: organoid models. *Diabetologia* **63**, 1093–1102 (2020).
- 184. Lehmann, R. *et al.* Human organoids: a new dimension in cell biology. *Molecular Biology of the Cell* **30**, 1129–1137 (2019).
- 185. Lancaster, M. A. & Knoblich, J. A. Organogenesisin a dish: Modeling development and disease using organoid technologies. *Science* (1979) **345**, (2014).
- 186. Grenier, K., Kao, J. & Diamandis, P. Three-dimensional modeling of human neurodegeneration: brain organoids coming of age. *Molecular Psychiatry* **25**, 254–274 (2020).
- 187. Crespo, M. *et al.* Colonic organoids derived from human induced pluripotent stem cells for modeling colorectal cancer and drug testing. *Nature Medicine* **23**, 878–884 (2017).
- 188. Sato, T. *et al.* Long-term Expansion of Epithelial Organoids From Human Colon, Adenoma, Adenocarcinoma, and Barrett's Epithelium. *Gastroenterology* **141**, 1762–1772 (2011).
- 189. Cristobal, A. *et al.* Personalized Proteome Profiles of Healthy and Tumor Human Colon Organoids Reveal Both Individual Diversity and Basic Features of Colorectal Cancer. *Cell Reports* **18**, 263–274 (2017).
- 190. Boj, S. F. *et al.* Organoid models of human and mouse ductal pancreatic cancer. *Cell* **160**, 324–338 (2015).
- 191. Takasato, M. *et al.* Kidney organoids from human iPS cells contain multiple lineages and model human nephrogenesis. *Nature* **526**, 564–568 (2015).
- 192. Homan, K. A. *et al.* Flow-enhanced vascularization and maturation of kidney organoids in vitro. *Nature Methods* **16**, 255–262 (2019).
- 193. Bartfeld, S. Modeling infectious diseases and host-microbe interactions in gastrointestinal organoids. *Developmental Biology* **420**, 262–270 (2016).
- 194. Lian, X. *et al.* Directed cardiomyocyte differentiation from human pluripotent stem cells by modulating Wnt/β-catenin signaling under fully defined conditions. *Nature Protocols* **8**, 162–175 (2013).
- 195. Martínez-Estrada, O. M. *et al.* Wt1 is required for cardiovascular progenitor cell formation through transcriptional control of Snail and E-cadherin. *Nature Genetics* **42**, 89–93 (2010).
- 196. Giacomelli, E. *et al.* Human-iPSC-Derived Cardiac Stromal Cells Enhance Maturation in 3D Cardiac Microtissues and Reveal Non-cardiomyocyte Contributions to Heart Disease. *Cell Stem Cell* **26**, 862-879.e11 (2020).
- 197. Giacomelli, E. *et al.* Three-dimensional cardiac microtissues composed of cardiomyocytes and endothelial cells co-differentiated from human pluripotent stem cells. *Development* **144**, 1008–1017 (2017).
- 198. Bargehr, J. *et al.* Epicardial cells derived from human embryonic stem cells augment cardiomyocyte-driven heart regeneration. *Nature Biotechnology* **37**, 895–906 (2019).
- 199. Bargehr, J. *et al.* Epicardial cells derived from human embryonic stem cells augment cardiomyocyte-driven heart regeneration. *Nature Biotechnology* **37**, 895–906 (2019).
- 200. Brade, T., Pane, L. S., Moretti, A., Chien, K. R. & Laugwitz, K. L. Embryonic heart progenitors and cardiogenesis. *Cold Spring Harbor Perspectives in Medicine* **3**, 1–18 (2013).
- 201. George, R. M. & Firulli, A. B. Hand Factors in Cardiac Development. *The Anatomical Record* **302**, 101–107 (2019).
- 202. Kelly, R. G., Buckingham, M. E. & Moorman, A. F. Heart fields and cardiac morphogenesis. *Cold Spring Harbor Perspectives in Medicine* **4**, 1–11 (2014).

- 203. Pinto, A. R. *et al.* Revisiting Cardiac Cellular Composition Alexander. *Circ Res.* **118**, 400–409 (2017).
- 204. Scott F. Gilbert, M. J. F. B. Lateral Plate Mesoderm: Heart and Circulatory System. in *Developmental Biology* 591–610 (Sinauer Associates is an imprint of Oxford University Press, 2019).
- 205. Sa, S. & McCloskey, K. E. Activin A and BMP4 signaling for efficient cardiac differentiation of H7 and H9 human embryonic stem cells. *Journal of Stem Cells and Regenerative Medicine* **8**, 198–202 (2012).
- 206. Kattman, S. J. *et al.* Stage-Specific Optimization of Activin/Nodal and BMP Signaling Promotes Cardiac Differentiation of Mouse and Human Pluripotent Stem Cell Lines. *Cell Stem Cell* **8**, 228–240 (2011).
- 207. Elliott, D. A. *et al.* NKX2-5eGFP/w hESCs for isolation of human cardiac progenitors and cardiomyocytes. *Nature Methods* **8**, 1037–1040 (2011).
- 208. Zhang, Q. *et al.* Designing a Green Fluorogenic Protease Reporter by Flipping a Beta Strand of GFP for Imaging Apoptosis in Animals. *J Am Chem Soc* **141**, 4526–4530 (2019).
- 209. Barnes, R. M., Firulli, B. A., Conway, S. J., Vincentz, J. W. & Firulli, A. B. Analysis of the Hand1 cell lineage reveals novel contributions to cardiovascular, neural crest, extra-embryonic, and lateral mesoderm derivatives. *Developmental Dynamics* **239**, 3086–3097 (2010).
- 210. Barnes, R. M. *et al.* Hand2 Loss-of-Function in Hand1 -Expressing Cells Reveals Distinct Roles in Epicardial and Coronary Vessel Development. *Circulation Research* **108**, 940–949 (2011).
- 211. Tsuchihashi, T. *et al.* Hand2 function in second heart field progenitors is essential for cardiogenesis. *Developmental Biology* **351**, 62–69 (2011).
- 212. Lian, X. *et al.* Directed cardiomyocyte differentiation from human pluripotent stem cells by modulating Wnt/β-catenin signaling under fully defined conditions. *Nature Protocols* **8**, 162–175 (2013).
- 213. Später, D., Hansson, E. M., Zangi, L. & Chien, K. R. How to make a cardiomyocyte. *Development (Cambridge)* **141**, 4418–4431 (2014).
- 214. Breckwoldt, K. *et al.* Differentiation of cardiomyocytes and generation of human engineered heart tissue. *Nature Protocols* **12**, 1177–1197 (2017).
- 215. Kim, M. *et al.* Activin-A and Bmp4 Levels Modulate Cell Type Specification during CHIR-Induced Cardiomyogenesis. 1–16 (2015) doi:10.1371/journal.pone.0118670.
- 216. Doppler, S. A. *et al.* Cardiac fibroblasts: More than mechanical support. *Journal of Thoracic Disease* **9**, S36–S51 (2017).
- 217. Moore-Morris, T., Guimarães-Camboa, N., Yutzey, K. E., Pucéat, M. & Evans, S. M. Cardiac fibroblasts: from development to heart failure. *Journal of Molecular Medicine* **93**, 823–830 (2015).
- 218. Feng, W. *et al.* Computational profiling of hiPSC-derived heart organoids reveals chamber defects associated with Ebstein's anomaly. *bioRxiv* 2020.12.24.424346 (2020) doi:10.1101/2020.12.24.424346.
- 219. Subramanian, A. *et al.* Single cell census of human kidney organoids shows reproducibility and diminished off-target cells after transplantation. *Nature Communications* **10**, 5462 (2019).
- 220. Mills, R. J. *et al.* Drug Screening in Human PSC-Cardiac Organoids Identifies Pro-proliferative Compounds Acting via the Mevalonate Pathway. *Cell Stem Cell* **24**, 895–907 (2019).
- 221. Dekkers, J. F. *et al.* High-resolution 3D imaging of fixed and cleared organoids. *Nature Protocols* **14**, 1756–1771 (2019).

- 222. Silva, A. C. *et al.* Developmental co-emergence of cardiac and gut tissues modeled by human iPSC-derived organoids. *bioRxiv* 2020.04.30.071472 (2021) doi:10.1101/2020.04.30.071472.
- 223. Beghin, A. *et al.* High content 3D imaging method for quantitative characterization of organoid development and phenotype. *bioRxiv* 2021.03.26.437121 (2021) doi:10.1101/2021.03.26.437121.
- 224. Richards, D. J. *et al.* Human cardiac organoids for the modelling of myocardial infarction and drug cardiotoxicity. *Nature Biomedical Engineering* **4**, 446–462 (2020).
- 225. Lees, J., Kong, A., Mitchell, G. & Lim, S. Human Vascularised Cardiac Organoids for Disease Modelling. *Heart, Lung and Circulation* **28**, S216 (2019).
- 226. Tulloch, N. L. *et al.* Growth of engineered human myocardium with mechanical loading and vascular coculture. *Circulation Research* **109**, 47–59 (2011).
- 227. Mansour, A. A. *et al.* An in vivo model of functional and vascularized human brain organoids. *Nature Biotechnology* **36**, 432–441 (2018).
- 228. Homan, K. A. *et al.* Flow-enhanced vascularization and maturation of kidney organoids in vitro. *Nature Methods* **16**, 255–262 (2019).
- 229. Kupfer, M. E. *et al.* In Situ Expansion, Differentiation, and Electromechanical Coupling of Human Cardiac Muscle in a 3D Bioprinted, Chambered Organoid. *Circulation Research* **127**, 207–224 (2020).
- 230. Richards, D. J. *et al.* Generation of spatial-patterned early-developing cardiac organoids using human pluripotent stem cells. *Nature Protocols* **9**, 723–737 (2020).
- 231. Gessert, S. & Kühl, M. The multiple phases and faces of Wnt signaling during cardiac differentiation and development. *Circulation Research* **107**, 186–199 (2010).
- 232. Kathiresan, S. & Srivastava, D. Genetics of Human Cardiovascular Disease. *Cell* **148**, 1242–1257 (2012).
- 233. Sun, R., Liu, M., Lu, L., Zheng, Y. & Zhang, P. Congenital Heart Disease: Causes, Diagnosis, Symptoms, and Treatments. *Cell Biochemistry and Biophysics* **72**, 857–860 (2015).
- 234. Hoffman, J. I. E. & Kaplan, S. The incidence of congenital heart disease. *J Am Coll Cardiol* **39**, 1890–1900 (2002).
- 235. Fahed, A. C., Gelb, B. D., Seidman, J. G. & Seidman, C. E. Genetics of Congenital Heart Disease. *Circulation Research* **112**, 707–720 (2013).
- 236. Narchi, H. & Kulaylat, N. Heart disease in infants of diabetic mothers. *Images Paediatr Cardiol* **2**, 17–23 (2000).
- 237. Ritchie, R. H. & Dale Abel, E. Basic Mechanisms of Diabetic Heart Disease. *Circulation Research* 1501–1525 (2020) doi:10.1161/CIRCRESAHA.120.315913.
- 238. Correa, A. Pregestational Diabetes Mellitus and Congenital Heart Defects. *Circulation* **133**, 2219–2221 (2016).
- 239. Øyen, N. *et al.* Prepregnancy Diabetes and Offspring Risk of Congenital Heart Disease: A Nationwide Cohort Study. *Circulation* **133**, 2243–2253 (2016).
- 240. Lisowski, L. A. *et al.* Congenital heart disease in pregnancies complicated by maternal diabetes mellitus: An international clinical collaboration, literature review, and meta-analysis. *Herz* **35**, 19–26 (2010).
- 241. Wu, Y. *et al.* Type 2 diabetes mellitus induces congenital heart defects in murine embryos by increasing oxidative stress, endoplasmic reticulum stress, and apoptosis. *American Journal of Obstetrics and Gynecology* **215**, 366.e1-366.e10 (2016).

- 242. Emsley, R. *et al.* Safety of the omega-3 fatty acid, eicosapentaenoic acid (EPA) in psychiatric patients: Results from a randomized, placebo-controlled trial. *Psychiatry Research* **161**, 284–291 (2008).
- 243. Hamden, K. *et al.* Inhibitory potential of omega-3 fatty and fenugreek essential oil on key enzymes of carbohydrate-digestion and hypertension in diabetes rats. *Lipids in Health and Disease* **10**, 226 (2011).
- 244. Min, Y. *et al.* Fetal erythrocyte membrane lipids modification: preliminary observation of an early sign of compromised insulin sensitivity in offspring of gestational diabetic women. *Diabetic Medicine* **22**, 914–920 (2005).
- 245. Devarshi, P. P., Grant, R. W., Ikonte, C. J. & Hazels Mitmesser, S. Maternal Omega-3 Nutrition, Placental Transfer and Fetal Brain Development in Gestational Diabetes and Preeclampsia. *Nutrients* **11**, 1107 (2019).
- 246. Lewis-Israeli, Y. R. *et al.* Self-assembling human heart organoids for the modeling of cardiac development and congenital heart disease. *Nature Communications* **12**, 5142 (2021).
- 247. Schwartz, R. *et al.* Hyperinsulinemia and Macrosomia in the Fetus of the Diabetic Mother. *Diabetes Care* **17**, 640–648 (1994).
- 248. Wang, F., Reece, E. A. & Yang, P. Oxidative stress is responsible for maternal diabetes-impaired transforming growth factor beta signaling in the developing mouse heart. *American Journal of Obstetrics and Gynecology* **212**, 650.e1-650.e11 (2015).
- 249. van Heeswijk, M., Nijhuis, J. G. & Hollanders, H. M. G. Fetal heart rate in early pregnancy. *Early Human Development* **22**, 151–156 (1990).
- 250. Benson, C. B. & Doubilet, P. M. Slow embryonic heart rate in early first trimester: indicator of poor pregnancy outcome. *Radiology* **192**, 343–344 (1994).
- 251. Cao, J. & Poss, K. D. The epicardium as a hub for heart regeneration. *Nature Reviews Cardiology* **15**, 631–647 (2018).
- 252. Andersen, P. *et al.* Precardiac organoids form two heart fields via Bmp/Wnt signaling. *Nature Communications* **9**, 1–13 (2018).
- 253. Pang, L. *et al.* Prostaglandin e receptor subtype 4 signaling in the heart: Role in ischemia/reperfusion injury and cardiac hypertrophy. *Journal of Diabetes Research* **2016**, (2016).
- 254. Kuhn, H., Banthiya, S. & van Leyen, K. Mammalian lipoxygenases and their biological relevance. *Biochim Biophys Acta* **1851**, 308–30 (2015).
- 255. Wende, A. R. & Abel, E. D. Lipotoxicity in the heart. *Biochimica et Biophysica Acta Molecular and Cell Biology of Lipids* **1801**, 311–319 (2010).
- 256. Kc, K., Shakya, S. & Zhang, H. Gestational diabetes mellitus and macrosomia: A literature review. *Annals of Nutrition and Metabolism* **66**, 14–20 (2015).
- 257. Engineer, A., Saiyin, T., Greco, E. R. & Feng, Q. Say NO to ROS: Their roles in embryonic heart development and pathogenesis of congenital heart defects in maternal diabetes. *Antioxidants* **8**, (2019).
- 258. Gandhi, J. A., Zhang, X. Y. & Maidman, J. E. Fetal cardiac hypertrophy and cardiac function in diabetic pregnancies. *American Journal of Obstetrics and Gynecology* **173**, 1132–1136 (1995).
- 259. Zhong, J., Xu, C., Gabbay-Benziv, R., Lin, X. & Yang, P. Superoxide dismutase 2 overexpression alleviates maternal diabetes-induced neural tube defects, restores mitochondrial function and suppresses cellular stress in diabetic embryopathy. *Free Radical Biology and Medicine* **96**, 234–244 (2016).
- 260. Manivannan, S. *et al.* Single-cell Transcriptomic Profiling Unveils Cardiac Cell-type Specific Response to Maternal Hyperglycemia Underlying the Risk of Congenital Heart Defects. *bioRxiv* (2022).

- 261. Filippo Buono, M. *et al.* Human Cardiac Organoids for Modeling Genetic Cardiomyopathy. *Cells* **9**, 1733 (2020).
- 262. Giacco, F. & Brownlee, M. Oxidative stress and diabetic complications. *Circulation Research* **107**, 1058–1070 (2010).

APPENDIX

ANTIBODIES AND MOLECULAR PROBES USED THROUGHOUT THE DISSERTATION

Table 4. Antibodies, dyes, and molecular probes used for immunofluorescence in this dissertation. ABs: antibodies

	Antibody name	Host Species	Dilution	Catalogue Number	Vendor
	cTnT (TNNT2)	Mouse	1:200	ab8295	Abcam
	WT1	Rabbit	1:200	ab89901	Abcam
	ZO1 (TJP1)	Goat	1:250	PA5-19090	Thermo Fisher Scientific
	HAND1	Rabbit	1:200	ab196622	Abcam
	HAND2	Rabbit	1:200	ab200040	Abcam
ABs	MLC2V (MYL2)	Rabbit	1:200	ab79935	Abcam
	MLC2A (MYL7)	Mouse	1:200	311-011	Synaptic Systems
ary	Vimentin (VIM)	Goat	1:200	ab11256	Abcam
Primary	CD90/Thy1	Rabbit	1:200	ab133350	Abcam
ď	NFAT2 (NFATC1)	Rabbit	1:200	ab25916	Abcam
	CD31 (PECAM1)	Rabbit	1:50	ab28364	Abcam
	COL1A1	Mouse	1:200	M-38	DSHB
	COL4A1	Mouse	1:200	M3F7	DSHB
	FBN1	Mouse	1:200	CPTC- FBN1-1	DSHB
	Alexa Fluor 488	Donkey anti- mouse	1:200	A-21202	Thermo Fisher Scientific
ABs	Alexa Fluor 488	Donkey anti-rabbit	1:200	A-21206	Thermo Fisher Scientific
Secondary	Alexa Fluor 594	Donkey anti- mouse	1:200	A-21203	Thermo Fisher Scientific
Seco	Alexa Fluor 594	Donkey anti-rabbit	1:200	A-21207	Thermo Fisher Scientific
	Alexa Fluor 647	Donkey anti-goat	1:200	A32849	Thermo Fisher Scientific
	Dye/ Probe name	Target	Dilution	Catalogue Number	Vendor
Probes	DAPI	Nucleus (DNA)	1:1000	62248	Thermo Fisher Scientific
	ER Tracker	Endoplasmic Reticulum	1 μΜ	E34250	Thermo Fisher Scientific
ంర	Fluo-4, AM	Calcium ions	1 μΜ	F14201	Fisher Scientific
Dyes	MitoTracker	Mitochondria	100 nM	M22426	Thermo Fisher Scientific
	WGA/FITC	T-tubules	1:200	L4895	Sigma-Aldrich

CELL LINE SOURCES

Table 5. Cell lines used throughout this dissertation

Cell Line	Stem Cell Type	Source
AICS-0037-172	Human iPSC	Coriell Institute for Medical
AICG-0037-172	Tidilali ir 30	Research
iPSC-GCaMP6f	Human iPSC	From another lab ^{127,128}
		Developed in house at
iPSC-L1	Human iPSC	University of California San
		Diego
iPSC-L1_FlipGFP	Human iPSC	Developed in house at
IF3C-L1_FIIPGFF	Human if 3C	Michigan State University
iPSCORE_16_3	Human iPSC	WiCell
H9	Human ESC	WiCell
HEK293T	Human Cancer Cells	ATCC

CRITICAL PROTOCOL PARAMETERS

Stem Cell Culture

Diligent stem cell culture technique is crucial for the success of the protocols listed here. Stem cells must remain pluripotent until the directed differentiation protocol begins in Basic Protocol 2. Successful maintenance of stem cells is line dependent. hPSCs should be cultured and passaged at least twice after thawing from cryopreservation before embryoid body generation. Cell culture in defined media is crucial for success of this protocol. PSCs cultured in serum-based media are susceptible to variability and may result in suboptimal organoids or an unsuccessful differentiation of cardiac lineages.

Embryoid Body Generation

This protocol utilizes round bottom ultra-low attachment plates to help shape the embryoid bodies into spheres. This results in the 3D spherical embryoid bodies sitting at the bottom of the well at the lowest point, but not being attached to the plate itself. The embryoid bodies are very delicate, especially on the day after aggregation, and can very easily come apart. For this reason, the very first media change in after aggregation (Basic Protocol 1, Cell aggregation into embryoid bodies, step 5) should be executed slowly and with care to not cause movement of the EBs that may cause breakage. Broken EBs may result in unsuccessful differentiation, or multiple smaller organoids in the same well which will not be reproducible or representative of the rest of the plate. This is true for both media removal and media addition.

Organoid Differentiation

For successful differentiation into functional cardiac organoids, it is recommended that all media changes take place at the same time of day within a 20-minute window. This allows differentiation to occur as intended and to minimize variability between plates. The differentiation and maintenance of media should be warmed to 37 °C prior to media changes to minimize any temperature shocks to the organoids during the protocol (this is especially important in the early days of differentiation). For organoid cultures over 15 days, the user should note that a slight decrease in size of the organoids is to be expected. Organoids achieve human-fetal-like heart features, and therefore, studies into development and diseases of the adult/mature human heart may need to incorporate additional maturation steps that are outside the scope of this protocol.

Analysis and testing

When transferring organoids from the 96-well culture plate to a secondary location for live analysis, fixation, or molecular biology assays, it is strongly recommend cutting the tip off a p200 tip to allow a wide opening to avoid any damage or stress to the organoids (see **Figure 3**). When fixing organoids using 4% PFA, it is recommended to use fixing time of 30-45 minutes, as shorter times would fail to properly fix the internal regions of the organoids, and longer fixing times may require an additional antigen retrieval step. It is also recommend not surpassing 8 organoids per tube for fixation and immunostaining, as it may result in diminished immunofluorescence quality.

Time Considerations

Allow at least two passages of PSCs after thawing which can take 1-2 weeks depending on the cell line. Basic Protocol 1 can be initiated as soon as healthy and pluripotent stem cells reach the required confluency. The dissociation of the stem cells and subsequent aggregation should take about 1-2 hours depending on user experience. EBs are ready for differentiation 2 days after aggregation. The differentiation protocol is 15 days long unless further culture is desired for other specific applications. Allow for at least 1 hour on every media change day for media preparation and slow and careful media changes. Changing the media on a single 96 well plate should take anywhere from 10 to 30 minutes depending on user experience.

TROUBLESHOOTING

 Table 6. Troubleshooting embryoid body generation

Problem	Possible Cause	Solution	
Visible differentiation on stem cell wells	Stress inducing passage or thawing	Mark differentiated areas using an object marker under a microscope and scratch differentiated cells using a pipette tip before proceeding to another passage.	
Stem cell colonies are growing in 3D (yellowish center appearing on colonies)	Colonies were too large or too confluent when last passaged.	Pass cells at lower confluency and ensure colonies are small when dissociated.	
Stem cells are not dissociating to single cells with Accutase	Accutase not at room temperature, or is expired/inactive	Make sure to allow enough time for Accutase to reach room temperature before proceeding with dissociation. Never place Accutase in temperatures above RT.	
EBs did not form the day after plate was centrifuged	Media was cold or centrifuge was not at room temperature. TZV was not added	Make sure that the cell culture media is at room temperature or 37°C and contained TZV. Make sure that the centrifuge was set to room temperature if it has temperature control.	
More than 1 EBs has formed in a single well Media change after aggregation was too aggressive resulting in the EBs splitting.		Change the media with extra care, gently removing and slowly adding the media.	

Table 7. Troubleshooting organoid differentiation

Problem	Possible Cause	Solution
Organoids are not	Unsuccessful differentiation due	This protocol was optimized with PSCs
beating by day 10	to serum-based stem cell culture	grown in E8-based media; less defined
	media.	media will result in inferior differentiation
	Unsuccessful differentiation	results.
	nonadherence to protocol	It is crucial to follow this protocol
		exactly, especially when it comes to
		concentrations and media changing
		times.
Organoids are broken,	Organoid was in contact with	Media changes should be conducted
or have broken pieces	pipette tip or media was changed	with care, with minimal disturbance to
	too aggressively	the organoids. The pipette tips should
		never be in contact with the organoid.

Table 8. Troubleshooting organoid collection and analysis

Problem	Possible Cause	Solution
Unable to collect	Users are being too gentle with	While it is important to collect the organoids
organoid into the	the pipette suction, or organoids	with care, it is recommended to pipette up
pipette tip.	have been lost.	slightly fast when collecting organoids
		compared to regular media changes.
		Ensure that there is an organoid in the well,
		organoids should be visible to the naked eye
		when looking at the plate from the bottom.
Organoids keep	The collection tip opening isn't	Make sure that the tip is cut about 10 mm from
breaking during	large enough, or organoids are	the bottom so that the opening is 3 times larger
collection	extra delicate	than an organoid.
		Depending on additional treatments to the
		organoids, they may become more delicate
		than usual, in which case the user should
		proceed with extra care or consider analyzing
		or fixing the organoids in the culture plate
		before transferring them (if possible).
No or little RNA	Organoids were not pooled before	Make sure to pool 3-4 organoids at least for
was extracted	extraction or were not submerged	sufficient RNA.
from the	in RNAprotect reagent.	Ensure that the organoids are completely
organoids		submerged in the RNAprotect reagent to
		preserve the RNA.
Immunofluoresce	Immunofluorescence antibody	It is crucial that the antibody solution be
nce images only	solution was not well prepared or	prepared according to recipe and that the
stain the surface	mixed	Triton X-100 detergent be at 0.5% (v/v) and
or the organoids		mixed well so that the detergent is no longer
		visible and the solution in uniform and
		transparent.
		If the problem persists, consider longer
		incubation time with antibodies, and ensure
		that enough antibodies are used.

PUBLICATIONS, CONFERENCE PRESENTATIONS, AND PATENTS

Publications, preprints and submitted manuscripts at time of writing

Lewis-Israeli, Y.R., Wasserman, A.H., Gabalski, M.A., Volmert, B.D., Ming, Y., Ball, K.A., Yang, W., Zou, J., Ni, G., Pajares, N. and Chatzistavrou, X., 2021. Self-assembling human heart organoids for the modeling of cardiac development and congenital heart disease. *Nature communications*, 12(1), pp.1-16. https://doi.org/10.1038/s41467-021-25329-5

- Lewis-Israeli, Y.R., Wasserman, A.H. and Aguirre, A., 2021. Heart organoids and engineered heart tissues: Novel tools for modeling human cardiac biology and disease. *Biomolecules*, 11(9), p.1277. https://doi.org/10.3390/biom11091277
- 3) <u>Lewis-Israeli, Y.R.</u>, Volmert, B.D., Gabalski, M.A., Huang, A.R. and Aguirre, A., 2021. Generating Self-Assembling Human Heart Organoids Derived from Pluripotent Stem Cells. *J. Vis. Exp. https://dx.doi.org/10.3791/63097-v*
- 4) Ming, Y., Hao, S., Wang, F., <u>Lewis-Israeli, Y.R.</u>, Volmert, B.D., Xu, Z., Goestenkors, A., Aguirre, A. and Zhou, C., 2022. Longitudinal morphological and functional characterization of human heart organoids using optical coherence tomography. *Biosensors and Bioelectronics*, 207, p.114136. https://doi.org/10.1016/j.bios.2022.114136
- 5) Wasserman, A.H., <u>Lewis-Israeli, Y.R.</u>, Huang, A.R., Dooley, M.D., Mitchell, A.L., Venkatesan, M. and Aguirre, A., 2021. Oxytocin promotes epicardial cell activation and heart regeneration after cardiac injury. *bioRxiv*. (Under review at *eLife*). https://doi.org/10.1101/2021.11.01.466355
- 6) <u>Lewis-Israeli, Y.R.</u>, Abdelhamid, M., Olomu, I., Aguirre, A., 2022. Modeling the effects of maternal diabetes on the developing human heart using pluripotent stem cell-derived heart organoids. (Accepted at *Current Protocols in Toxicology*).

Conference presentations

- Lewis-Israeli, Yonatan, et al. Self-assembling human heart organoids modeling cardiac development and congenital heart disease. Talk presented at The International Society for Stem Cell Research (ISSCR) and the Japanese Society for Regenerative Medicine (JSRM) International Symposium, October 2021. Tokyo, Japan (Virtual).
- Lewis-Israeli, Yonatan, et al. Self-assembling human pluripotent stem cell-derived heart organoids modeling development and congenital heart disease. Poster presented at EMBO Cardiomyocyte Biology, May 2021. Ascona, Switzerland (Virtual).
- Israeli, Yonatan, et al. Self-assembling human pluripotent stem cell-derived heart organoids for the study of cardiac development and disease. Poster presented at ISSCR Annual Meeting, June 2020. Boston, USA (Virtual).

Patents

1) A. Aguirre, Y.R. Israeli. Pluripotent stem cell-derived heart organoid. WO2021257812A1.

Published: 2021-12-23.

https://patents.google.com/patent/WO2021257812A1/en?oq=WO2021257812A1